- The "Nitrogen Interface Test," or NIT, consists of injecting nitrogen into the annular space to develop a nitrogen/liquid interface below the last cemented casing. The central string remains filled with brine, and a logging tool is used to measure the brine/nitrogen interface location. Two or three measurements, generally separated by 24 hours, are performed; an upward movement of the interface is deemed to indicate a nitrogen leak. Pressures are measured at the wellhead, and temperature logs are performed to allow precise calculation of nitrogen seepage. A slightly different method is the In-Situ Compensation Method. No logging tool is used; instead, gas is injected until it reaches a weep-hole in the inner pipe. When the interface depth rises, the interface level is reset by injecting additional gas until the weep-hole is reached again. The amount of additional gas injected to reset the interface can be measured with great precision at the surface [Crotogino, 1996]. A case history is described in Edler et al. [2003].
- The "Liquid-Liquid Interface Test" consists of injecting a liquid hydrocarbon (instead of nitrogen, as for the NIT) into the annular space to below the last cemented casing. During the test, attention is paid to the evolution of the brine and liquid pressures as measured at the wellhead. A severe pressure-drop rate is a clear sign of poor tightness. In addition, the annular liquid can be withdrawn after the test and weighed, allowing comparison with the weight of the injected liquid volume (the so-called Above-Ground Balance Method; a case history is described in Branka et al. [2002]).

In the following, the accuracy and meaning of these two test types are discussed in more detail.

4.3 BIBLIOGRAPHY

Literature addressing cavern well testing is relatively abundant. Van Fossan [1983] and Van Fossan and Whelply [1985] discuss both the legal and technical aspects of cavern-well testing and strongly support the Nitrogen Interface Test (NIT). They point out the significance of the Minimum Detectable Leak Rate (MDLR) or the accuracy of the test method.

Goin [1983] discusses the effect of testing-fluid viscosity on leak rate.

The ATG Manual [1985, in French] describes an Above-Ground Liquid Balance Test performed before the first natural-gas injection in a leached-out cavern. A light hydrocarbon is injected in the annular space to a depth of 15 m below the last cemented casing shoe. Test duration is 4–5 days. The hydrocarbon mass is measured accurately at ground level before injection and again after withdrawal. The pass/fail criterion is a hydrocarbon loss rate smaller than 250 liters per day. The test pressure is 110 percent of the maximum operating gas pressure.

Heitmann [1987] presents a set of case histories that illustrate several difficulties encountered when testing real caverns.

Vrakas [1988] (see also Beasley [1982]) discusses the cavern integrity program used by the U.S. Strategic Petroleum Reserve (SPR). This program includes "Hydrostatic Testing" (i.e., Pressure Observation Tests) and "Nitrogen Interface" testing. Hydrostatic tests include a 48-hour-long test at 90 percent of the overburden pressure followed by a 48-hour-long test at 83 percent of the overburden pressure. The caverns are filled partly with oil. Results are somewhat erratic; in several cases, the wellhead pressure rises instead of decreases. (In hindsight, these results maybe attributed to the effects of fluid thermal expansion, which are especially severe in a large cavern filled with oil whose thermal expansion coefficient is larger than that of brine.) Vrakas suggests that, during an NIT, the optimum test duration is 0.65 day per square foot of cross-sectional area of the borehole (at interface depth). The pass/fail criterion acceptable to the SPR is 100 bbls/year.

Diamond [1989] and Diamond et al. [1993] propose the Water-Brine Interface Method, which originally was designed to test multiple-well caverns operated for brine production. The cavern is filled with brine and wells are shut in. Soft water is injected in one well to fill all but the bottom 50 ft; the remaining wells remain brine filled. Any upward displacement of the water-brine interface results in a pressure drop at the wellhead, which is compared to the pressure evolution in a reference brine-filled well. The same method can be used in a single well equipped with a brine-filled central string, which plays the role of the reference well: soft water is injected in the annular space to create the brine-water interface. Diamond et al. [1993] recommend letting the well idle for 36 hours before performing the test to provide sufficient time for the well fluids to reach thermal equilibrium.

Brasier [1990], a member of the U.S. Environmental Protection Agency, assesses the Pressure Observation Test (POT), stating [p.6] that:

> "The theory ... is if the salt cavity is "shut in" and a leak develops ... a pressure decrease can be observed at the surface. This test was deemed inappropriate for two reasons ... given the enormous size of ... the cavities, a massive leak would have to be present in order to detect any pressure decrease. Any uncalculated pressure changes in the "shut in" cavity due to temperature fluctuations of cavity fluid, further dissolution of salt and salt heaving will interfere with the interpretation of the results making the test unreliable."

Based on this, Brasier strongly supports the interface method described by Diamond, compared to the POT test.

Thiel [1993] (see also Thiel [1990]), describes several test methods based on the measurement of cavern compressibility, which is the ratio between the volume of injected liquid in a shut-in cavern and the resulting pressure build-up. This notion is used to caliper the interface cross-sectional area, an essential issue for the accuracy of the Nitrogen Interface Test. Cavern compressibility is also used to interpret the Pressure Observation Test: a hydrocarbon cap is established in the cavern; the pressure-drop rate, as observed at ground level, is then

converted into a seep rate by multiplying the pressure drop rate and the cavern compressibility. Interesting comments are provided on the effects of ground temperature variation during a Nitrogen Interface Test. Thiel suggests prepressurizing the cavern 2–4 weeks before the actual test to minimize the effects of cavern destabilization caused by pressurization. He suggests a 1,000-bbls/year (160-m^3/year) Maximum Admissible Leak Rate.

CH2M HILL, Inc. [1995], in a report prepared for the Solution Mining Research Institute (SMRI), gives a practical description of the Nitrogen Interface Test. Cavern-neck diameter and test duration are important parameters affecting test accuracy. Influence of the following factors is considered: additional dissolution, cavern expansion/contraction, cavern shape and size, adjacent caverns influence, and nitrogen temperature evolution.

Crotogino [1995] prepared one of the most important papers dedicated to MIT published in recent years; a summary is provided in Crotogino [1996]. Crotogino distinguishes between (a) the *In-Situ Balance Method* (or Nitrogen Interface Test), which involves tracking a nitrogen/brine interface through a logging tool; (b) the *In-Situ Compensation Method*, in which a weep-hole is located in the central string; nitrogen (or liquid) is injected in the annular space at the beginning and at the end of the test till overflowing; and (c) the *Above-Ground Balance Method*, whose principle is based on the comparison at the surface between the volume of the injected test fluid (a liquid, in most cases) and the volume of the fluid recovered after the test. Crotogino proposes an SMRI-Reference leak rate value. In fact, he distinguishes between the Minimum Detectable Leak Rate, or MDLR (resolution of the testing method), and the Maximum Allowable Leak Rate, or MALR. Based on a pragmatic approach, Crotogino suggests that the MDLR be 50 kg (of nitrogen) per day and that the MALR be 150 kg per day. Assuming a pressure of 17 MPa and a temperature of 300 K, 150 kg/day is equivalent to 800 l/day or 300 m^3/year. The actual MALR must be reduced by a factor of 2 when LPG is considered instead of nitrogen.

Bérest et al. [1995; 1996; 2001a; 2002] address various aspects of cavern-tightness testing. They suggest distinguishing between the "apparent leak" (directly deduced from observations), the "corrected leak" (obtained when taking into account well-known mechanisms, other than an actual leak, contributing to the apparent leak) and the "actual leak." They describe a specific Pressure Difference Observation Test where a light hydrocarbon fluid was accurately injected in the annular space of a brine-filled cavern. Test interpretation was based on the analysis of the evolution of the difference between the annular-space pressure and the central-string pressure, rather than on the evolution of the pressures themselves–a technique reminiscent of the method proposed by Diamond et al. [1993]. Bérest and his coworkers performed a Nitrogen Interface Test and simulated artificial leaks by withdrawing calibrated amounts of brine or nitrogen to assess NIT accuracy. Thus they demonstrated that the interface displacement could be inferred from analysis of the differential evolution of wellhead pressures.

Thoms and Kiddoo [1998] provide a general description of the NIT and an additional bibliography.

The Solution Mining Research Institute [1998] organized a technical class dedicated to Mechanical Integrity Testing of brine production and storage caverns to provide a comprehensive assessment of the state of the art.

Remizov et al. [2000] recommend that cavern wells be tested 28–45 days after leaching is completed. Several methods can be used. The pass/fail criteria they propose are (a) the leak rate must be smaller than 20–27 liters per day (when testing with liquid) or 50 kg per day (when testing with gas), and (b) the pressure drop rate (during a Pressure Observation Test) must become constant and be less than 0.05 percent (of test pressure) per hour. The Pressure Observation Test interpretation takes into account the following influential factors: additional dissolution, cavern convergence, changes in brine and test fluid temperatures, and transient creep. Transient creep is deemed to be effective for only 1–2 days after pressure build-up. According to Remizov et al., cavern compressibility during depressurization is 2–20 percent smaller than when measured during pressurization. Formulas establishing a correspondence between the wellhead pressure drop rate and leakage rate are proposed.

Branka et al. [2002] describe an MIT performed in Gora Underground Cavern Oil and Fuel Storage (Poland). The Above-Ground Balance Method was used to avoid "... complicated and expensive installation and survey." The authors state that testing a liquid-storage cavern using a liquid test fluid (rather than a gas) seems reasonable. The procedure basically consists of injecting the test liquid ("blanket oil") down the central-tubing to the level of a weep-hole, which is located below the last cemented casing shoe. Both the injected volume and the overflowed volume are measured carefully, taking temperature and pressure changes into account. Test pressures equal to 105 percent of the maximum operating pressure are recommended. The pressurized well is kept idle for 10 days, at which time, the test liquid is again injected to reach overflow. Volumes are measured carefully, and the "lost" volume is computed. Observed leak rates are in the range of 3.7–29.2 kg/day (of blanket oil); the larger leak rate applying to newly created wells.

Edler et al. [2003] describe use of the In-Situ Compensation Method. Before leaching, or when leaching is completed, the well is equipped with a central gas-tight string to below the last cemented casing. A 1-cm-diameter hole is located at the lower end of this central string. A gas (nitrogen or air) column is injected to below the last cemented casing. When the gas-brine interface reaches the hole (overflow), gas rises in the string and wellhead pressure increases. After several hours, gas is injected again until the brine/gas interface reaches the hole located in the central string. The amount of gas leaked between the two injections is computed via a spreadsheet that allows temperature and pressure variations with depth, as well as changes in central volume composition, to be taken into account. The accuracy of the method is discussed.

Nelson and Van Sambeek [2003] address the issue of MIT techniques that can be implemented for gas-filled storage caverns. They discuss existing test methods (advantages, disadvantages, and estimated uncertainty). Uncertainties are much larger than in fluid-filled caverns because (1) no interface method can be used in a gas-filled cavern, and (2) gas compressibility is much larger than liquid compressibility, resulting in poor accuracy of any pressure observation method. Novel MIT techniques are explored.

Thiel and Russel [2004] proposed the Pressure Observation Test (POT) method, which is a liquid-liquid method. Whereas the standard Nitrogen Interface Test (NIT) can be used conveniently when the tested cavern has a narrow and consistent neck, a situation often met in domal caverns; in the bedded-salt caverns whose thickness is small, the caverns tend to be shallow and small with no neck. For bedded-salt caverns, the authors strongly suggest using the POT method, which is based on accurate measurement of wellhead pressures in a pressurized liquid-filled cavern. The cavern remains filled with brine, except for a small hydrocarbon cap that is injected in the annular space to establish the brine/hydrocarbon interface below the last cemented casing. Advantage is taken of the end of the pressure build-up phase to measure cavern compressibility. After a stabilization period, the wellhead pressure decay rate (accounting for ground temperature variations) is divided by cavern compressibility to get the leak rate, which must be smaller than 1,000 bbls/year. If this criterion is not met, a second observation cycle is performed. Real-life examples are discussed, as are the advantages of the two methods (POT and NIT).

4.4 APPARENT, CORRECTED, AND ACTUAL LEAKS

Testing the tightness of an underground storage facility involves recording the decrease of wellhead pressure and/or tracking a fluid/fluid interface in the well. The pressure decrease rate, or the interface velocity, must then be converted into a "fluid leak rate" through relevant calculations. In fact, several different mechanisms, of which the actual leak is just one, combine to produce fluid-pressure decreases or interface movements. The combined effects of these mechanisms may lead to an over- or an underestimation of the leak. Several of these mechanisms can be identified clearly and quantified precisely. Field data can be corrected for the effects of these mechanisms, leading to a better estimation of the leak.

More precisely, one must distinguish between:

- The "**actual**" leak, whether measured or not.
- The "**apparent**" leak, which is directly deduced from the observed pressure decrease or interface displacement.
- The "**corrected**" leak, obtained when the effects of known and quantifiable mechanisms contributing to the apparent leak are taken into account.

During a Pressure Observation Test (POT), the apparent leak rate is

$$Q_{app} = -\beta V \cdot \dot{P}_{tub}^{wh}$$

where $\dot{P}_{tub}^{wh}$ (in most cases, $\dot{P}_{tub}^{wh} < 0$) is the wellhead pressure decrease rate as measured in the tubing; βV is the cavern compressibility. In most cases, $Q_{app} > 0$. For this reason, the cavern compressibility is of utmost importance when interpreting an POT; this will be discussed in Chapter 5.0.

During an interface test (Nitrogen Interface Test (NIT) or Pressure Difference Observation (PDO) test, the apparent leak rate is

$$Q_{app} = -\Sigma \dot{h}$$

where $\dot{h}$ (in most cases, $\dot{h} < 0$) is the interface displacement rate either measured directly (NIT) or calculated from pressure difference evolution (PDO) and Σ is the annular cross-sectional area at interface depth. For this reason, an NIT or PDO can only be effectively performed when the cavern neck is consistent; i.e., when Σ is well known.

The objective of the remainder of this chapter is to identify those mechanisms that might contribute to the apparent leak and which, when properly accounted for, can potentially reduce the gap between the corrected leak and the actual leak.

4.5 PREEXISTING AND TEST-TRIGGERED PHENOMENA

The mechanisms contributing to pressure changes or interface displacement in an MIT are those that produce a change in cavern or fluid volumes. For example, brine warming leads to brine thermal expansion, additional dissolution leads to brine+cavern volume variation, and steady-state creep leads to cavern shrinkage.

It is convenient to distinguish between the two types of effects contributing to pressure evolution or interface displacement during an MIT: phenomena existing before the test and phenomena triggered by the test. The importance of each phenomenon will be assessed in Chapters 5.0 through 9.0.

4.5.1 Preexisting Test Phenomena

For all practical purposes, a steel pressure vessel (say, a steel pipe line tested before being used for pressurized gas transport) can be assumed to be in an equilibrium state before a pressure build-up test is performed. The same cannot be said of an underground cavern, which, in most cases, is still out of equilibrium even several years after creation. For instance, equilibrium might be expected when both the well and the cavern are filled with saturated

brine and the well has been kept open to the atmosphere for several weeks; however, common experience proves that, even after several years, an open (but filled) cavern expels a significant flow of brine–clear evidence of ongoing deformation mechanisms even after long periods of time.

Preexisting phenomena that are potentially active during an MIT are:

- Cavern brine thermal expansion (or contraction) Q_{th}.
- Steady-state salt creep (cavern closure) Q_{cr}^{ss}.
- Wellbore warming or cooling.
- Steady-state brine micropermeation into the surrounding rock mass Q_{perm}^{ss}.
- Ground and air temperature variations.
- Earth tides and atmospheric pressure variations.
- Additional dissolution because of brine undersaturation (usually does not occur).

With the exception of brine permeation, several preexisting phenomena produce effects that, in an LLI, appear to "increase" the amount of brine in the closed container–they will act to mask the amount of leaking fluid. Hence, the apparent leak results for an LLI are nonconservative as regards to the listed preexisting phenomena, while the inverse is true for an NIT.

4.5.2 Phenomena Triggered by the Test

The rapid pressure increase at the beginning of a test triggers several transient phenomena. Test-triggered phenomena are:

- Transient salt creep Q_{cr}^{tr}.
- Transient brine permeation Q_{perm}^{tr}.
- Cooling following adiabatic pressure build-up Q_{th}^{ad}.
- Additional dissolution because of pressure saturation effects Q_{diss}.

According to the Le Chatelier (or Braun) principle, these test-triggered phenomena tend to restore the preexisting pressure. During an LLI, the effects of the phenomena make the apparent leak rate greater than the actual leak. Thus as far as the phenomena triggered by the test are concerned, the apparent leak result is conservative because it overestimates the actual leak. The inverse (as compared to an LLI) is true during an NIT.

4.5.3 Effect of all the Phenomena

The effect of all these phenomena can be expressed as[1]

$$Q = Q_{cr}^{ss} - Q_{cr}^{tr} + Q_{th} - Q_{th}^{ad} - Q_{perm}^{tr} - Q_{diss} - Q_{perm}^{ss} \tag{1}$$

In fact, some of these phenomena are slow to occur. A mechanism leading to even very large deformation can be disregarded when it is so slow that its influence is significant only after a time period much longer than the test duration. Other phenomena are difficult to quantify precisely. Q^* will be the estimation that can be made of all these phenomena. During an LLI, for instance, the actual leak Q_{leak} must be added to these phenomena and

$$Q_{leak} = Q_{app} - Q \tag{2}$$

However, only Q_{app} can be measured; Q can be estimated as Q^* and the corrected leak is

$$Q_{leak}^{corr} = Q_{app} - Q^* \tag{3}$$

And, hopefully Q_{leak}^{corr} is close to Q_{leak}, $Q_{leak}^{corr} \approx Q_{leak}$.

In an NIT, the situation is more complicated and, as will be seen in Chapter 11.0,

$$Q_{leak}^{corr} = Q_{app} \cdot \left(1 + \frac{\beta_g V_g^o}{\beta V}\right) - \frac{\beta_g V_g^o}{\beta V} \cdot Q^* \tag{4}$$

where $\beta_g V_g^o$ is the compressibility of the nitrogen column.

4.6 COMPARISON BETWEEN THE NITROGEN AND LIQUID-LIQUID TESTS

Consider the case of a one-phase fluid flow through a long permeable cylinder with cross-sectional area s and length l when a $(P_2 - P_1)$ pressure difference is applied between the two ends of the cylinder. The calculated flow rate is proportional to intrinsic permeability K^{hyd}, and inversely proportional (according to the Darcy's law) to fluid dynamic viscosity, or μ:

$$Q_{perm}^{ss} = -s\frac{K^{hyd}}{\mu}\left(\frac{P_2 - P_1}{l}\right) \tag{5}$$

---

[1] In Equation (1), the plus/minus sign for each phenomena accounts for the way the apparent leak is affected. A plus sign means the phenomena makes the volume of cavern fluid appear to increase while a minus sign means the volume of cavern fluid appears to decrease relative to the cavern volume.

For nitrogen, $\mu_g = 2 \cdot 10^{-5}$ Pa·s; for brine, $\mu_b = 1.2 \cdot 10^{-3}$ Pa·s; for LPG, $\mu_{LPG} = 1.3 \cdot 10^{-4}$ Pa·s; and for crude oil, $\mu_{oil} = 10^{-3}$ to 10^{-2} Pa·s. When such a simplistic formula is accepted, the calculated volumetric flow rate of nitrogen is 60 times larger than that of brine and 6.5 times larger than that of LPG. In fact, however, the following is observed:

- Hydrocarbon and nitrogen leaks through a porous brine-saturated formation (typically, the cemented annular space behind the casing) are not easy to compare: fluid flow is governed by such phenomena as capillary pressure and two-phase flow in a porous medium, which are difficult to assess precisely.
- Flow rates depend on such factors as flow regime (Reynolds number), geometry of flow path, etc.
- Some "threshold" probably exists below which high viscosity liquids are immobile. (No liquid leak occurs in a context where nitrogen leaks are observed.)
- Rather than volumetric flow rate, mass flow rate, or ρQ, is of interest. When mass flow rate is considered, the figures change: nitrogen density (in kg/m^3) is $\rho_g = 11.5 \cdot P_g$, where P_g is the gas pressure (in MPa); typically, P_g = 10 MPa and ρ_g = 115 kg/m^3 ; brine density is ρ_b = 1,200 kg/m^3, LPG density is ρ_h = 500 kg/m^3; and crude oil density is ρ_{oil} = 850 kg/m^3.

In other words, the mass flow rate is proportional to ρ/μ. If the brine-mass leak rate is taken as a reference, the LPG-mass leak rate is 4 times larger and the nitrogen-mass leak rate is 55 times larger! A tentative analysis of all these factors can be found in Goin [1983].

From a practical point of view, Crotogino [1995] suggests that, when comparing the flow rates of viscous fluids to the flow rate of nitrogen in similar pressure conditions, the nitrogen-mass flow rate must be divided by 2 (LPG), 3 (gas oil), or 10 (crude oil), assuming the cavern temperature and pressure are 300 K and 17 MPa. These ratios are smaller than those suggested by direct application of Darcy's law, so clearly, this issue is open to discussion.

5.0 CAVERN COMPRESSIBILITY

Measuring cavern compressibility provides information so that a measured pressure evolution can be converted into an apparent leak rate. Measuring the cavern compressibility during the course of an MIT is a convenient operation because liquid is injected in the cavern to reach the test pressure. Careful measurement of the amount of injected liquid and the resulting pressure increase provides data for computation of cavern compressibility. Before a nitrogen MIT, brine is injected in the cavern to "prepressurize" the cavern, and the cavern compressibility can be calculated from data gathered during this pressure increase.

In most cases, an order of magnitude estimate of cavern compressibility can be made before the test. The cavern volume, V, is usually known from sonar surveys; however, when the formation contains a high amount of insolubles, the actual brine volume is larger than the volume that is "seen" by the sonar survey. The compressibility factor[2] is usually about $\beta = 4$ to $5 \cdot 10^{-4}$/MPa (2.8 to $3.6 \cdot 10^{-6}$/psi) in a standard cavern. When the measured cavern compressibility is significantly different from the estimated βV product, the potential existence of an anomaly should be considered (a gas pocket or a large sump, for instance; see Example 2, Section 5.2.2.4).

5.1 COMPRESSIBILITY MEASUREMENT

When a certain amount of liquid, v_{inj} is injected in a closed cavern, the wellhead pressure increases by δP^{wh}, which is also, at first approximation, the cavern pressure increase, δP_i (see Figure 4). The relation between the two quantities (v_{inj} and δP^{wh}) generally is linear during a rapid test and the cavern compressibility (βV) is the proportionality constant. A similar test can be performed by withdrawing liquid from a pressurized cavern.

An example of such a cavern compressibility measurement is described in Thiel [1993]; see Figure 4. The slope of the curve (injected brine versus brine pressure) is called the cavern compressibility (in m^3/MPa or bbls/psi):

$$v_{inj} = \beta V \cdot \delta P^{wh} \tag{6}$$

The cavern compressibility, βV, is influenced to some extent by test duration and other factors [Bérest et al., 1999]; however, in the context of an MIT, interest is mainly in relatively rapid injections. Figure 4 shows that, from an engineer's perspective, the notion of cavern compressibility is defined sufficiently.

---

[2] Compressibility factor (β) relates pressure change to the volumetric strain; i.e., $\delta P = \delta V / \beta V$.

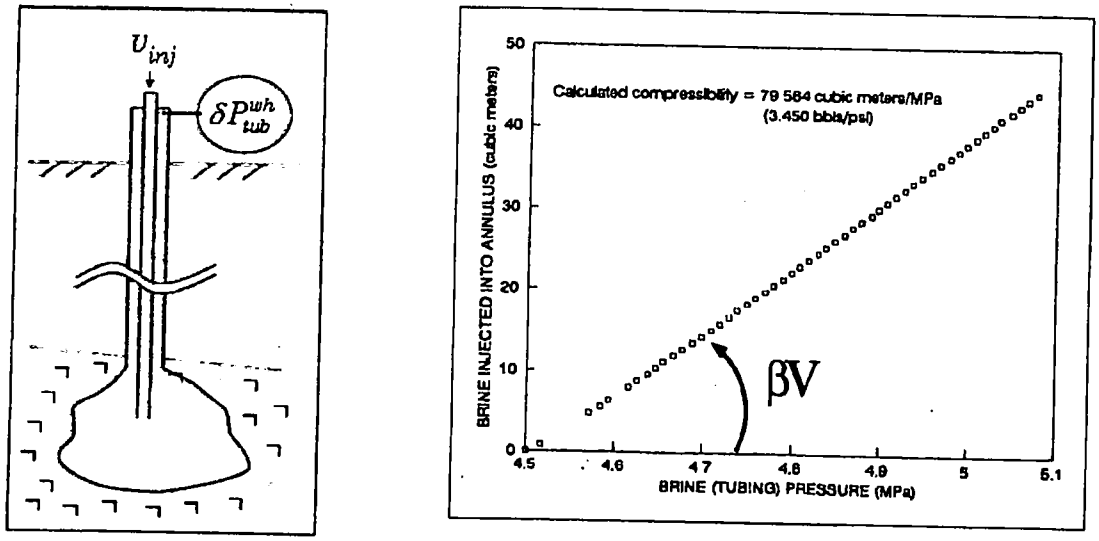

Figure 4. Measurement of Cavern Compressibility (After Thiel [1993]).

5.2 COMPRESSIBILITY ANALYSIS

Cavern compressibility, βV, can be expressed as the product of the cavern volume, V (in m^3 or bbls), and a *compressibility factor*, β (in /MPa or /psi). The compressibility factor, β, is a constant–at least for caverns of similar shapes located at the same site, filled with the same fluid, and tested for a relatively short period of time (1 hour); in other words, the compressibility factor does not depend upon the *size* of the cavern.

For instance, for the Etrez natural gas storage site, operated by Gaz de France in the north of Lyon (France), Boucly [1981] has measured an average compressibility factor as

$$\beta = 4.0 \cdot 10^{-4}/\text{MPa} = 2.8 \cdot 10^{-6}/\text{psi} \tag{7}$$

Smaller values, from $3.4 \cdot 10^{-4}$ to $3.9 \cdot 10^{-4}$/MPa have been found for the Tersanne caverns.

Similarly, for the case of the Manosque oil storage site operated by Géostock in southeastern France, Colin and You [1990] give the measured compressibility factor for brine-filled caverns as

$$\beta = 5.0 \cdot 10^{-4}/\text{MPa} = 3.6 \cdot 10^{-6}/\text{psi} \tag{8}$$

For the caverns of the Total-operated Vauvert site in southeastern France, You et al. [1994] have measured values from $\beta = 3.2 \cdot 10^{-4}$ to $8.5 \cdot 10^{-4}$/MPa. At this particular site, however,

(1) the caverns are very deep, resulting in large creep rates, (2) the salt formation is probably gassy, and (3) caverns were developed between two wells linked by hydrofracturing. These factors all contribute to this unusual range.

Thiel (personal communication) suggests that $\beta = 2.94 \cdot 10^{-6}$/psi ($4.26 \cdot 10^{-4}$/MPa) works well as a "starting point." According to Blair [1998], "compressibility of the brine filled cavern can be approximated as the compressibility of the brine," or $\beta = 3 \cdot 10^{-6}$/psi ($4.35 \cdot 10^{-4}$/MPa).

5.2.1 The Cavern Compressibility Factor

5.2.1.1 Theoretical Analysis

First consider the case of a brine-filled cavern and restrict discussion to a simple derivation. Difficulties with the simple derivation will be discussed later. Let M_b be the cavern brine mass:

$$M_b = \rho_b V_b \tag{9}$$

where ρ_b (kg/m^3) is the average brine density, and $V_b = V$ (m^3) the same as the cavern volume.

When the cavern pressure is rapidly increased by δP_i ("rapidly" means that neither salt creep nor salt dissolution have enough time to play a significant role), the following occurs:

1. The brine density increases by $\delta\rho_b = \rho_b \beta_b^{ad} \cdot \delta P_i$, where β_b^{ad} is the brine adiabatic compressibility factor, which does not depend upon cavern shape or cavern volume.
2. The cavern volume increases by $\delta V = \beta_E V \cdot \delta P_i$, where β_E is the "cavern elasticity," which depends upon rock-mass elastic properties and cavern shape (but *not* upon cavern volume).

Thus when an additional mass of saturated brine, $\delta M_b = \rho_b v_{inj}$, is forced into a closed cavern, its density and volume will increase by $M_b + \delta M_b = (\rho_b + \delta\rho_b)(V + \delta V)$, or, after linearization:

$$\beta V \cdot \delta P_i = v_{inj} \qquad \text{and} \qquad \beta = \beta_b^{ad} + \beta_E \tag{10}$$

The cavern compressibility factor, β, is the sum of the brine compressibility factor, β_b^{ad}, and the cavern elasticity, β_E. The cavern elasticity, β_E, obviously depends upon both rock-salt elastic properties and the cavern shape. For simple cavern shapes, analytical calculations of cavern elasticity can be made. If E is the Young's modulus and ν is Poisson's ratio of the salt, the cavern elasticity is calculated in the following table.

	Cavity Shape		
	Sphere	**Infinite Cylinder**	**Real-World**
β_E	$[3(1+\nu)/2E]$	$[2(1+\nu)/E]$	$f(\nu)\cdot(1+\nu)/E$

where $f = f(\nu)$ is a cavern *shape factor* that depends on the "real-world" cavern's shape and, to a smaller extent, on the Poisson's ratio of the rock. The function f is always greater than 3/2, which corresponds to a spherical case, which is the least compressible shape of a cavern. For the pear-shaped TE04 cavern (see Figure 5), Gaz de France computed a shape factor of $f = 1.6$.

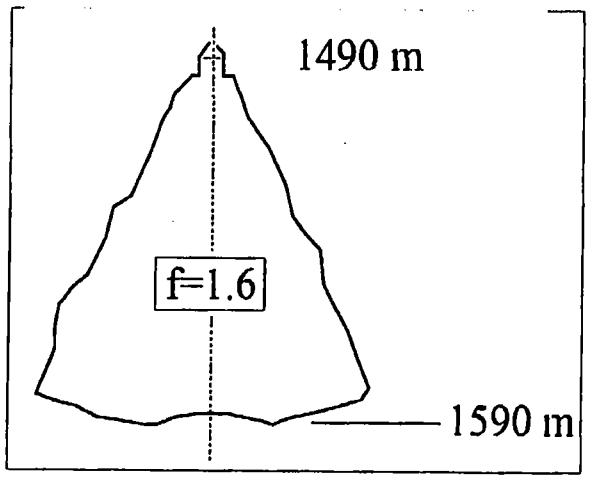

Figure 5. Tersanne TE04 Cavity (Gaz de France).

Another interesting shape is the case of a spheroidal cavern (obtained by rotation of an ellipse around its vertical axis; see Figure 6) for which a closed-form solution is available [Ballard and Constantinescu, personal communication]. Let the aspect ratio be the ratio of the semiaxes, b/a. A prolate spheroidal cavern (b/a = 6) behaves like a cylindrical cavern ($\beta_E \approx 2(1+\nu)/E$.) When $b = a$, the cavern behaves according to the spherical case. However, for an oblate (flat) cavern with large a/b, the cavern compressibility factor rapidly increases, $\beta_E \approx \left[4(1-\nu)^2/E\pi\right]\cdot(a/b)$, and cavern compressibility (see Figure 6) is $\beta V \approx \beta_E V = (16/3)a^3(1-\nu)^2/E$. In other words, the cavern compressibility factor becomes very large for a "flat" cavern.

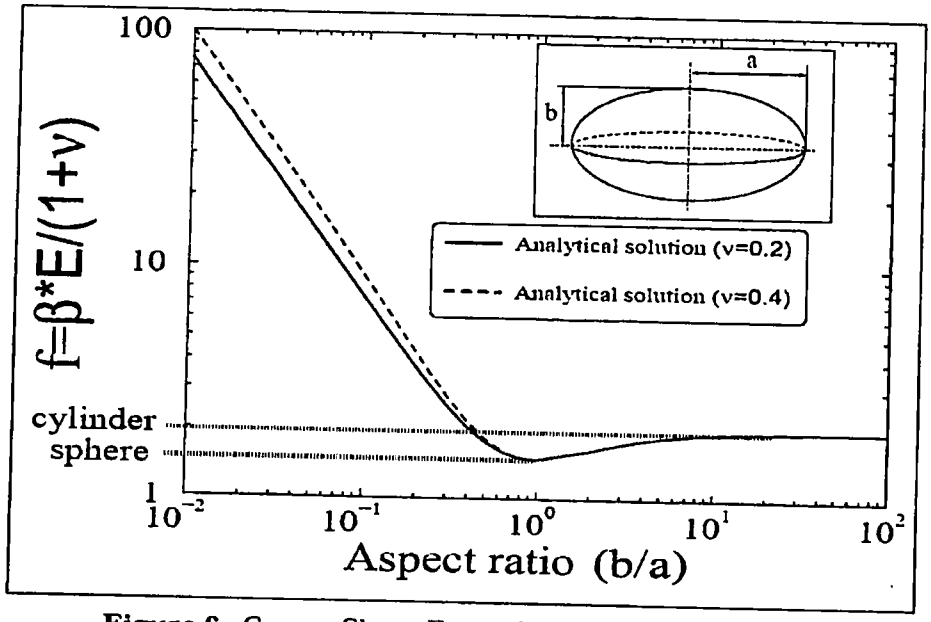

Figure 6. Cavern Shape Factor for a Spheroidal Cavern.

5.2.1.2 Field Data

From cavern compressibility factor data, Boucly [1981] infers that the cavern compressibility is

$$\beta_E = 1.3 \cdot 10^{-4}/\text{MPa}\ \left(9.0 \cdot 10^{-7}/\text{psi}\right) \tag{11}$$

which is consistent, for instance, with the following estimates:

$$\nu = 0.3,\ E = 17{,}000\ \text{MPa},\ \text{and}\ f = 1.6. \tag{12}$$

This shape-factor value corresponds to caverns from the Tersanne and Etrez sites, which have shapes that are intermediate between cylindrical and spherical (see Figure 5). The elastic properties of rock salt can vary from one site to another; reasonable ranges of variation are

$$\begin{cases} 10{,}000 \le E \le 35{,}000\ \text{MPa} \\ 0.25 \le \nu \le 0.35 \end{cases} \tag{13}$$

With such figures, the cavern compressibility factor can vary from $\beta_E = 0.5 \cdot 10^{-4}$/MPa ($3.4 \cdot 10^{-7}$/psi) to $\beta_E = 2 \cdot 10^{-4}$/MPa ($1.4 \cdot 10^{-6}$/psi) for a spherical cavern (the least compressible shape) and up to 4 or 5 times more for a somewhat flat cavern.

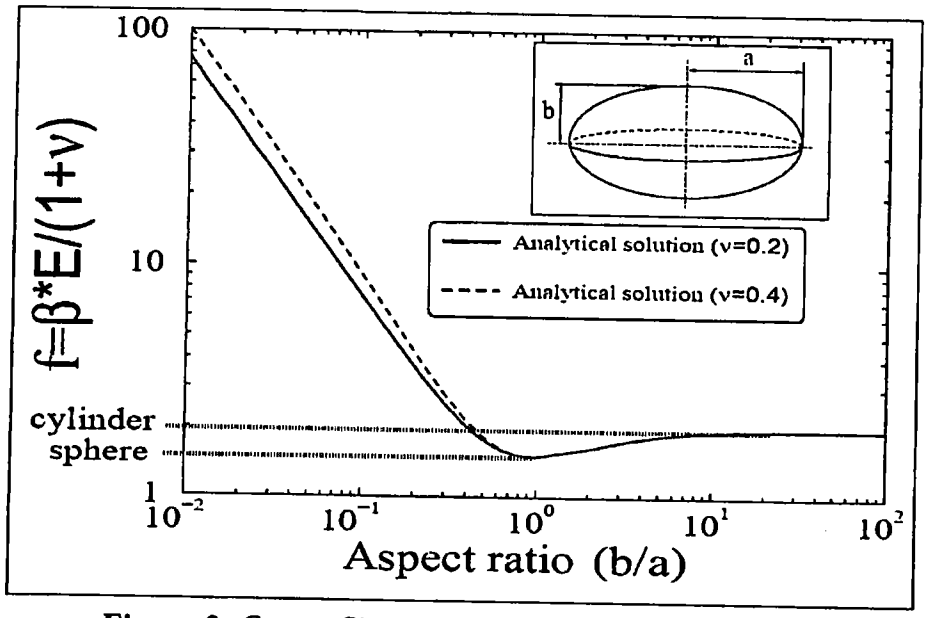

Figure 6. Cavern Shape Factor for a Spheroidal Cavern.

5.2.1.2 Field Data

From cavern compressibility factor data, Boucly [1981] infers that the cavern compressibility is

$$\beta_E = 1.3 \cdot 10^{-4}/\text{MPa}\ \left(9.0 \cdot 10^{-7}/\text{psi}\right) \tag{11}$$

which is consistent, for instance, with the following estimates:

$$\nu = 0.3,\ E = 17{,}000\ \text{MPa},\ \text{and}\ f = 1.6. \tag{12}$$

This shape-factor value corresponds to caverns from the Tersanne and Etrez sites, which have shapes that are intermediate between cylindrical and spherical (see Figure 5). The elastic properties of rock salt can vary from one site to another; reasonable ranges of variation are

$$\begin{cases} 10{,}000 \le E \le 35{,}000\ \text{MPa} \\ 0.25 \le \nu \le 0.35 \end{cases} \tag{13}$$

With such figures, the cavern compressibility factor can vary from $\beta_E = 0.5 \cdot 10^{-4}$/MPa ($3.4 \cdot 10^{-7}$/psi) to $\beta_E = 2 \cdot 10^{-4}$/MPa ($1.4 \cdot 10^{-6}$/psi) for a spherical cavern (the least compressible shape) and up to 4 or 5 times more for a somewhat flat cavern.

5.2.2 The Fluid Compressibility Factor

5.2.2.1 Brine

The theoretical adiabatic brine-compressibility factor is related to the speed of sound (measured via a sonar survey) through the relation $\rho_b \beta_b^{ad} c_b^2 = 1$, where $\rho_b \approx 1{,}200$ kg/m^3, and $c_b^2 \approx 1{,}800$ m/s; thus, $\beta_b^{ad} \approx 2.57 \cdot 10^{-4}$/MPa. This figure is appropriate for rapid (adiabatic) evolutions.

In fact, β_b^{ad} is not different, from a practical point of view, from the brine isothermal compressibility factor, but it is a little too small when relatively slow pressure changes (lasting several hours or days) are considered, because the brine saturation concentration is modified by pressure change. Pressure increase triggers additional cavern leaching (as noted, for instance, by Ehgartner and Linn [1994]), and increases the cavern volume, resulting in a slightly higher effective brine compressibility factor. However, such an additional dissolution is somewhat a delayed phenomenon and is not usually effective during the course of a rapid pressure increase. This phenomenon will be further discussed in Chapter 8.0.

In conclusion, a reasonable value for the in situ brine compressibility factor seems to be $\beta_b = 2.7 \cdot 10^{-4}$/MPa ($1.9 \cdot 10^{-6}$/psi) [Boucly, 1981; Crotogino, 1981], but bear in mind that this value can be influenced by test duration.

5.2.2.2 Hydrocarbons

Hydrocarbons are much more compressible than brine or water, and their compressibility factors are influenced by pressure and temperature. A typical value for pure propane at 25°C and 7 MPa is $\beta_{prop} \approx 2.9 \cdot 10^{-3}$/MPa and up to $4.5 \cdot 10^{-3}$/MPa for LPG. Because the speed of sound, c_{LPG}, is measured during sonar surveys, the actual adiabatic hydrocarbon compressibility factor can be computed through the formula $\beta_{LPG}^{ad} = 1/\left(\rho_{LPG} \cdot c_{LPG}^2\right)$.

5.2.2.3 Nitrogen and Other Gases

When slow evolutions (occurring over more than 1 hour for a gas volume of a few cubic meters) are considered, gas evolutions can be considered to be isothermal; for an ideal gas, the isothermal compressibility factor is simply the inverse of the (absolute) pressure, P_g:

$$\beta_g^{Isoth} = 1/P_g \qquad (14)$$

When fast evolutions are considered, gas evolution is adiabatic, and the gas adiabatic compressibility factor is

$$\beta_g^{ad} = \gamma/P_g \qquad (15)$$

where $\gamma \approx 1.3$ to 1.4. It is difficult to specify whether a given evolution can be considered as "isothermal" or "adiabatic," as that depends on evolution rate, gas volume, and container shape. The following considers only small gas pockets and isothermal evolutions.

The compressibility factor of a gas pocket trapped at the top of a brine-filled cavern (where the pressure is, for example, $P_l = P_g = 12$ MPa at 1,000 meters), will be

$$\beta_g^{isot} = 1/P_g = 8.3 \cdot 10^{-2}/\text{MPa} \tag{16}$$

whereas the compressibility factor of a gas bubble trapped at the wellhead, where the absolute pressure is, for example, $P_g^{wh} = 0.1$ MPa, will be

$$\beta_g^{isot} = 1/P_g^{wh} = 10\ /\text{MPa} \tag{17}$$

For other gases, the inverse of absolute pressure provides a first estimate of the compressibility, which can be refined by consulting available physical constant tables.

5.2.2.4 The Case of Several Fluids in a Cavern

Theoretical Aspects—In a liquid-storage cavern, the cavity contains brine *and* a hydrocarbon (such as propane or oil). In this case, the global fluid-compressibility factor will be an average of the compressibility factors of the different fluids: β_b (for brine) and β_h (for hydrocarbon). Let x be the cavern volume fraction that is occupied by the other fluid (i.e., if V is the cavern volume, the hydrocarbon volume is xV and the brine volume is $(1-x)V$. Then, the global compressibility factor, β, may be written as

$$\beta = \beta_E + \left[(1-x)\beta_b + x\beta_h\right] \tag{18}$$

This will vary, to a large extent, with respect to the hydrocarbon volume fraction. Consider, for instance, the case of propane storage. If we take

$$\begin{cases} \beta_E = 1.3 \cdot 10^{-4}/\text{MPa} \\ \beta_b = 2.7 \cdot 10^{-4}/\text{MPa} \\ \beta_h = \beta_{prop} = 4.5 \cdot 10^{-3}/\text{MPa} \end{cases} \Rightarrow \beta = \left(1.3 \cdot 10^{-4} + \left[(1-x)2.7 \cdot 10^{-4} + x \cdot 45 \cdot 10^{-4}\right]\right)/\text{MPa} \tag{19}$$

the compressibility factor varies from approximately $\beta = 4 \cdot 10^{-4}$/MPa ($2.8 \cdot 10^{-6}$/psi) with no propane in the cavern to $\beta = 38 \cdot 10^{-4}$/MPa ($2.6 \cdot 10^{-5}$/psi) when propane fills 80 percent of the cavern. To illustrate the concept for several fluids in a cavern, three case history examples follow.

Example 1—The SPR1 cavern in the Carresse site in southwestern France was used by SNEA(P) (ELF), now Total E&P France, to store propane. The casing shoe depth is 348 meters below ground level and the depth of the cavern bottom is 381.5 meters. The cavern volume is 13,000 m^3 (as measured in 1992). Compressibility measurements were performed during three different periods when the product storage volume varied widely (see Figure 7). During the three tests, the cavern compressibility (βV) was measured during brine injection; the pressure measurement resolution was 500 Pa. The cavern compressibility for the three amounts of stored propane is listed in Figure 7.

RSI-1476-05-011

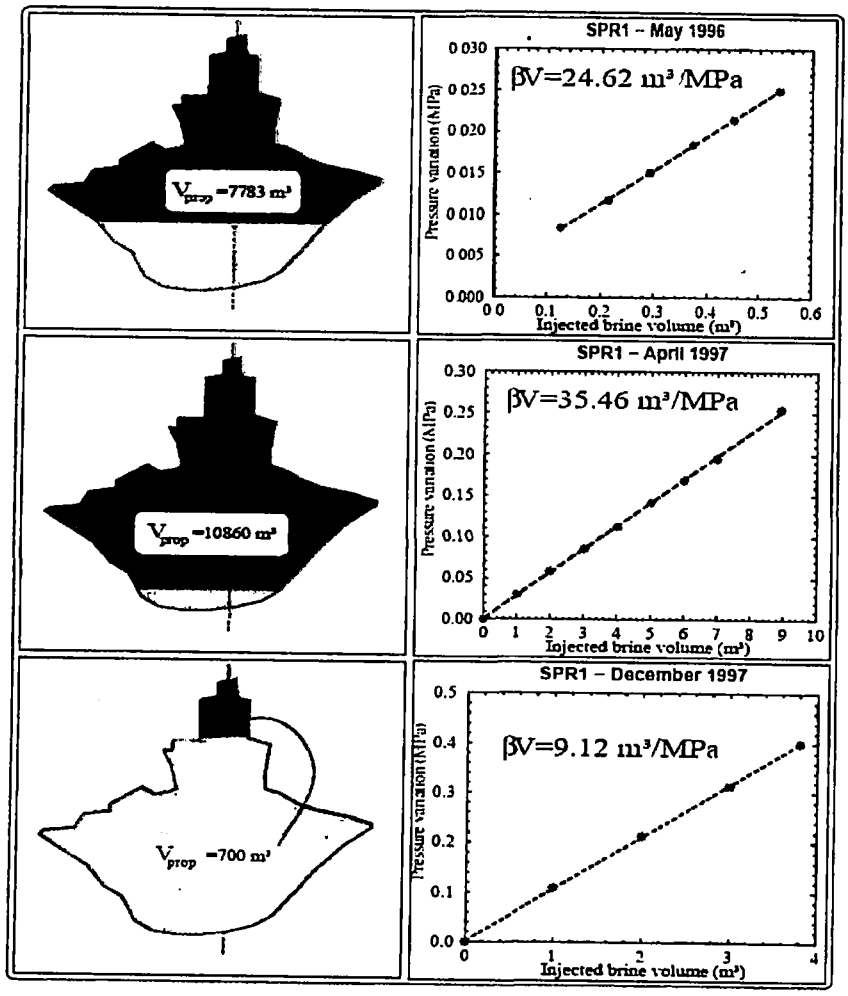

Figure 7. Three Cavern Compressibility Measurements for the Carresse SPR1 Cavern. (Propane is much more compressible than brine; cavern compressibility is greater when the stored propane volume increases.)

Example 2 — If a gas pocket is trapped in a cavern, the compressibility factor drastically increases, even if the gas pocket volume is small. The SPR3 cavern of the Total E&P France

Carresse site has the casing shoe depth 692 meters below ground level and the cavern bottom depth of 711 meters. A sonar survey performed a few months before the test in 1995 confirmed that this cavern exhibits a nonconvex shape (Figure 8). According to the latest sonar survey, the cavern volume was $V \approx 4{,}600$ m^3. The compressibility factor observed during the test was $\beta V \approx 11 \cdot 10^{-4}$/MPa, which is abnormally high for a brine-filled cavern. (The pressure resolution was 0.0005 MPa (0.07 psi). This greater-than-expected compressibility factor can be explained by the presence of gas trapped under the bell-shaped parts of the cavern. These pockets clearly are visible on the left and top of the cavern, as shown on Figure 8. The gas pressure at cavern depth is P_g = 8.3 MPa, which means that its isothermal compressibility factor is β_g^{isoth} = 0.12/MPa. The possible volume of the gas pocket can be back-calculated as being approximately 25 m^3, or about 0.5 percent of the cavern volume. However, the Carresse salt formation contains a relatively high amount of insolubles, and the actual brine volume might be larger– up to about 10,000 m^3 rather than the 4,600 m^3 estimated from the sonar survey, making the estimated gas pocket even smaller.

RSI-1476-05-012

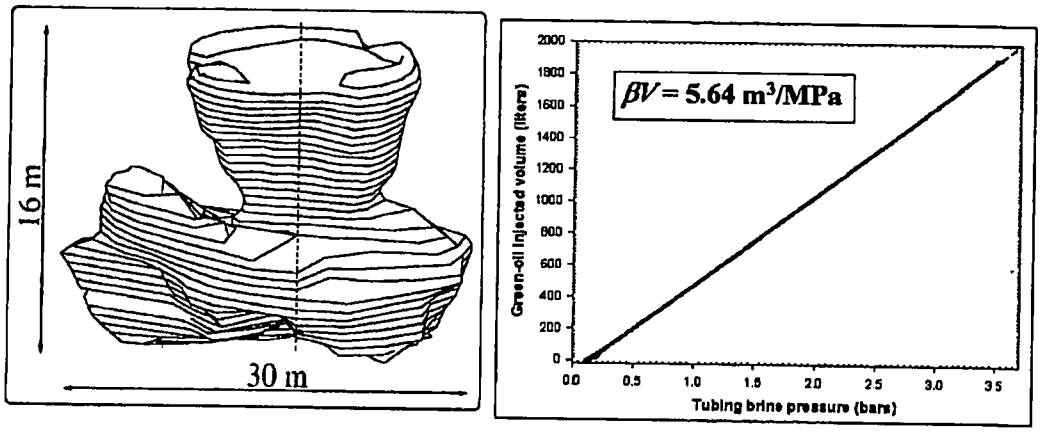

Figure 8. A Compressibility Test on the Carresse SPR3 Cavern.

Example 3 — In an NIT, nitrogen is injected in the annular space. When the casing shoe is 1,000 m deep and the tubing cross-sectional unit volume is 30 liters/m, the annular space volume is 30 m^3. When the nitrogen/brine interface is located, say, 10 m below the casing shoe, in the cavern neck whose cross-sectional area is 1 m^2, the nitrogen volume is V_g^o = 40 m^3. Gas pressure may be 20 MPa, its isothermal compressibility is $\beta_g = 1/P_g$ = 0.05 /MPa, and $\beta_g V_g^o$ = 2 m^3/MPa. In a large cavern, say $V >$ 100,000 m^3, $\beta V >$ 40 m^3/MPa, the gas pocket is "stiff" when compared to the brine-filled cavern: phenomena such as brine thermal expansion, which are influential during an LLI, result in a relatively small brine/nitrogen interface rise.

5.2.3 Phenomena Influencing the Measurement of Cavern Compressibility

5.2.3.1 Column Weight Changes

When brine is injected (or withdrawn) into (or from) the central tube, the cavern wellhead pressure, as measured in the annular space (P_{ann}^{wh}), can be compared to the central tube wellhead pressure (P_{tub}^{wh}). The pressure change, δP_{ann}^{wh}, in the annular space during a brine injection (or withdrawal) test is very close to the pressure change, δP_I, in the cavern, because the composition, temperature, and concentration of the fluid column in the annular space do not change during the test; only a very small difference because of brine compressibility can be observed. The same can not be said of the brine column (wellhead pressure) in the tube space (Figure 9). In many cases, the injected brine is not fully saturated (because, for example, it is stored in a brine pond and can be diluted by rain water), resulting in significant variations in the brine column weight.

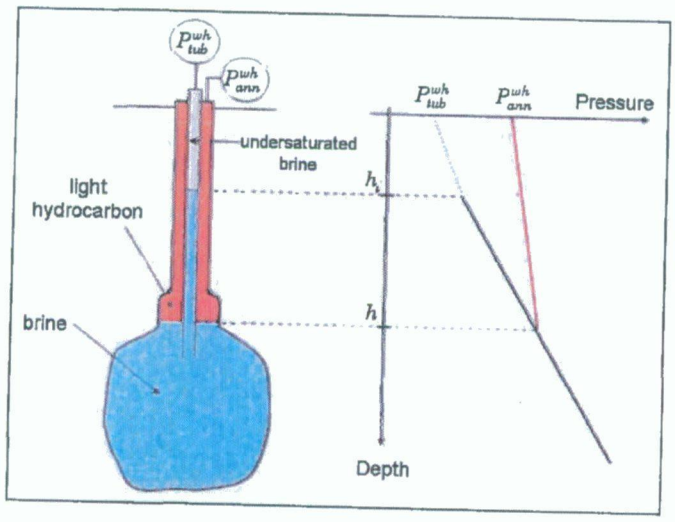

Figure 9. Injection of Nonsaturated Brine in the Central Tube.

For example, assume the density of the injected brine is slightly smaller than the density of saturated brine (temperature effects will be discussed later); for instance, $\rho_b = 1{,}180$ kg/m^3 instead of $\rho_b^{sat} = 1{,}200$ kg/m^3, which results in a ($\delta\rho_b = -20$ kg/m^3)-difference in densities. This means that when a volume of brine equal to v_{inj} is injected at the top of the central tube, the injected brine/saturated-brine interface is lowered by $h_1 = v_{inj}/S_t$, where S_t is the cross-sectional area of the central tubing (Figure 9). The cavern pressure and annular space pressure are changed by

$$\delta P_{ann}^{wh} = \delta P_I = \frac{v_{inj}}{\beta V} = \frac{S_t h_1}{\beta V} \qquad (20)$$

However, the tube pressure changes by

$$\delta P_{tub}^{wh} = \delta P_l - \delta\rho_b g h_l \tag{21}$$

because of the change in the brine column weight. (The tube column now contains some unsaturated brine.) In other words, provided that the injected brine volume, v_{inj}, is smaller than the tube volume, we get a relative error, e, when measuring the central tubing pressure:

$$e = \frac{\delta P_{ann}^{wh} - \delta P_{tub}^{wh}}{\delta P_{ann}^{wh}} = \frac{\beta V \cdot \delta\rho_b \cdot g}{S_t} \tag{22}$$

Reasonable values are $g = 10$ m/s², and $S_t = 2 \cdot 10^{-2}$ m², so for a standard brine-filled cavern, $\beta = 4 \cdot 10^{-10}$/Pa; then, e, the relative error made by measuring the central tube brine pressure instead of the annular brine pressure is a function of cavern volume (V) and brine undersaturation ($\delta\rho_b$):

$$e = 2.10^{-7} \cdot V \text{ (in m}^3\text{)} \; \delta\rho_b \text{ (in kg/m}^3\text{)} \tag{23}$$

from:

$$e = \frac{\left(4 \cdot 10^{-10}\right) \; V \; \delta\rho_b \; 10}{2 \cdot 10^{-2}} = 2 \cdot 10^{-7} \; V \delta\rho_b \tag{24}$$

where V (m³) is the cavern volume and $\delta\rho_b$ (kg/m³) is the difference between saturated brine density and actual brine density. For example, if $V = 10{,}000$ m³ and $\delta\rho_b = 10$ kg/m³, then $e = 0.02$ (2 percent).

Large underestimates of cavern compressibility can also be made by measuring the pressure change on the wrong tube (Figure 10). Such error can be avoided by either (a) measuring the wellhead pressure changes in the annular space, which experiences no change in brine composition, or (b) pressurizing the cavern and performing a test by withdrawing (instead of injecting) brine. (Note, however, that, in this case, transient creep effects may be activated.)

A similar effect can be obtained when a volume $v_{inj} = S_t h_l$ with $h_l < h_{tub}$, where h_{tub} is the central tubing length, is injected or withdrawn so rapidly that thermal equilibrium with the rock mass is not reached during the test. For instance, if brine is withdrawn, the average tubing temperature will increase by $\delta\theta_{av} = h_l\left(1 - h_l/2h_{tub}\right)G^{th}$, where G^{th} is the average geothermal gradient ($G^{th} = 0.03$°C/m is typical, but smaller values are expected in salt formations), resulting in a density change $\delta\rho_b = -\alpha_b \rho_b \delta\theta_{av}$, where the thermal expansion coefficient of brine is $\alpha_b = 4.4 \cdot 10^{-4}$/°C. For $h_l = 500$ meters and $h_{tub} = 1{,}000$ meters, $\delta\rho_b = -6$ kg/m³, leading to large overestimates–at least in large caverns. Further discussions of this effect can be found in Chapter 6.0.

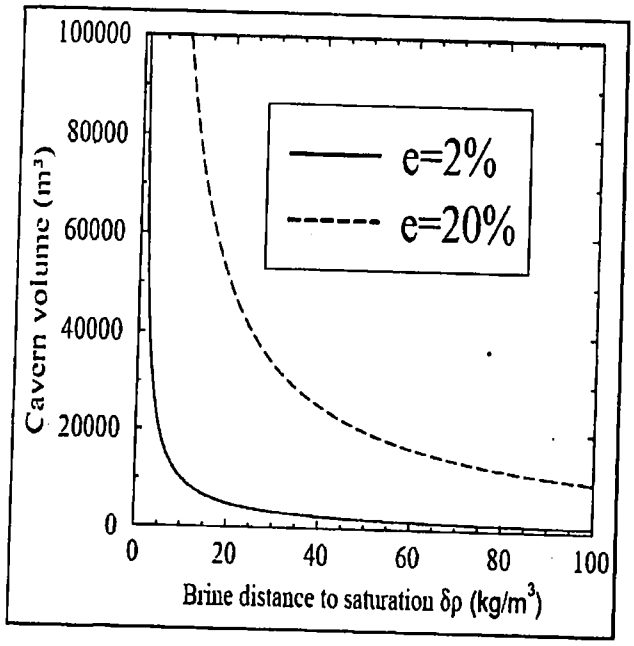

Figure 10. Iso-Underestimates of Cavern Compressibility βV When Injecting Under-saturated Brine.

5.2.3.2 Transient Creep and Additional Dissolution

These two phenomena may affect compressibility measurement when the injection is slow. An MIT brine injection for pressure build-up is relatively fast, and the effects of these two phenomena are effective *after* the brine injection; i.e., during the leak test. These effects are discussed in Chapters 8.0 and 9.0. Compressibility measured during a slow injection (when compared to a rapid injection) is smaller by 4 percent when additional dissolution is taken into account, and still smaller when transient creep is also taken into account.

5.2.3.3 Bedded Salt Formation

Bedded salt formations contain a fair amount of insolubles. When salt is washed out, insolubles fall to the cavern bottom; the insolubles bulking factor is of the order of 1.5, and brine is trapped in the sedimented insolubles. The as-measured cavern compressibility (from pressure build-up) in most cases is greater than the cavern compressibility inferred from the apparent cavern volume measured by sonar survey.

6.0 THERMAL EFFECTS

In this chapter, we discuss several mechanisms contributing to the apparent leak "measured" in an MIT. Two of these effects (well temperature, Section 6.1, and adiabatic pressure build-up, Section 6.4) are triggered by the test and two (wellhead temperature, Section 6.2, and brine warming, Section 6.3) occur before the test. Another phenomena, earth tides and atmospheric pressure variations, although they are not thermal effects, are included in Section 6.5 because their similarity to the effects from brine or rock temperature.

6.1 WELL TEMPERATURE

The well diameter is relatively small (a few decimeters), so thermal equilibrium between the rock mass and the well fluid is reached must faster than it is in the cavern itself. (The characteristic time, which is inversely proportional to the square of the characteristic dimension; i.e., cavern radius or well radius, is much shorter in a well than it is in a cavern.) Diamond [1989] suggests that: "...48 hours is adequate to achieve temperature equilibrium".

However, if the well was active just before the test (for example, if large amounts of fluids were circulated in the well for a period lasting several weeks or months before the test), the rock temperature in the vicinity of the well can be significantly different from the natural geothermal temperature. When the well is kept idle, the natural geothermal temperature will be restored in the well, but this is a long process (as long as the circulating period or even longer). Note that the two phenomena (cooling the rock while cold water circulates in the well compared to the warming of the rock and the well liquid while the well sits idle) are not perfectly symmetrical. When cold water circulates in the well, the boundary condition at the well wall is a fixed-temperature condition; when liquid keeps idle, the boundary condition stipulates that the heat flux through the well wall causes the liquid temperature to increase. The former process is slightly slower than the latter. The consequences of well liquid warming are twofold:

1. The volume of the well liquid increases but the effect of this volume increase is minute because the well volume is very much smaller than the cavern volume.

2. The density of the well liquid decreases, leading to a change in the difference between the wellhead pressure and the cavern pressure (see Section 5.2.3.1). This difference is $P_{tub}^{wh} - P_l = \rho_b g h_{tub}$ = 12 MPa when the central tubing length is h_{tub} = 1,000 meters. When the tubing liquid (brine, for instance) temperature increases by $\delta\dot{\theta}_{av}$ = 1°C/day, the brine density decreases by $\delta\dot{\rho}_b = \alpha_b \rho_b \delta\dot{\theta}_{av} = -4.4 \cdot 10^{-4} \times 1{,}200 \times 1 = -0.53$ kg/m^3/day, and the pressure difference decreases by $\delta\dot{\rho}_b g h_{tub} = -5.3$ kPa/day (–0.8 psi/day). Furthermore, when the well has been kept idle for a couple of weeks before the test, the daily

temperature increase in the well is likely to be slower than 1°C per day, and this effect can be neglected.

6.2 WELLHEAD TEMPERATURE CHANGES

6.2.1 Temperature Change

Ground level temperatures experience daily fluctuations. Depending on the season and the geographical location of the storage site, the amplitude of these daily fluctuations may be 10°C to 30°C, usually with the lowest temperature at night and the highest temperature in the afternoon. The wellhead and the fluids in the wellhead are cooled or warmed accordingly. The "temperature wave" propagates downward into the well but the penetration depth is shallow.

École Polytechnique and Brouard Consulting performed a test in the well of the SPR3 cavern, a brine-filled cavern operated by Total E&P France in southwestern France. Temperature gauges were set at eight depths in the brine-filled central string (see Table 1). The annular space was filled with brine. Figure 11 shows the SPR3 wellhead and the location of the θ_8 gauge, which is also the reference location for depth. Figure 12 displays the temperature variation as measured by the eight temperature gauges over a 4-day period.

Table 1. Depths of Temperature Gauges in the SPR3 Well.

Gauge	1	2	3	4	5	6	7	8
Depth (m)	−10	−5.75	−1.5	−1	−0.6	−0.25	−0.125	0

The following conclusions were drawn about the measured temperatures:

1. Only small temperature changes are experienced at depths of 10 meters and 5.75 meters (θ_1 and θ_2, respectively). Temperature changes at 1.5 meters (θ_3) are about one-third of those observed at the "surface" gauge location (θ_8).
2. A time lag, increasing with depth, is observed. The existence of such a time lag is consistent with what is known from the propagation in the ground of a periodic "temperature wave." When the ground level temperature is a harmonic function, $\theta_{gr} = \theta^{o}_{gr} \cdot \cos(\omega t)$, the temperature at a depth "z" is

$$\theta(z,t) = \theta^{o}_{gr} \cdot \exp\left(-z\sqrt{\frac{\omega}{2k^{th}_{gr}}}\right) \cdot \cos\left(\omega t - z\sqrt{\frac{\omega}{2k^{th}_{gr}}}\right) \qquad (25)$$

where k^{th}_{gr} is the ground thermal diffusivity (typically 1 to $1.5 \cdot 10^{-6}$ m²/s). Both the attenuation and the time lag increase with depth. Equation (25) is for homogeneous soil; however, the situation is somewhat more complex in the case of a fluid-filled vertical

RSI-1476-05-015

Figure 11. SPR3 Wellhead.

RSI-1476-05-016

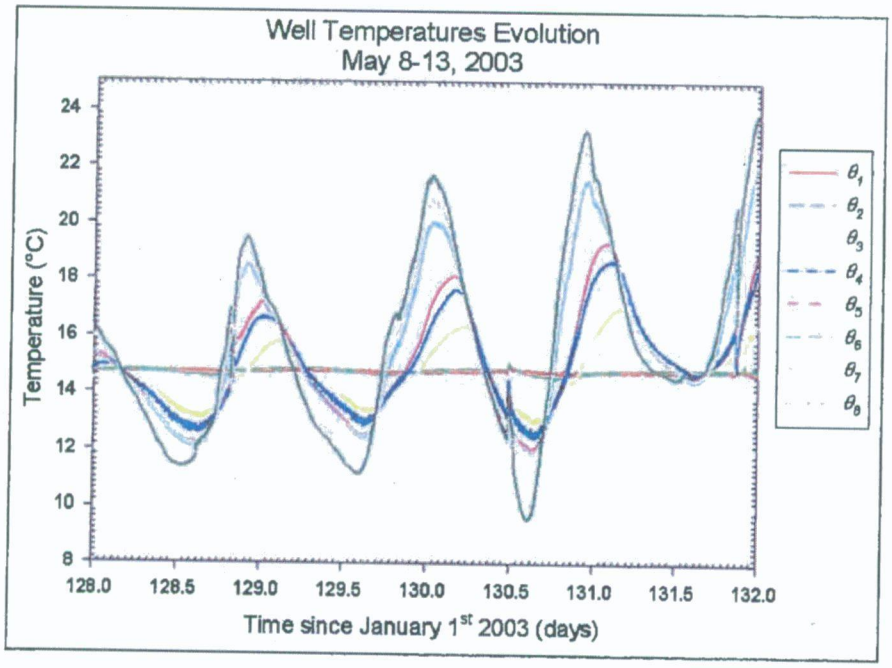

Figure 12. Temperature Measurements in the SPR3 Wellhead.

steel tube, but the equation gives a first approximation. A time lag is often observed between ground temperature variations and pressure variations. In fact, such factors as Christmas tree geometry, string diameter, and fluid heat capacity are influential. Heat is transferred in the vertical and radial directions through radiation, conduction, and convection. In some cases, a secondary time lag exists between temperature variations in the annular space and in the central tubing, resulting in differential variations of the pressures. A complete picture is beyond the scope of this effort. Examples of pressure fluctuations correlated to ground temperature variations can be found, for example, in Thiel [1993], Thiel and Russel [2004] and Brouard et al. [2004].

3. The effect of wellhead cooling at depth is smaller than the effect of wellhead warming. This fact is consistent with observations made at other sites and can be explained by natural heat convection in the well. When cooled, brine in the upper part of the well is denser than the deeper brine; therefore, warmer (and lighter) brine flows upward to replace the cooler brine, which flows downward, enhancing the effect of wellhead cooling. Conversely, such a density-driven convective flow cannot occur when the wellhead is warmed.

4. When integrated with respect to depth, the overall temperature change can be written as

$$h_{av}\delta\theta_{av} = \int_0^{\infty} \delta\theta(z)\,dz \approx 10 \text{ m°C (in the case of the SPR3 cavern).} \qquad (26)$$

In other words, the effect of brine warming, which is not homogeneous through the well depth in reality, is equivalent to a homogeneous warming by $\delta\theta_{av}$ = 10°C of a h_{av} = 1-meter-high brine column. The effects of brine warming are proportional to $h_{av}\delta\theta_{av}$, as will be shown below.

5. The above-mentioned figure ($h_{av}\delta\theta_{av}$ = 10 m°C) is typical of a brine-filled well. It is suspected that the effects of ground temperature might be more significant when, instead of brine, the well is filled with LPG or a light hydrocarbon, whose heat capacity is much smaller than that of brine, allowing faster and greater temperature change.

6.2.2 Effects of Temperature Change

6.2.2.1 Liquid-Filled Well

The effect of temperature change is twofold (see Section 5.3.2.1): liquid volume change and liquid density change.

- Let S_l be the volume of the well per unit length (e.g., liters/meter). The liquid volume increase will be $\delta v = \alpha S_l h_{av}\theta_{av}$, where α is the liquid (brine, for example) thermal-expansion coefficient. When S_l is 20 liters/meter, $h_{av}\delta\theta_{av}$ = 10 m°C, the volume change is

$$\delta v = 4.4 \cdot 10^{-4}/°C \times 20 \text{ l/m} \times 10 \text{ m°C} = 0.1 \text{ liters} \qquad (27)$$

- The brine density change lightens the liquid column, resulting in a wellhead pressure change by $\delta P^{wh} = \alpha_b \rho_b g h_{av} \delta\theta_{av}$, or

$$\delta P^{wh} = 4.4 \cdot 10^{-4}/°C \times 1{,}200\ kg/m^3 \times 10\ m/s^2 \times 10\ m\ °C = 53\ Pa. \quad (28)$$

Both effects are negligible in the context of an MIT. However when LPG or liquid hydrocarbons are considered (instead of brine), these effects are larger and pressure fluctuations whose amplitude is several kPa (1 psi) can be observed. Moreover, a significant time lag often is observed between annular space and central tubing responses to an external temperature change (Figure 13).

RSI-1476-05-017

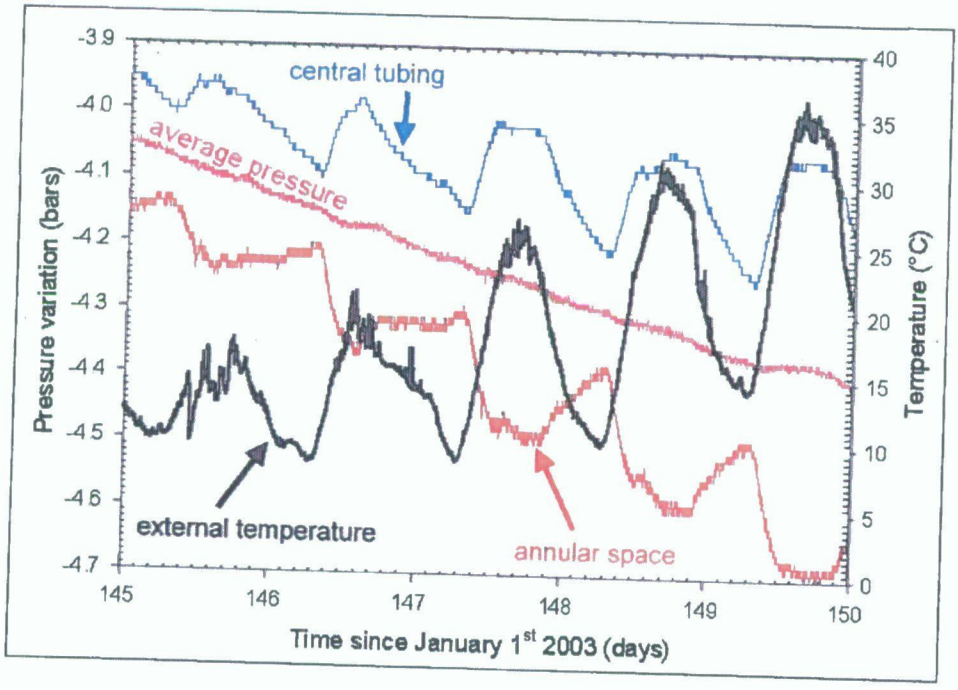

Figure 13. A Correlation Between External (i.e., Ground) Temperature and Oil-Filled Tubing Pressure Is Clearly Visible. An inverse correlation is observed when temperature and annular space pressure are concerned.

6.2.2.2 Gas-Filled Wellhead

The thermal expansion coefficient of a gas is much larger than the thermal expansion coefficient of a liquid, by at least a factor of 10. The exact temperature-pressure relation is difficult to calculate because gas may have a variable composition. A ±500-Pa pressure change can be expected, as shown in Figure 14, from Thiel [1993], which provides a good example of pressure fluctuations resulting from temperature fluctuations.

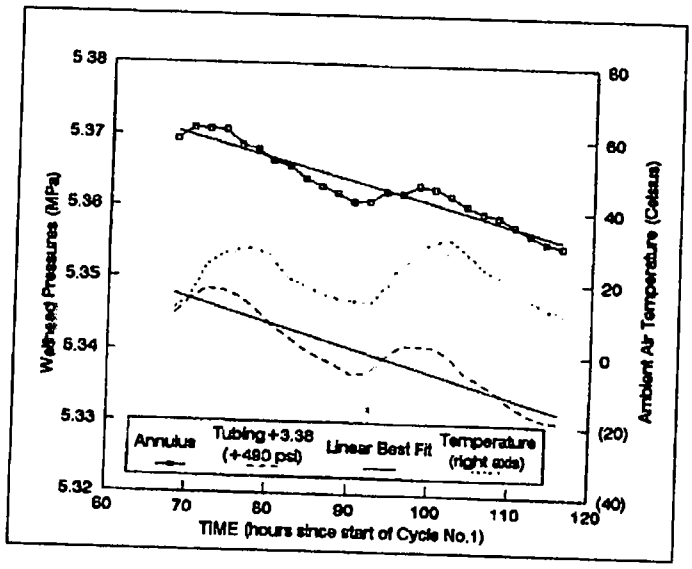

Figure 14. Measured Wellhead Pressure and Air Temperature Variations (After Thiel [1993]). In this example, the annulus is filled with nitrogen and the tubing is filled with brine. (Daily pressure variations clearly are correlated with temperature variations. Fluid-pressure decay rates are averaged on 48-hour-long intervals of time to smooth out diurnal temperature effects.)

6.2.2.3 Practical Conclusions

As stated by Thiel [1993, p.381]: "It is important to analyze 24-hour increments (i.e., the last 24 hours, 48 hours, 72 hours, etc.) to neutralize diurnal temperature effects." From Figure 14, it is obvious that the pressure decay rate would have been greater (and presumably less accurate) if only the last 15 h had been analyzed.

6.3 BRINE WARMING

In this section, the effect of brine thermal expansion is discussed, a phenomenon that precedes the test. The origin of this phenomenon is discussed in Section 6.3.1, the equations governing temperature variation are presented in Sections 6.3.2 and 6.3.3, and a case history is discussed in Section 6.3.4. The consequences of thermal expansion for pressure changes in an MIT are presented in Sections 6.3.5 to 6.3.9.

6.3.1 Initial Temperature Difference

The natural temperature of rock increases with depth. A typical value of the geothermal gradient in most rock formations is G^{th} = 3°C/100 meters; however, the geothermal gradient in salt is about half this value, because the thermal conductivity of salt (K^{th}_{salt} = 6 W/m-°C) is

larger than the average thermal conductivity of most rocks ($K_{gr}^{th} \approx 3$ W/m-°C) and the product of G^{th} and K^{th} at a given site does not depend upon depth.

A typical temperature profile is given in Figure 15. The cavern had been kept idle for 15 years. At a depth of $H = 1{,}000$ meters, a typical rock mass temperature is $\theta_R^{\sim} = 45$°C. The temperature depth profile shows a clear discontinuity at the salt/marls interface, at a depth of 700 meters, as explained above. A second discontinuity at shallow depth is related to low ground-surface temperature. The temperature log was performed in February 1996 when the ground temperature in central France was close to 0°C. Brine temperatures in the cavern are quite homogeneous (temperature gradient is 0.34°C/100 meters, or 0.18°F/100 feet) because of natural free convection. The brine is slightly warmer at the cavern bottom, its density is smaller, and the cavern is subject to a perennial convective flow. That is, an upward brine flow occurs close to the cavity wall, and a downward brine flow occurs in the vicinity of the cavern axis; the cavern brine is continuously stirred by natural convection.

RSI-1476-05-019

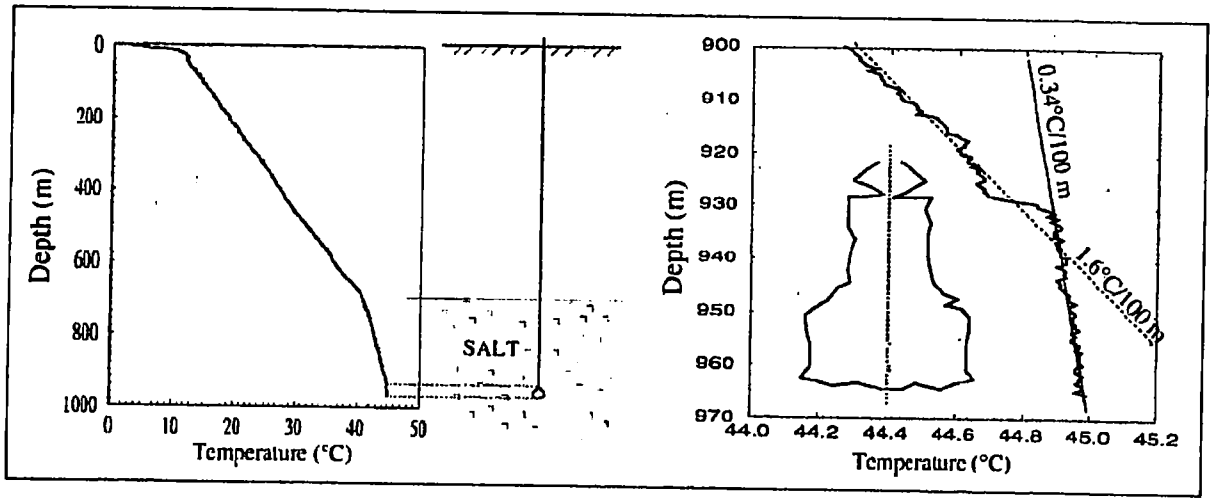

Figure 15. Geothermal Profile in the Gaz de France EZ53 Cavern and Well.

Caverns are leached using soft water pumped from a river, lake, or shallow aquifer. A typical leach water temperature might be 15°C; i.e., significantly colder than rock temperature at depth. The transit time of leach water in the cavern is a few days or weeks. When the injected water flow rate is 100 m^3/h, the transit time in a 10,000-m^3 cavern is 100 hours, or 4 days, and 40 days in a 100,000-m^3 cavern. This time is insufficient for brine to warm significantly, as will be shown later, when the characteristic time for brine warming is discussed.

In fact, the warming process during cavern leaching is complex. Salt solution mining is an endothermic reaction, and cold soft water circulating downward through the central string

exchanges heat with the warmer brine circulating upward through the annular space because the steel tubing separating the two flows is such a good heat conductor [Kunstman and Urbanczyk, 1995; Brouard et al., 1997].

As a whole, the temperature of the brine at the end of the leaching phase can be lower than the natural temperature of rock by several tens of degrees Celsius. The same can be said for an operating liquid storage cavern, when products frequently are injected in or withdrawn from the cavern. A substantial initial gap is present between the rock mass temperature, θ_R^{∞}, and the initial cavern brine temperature, $\theta_l(0)$. When the cavern remains idle, after leaching is completed or when no product movement takes place for a long period of time, the initial temperature gap, $\theta_R^{\infty} - \theta_l(0)$, slowly declines with time, and $\theta_l(t)$, the time-dependent cavern fluid temperature, slowly increases.

Note that in some cases (shallow cavern), the injected brine may be warmer than the rock mass at cavern depth. In such a case, the brine temperature slowly decreases in an idle cavern. Ignoring such a condition could mean that the apparent leak then overestimates the actual during an LLI test.

6.3.2 Temperature History

Temperature history, then, is governed by heat conduction through the rock mass and heat convection in the cavern: the time-dependent cavern-fluid temperature $\theta_l(t)$ is roughly homogeneous throughout the cavern, as the brine is continuously stirred by natural convection. However, the process is somewhat more complicated when the cavern is partially filled with hydrocarbons, as distinct convection cells develop separately in the hydrocarbon mass and in the brine mass, leading to distinctly different temperatures in the two liquids.

The following considers the case of a brine-filled cavern. The warming process is easy to compute; appropriate heat transfer equations can be written as follows:

$$\begin{cases} \dfrac{\partial \theta_R}{\partial t} = K_{salt}^{th} \cdot \Delta \theta_R \\ \iint_S K_{salt}^{th} \dfrac{\partial \theta_R}{\partial n} dS = \rho_{liq} C_{liq} V \dot{\theta}_l \text{ , } n \text{ is the outward normal} \\ \theta_R(\text{wall}, t) = \theta_l(t) \\ \theta_R(\text{rock mass}, 0) = \theta_R^{\infty} \end{cases} \tag{29}$$

The first equation holds in the rock mass: K_{salt}^{th} is the thermal conductivity of salt: $K_{salt}^{th} = k_{salt}^{th} \rho_{salt} C_{salt}$; $K_{salt}^{th} = 6$ W/m-°C ; $\rho_{salt} C_{salt} = 2 \cdot 10^6$ J/m^3-°C, leading to $k_{salt}^{th} = 3 \cdot 10^{-6}$ m^2/s $\approx$ 100 m^2/year; and Δ is the Laplacian operator. The second equation is the boundary equation at the cavern wall: heat flux crossing a cavern wall (the left-hand side of the second equation) warms up cavern brine with an average temperature of θ_l ($\rho_{liq} C_{liq}$ is the volumetric heat

capacity of the cavern liquid; when brine is considered, $\rho_b C_b = 1{,}200 \times 3{,}800 \approx 4.5 \cdot 10^6$ J/m^3–°C). The third equation stipulates that the rock temperature of the cavern wall is equal to the average brine temperature in the cavern, which is homogeneous. The last equation describes the initial temperature distribution in the rock formation. (At the end of the leaching process, for example, the rock temperature is close to the natural rock temperature. Indeed, while rock cooling is active during the leaching process, the rock that has been most significantly cooled is continually being removed by the leaching process and, as a whole, the temperature of the rock at a distance from the cavern wall has not been significantly modified.) The same cannot be said of a cavern that has experienced several fillings/withdrawals; in this case, determining the initial (beginning of test) rock temperature distribution is not an easy task.

6.3.3 Characteristic Time

It is convenient to rewrite the equation for liquid temperature in the cavern in a dimensionless form. If we set $t_c^{th} = R^2/\pi k_{salt}^{th} \approx V^{2/3}/8K_{salt}^{th}$, $\chi = \rho_{salt} C_{salt}/\rho_{liq} C_{liq}$

$$\theta_R^{\sim} - \theta_l(t) = \left[\theta_R^{\sim} - \theta_l(0)\right] \cdot \Omega\left(t/t_c^{th}, t_c^{th}/\chi\right) \tag{30}$$

In other words, the liquid warming process is governed by two characteristic times: t_c^{th} and t_c^{th}/χ. When the cavern is filled with liquid, no sharp contrast exists between $\rho_{salt} C_{salt}$ and $\rho_{liq} C_{liq}$, χ is not large (for example, when brine is considered, $\chi \approx 4/9$). Then, t_c^{th} and t_c^{th}/χ are of the same order of magnitude; when discussing warming rate, one can take t_c into account. (However, in a gas-filled cavern, $\rho_g C_g$ is much smaller than $\rho_{salt} C_{salt}$ and χ is very large, the second characteristic time, or t_c^{th}/χ, is much smaller than the first characteristic time, t_c^{th}, and the warming process is correspondingly much faster in a gas-filled cavern.)

The characteristic time is $t_c^{th} = V^{2/3}/8k_{salt}^{th}$, or t_c^{th} (year) = $V^{2/3}$ (m^3)/800, or t_c^{th} = 0.5 year when V = 8,000 m^3 and t_c^{th} = 8 years for V = 500,000 m^3; in a large cavern, thermal equilibrium is reached only after a long period of time.

For an idealized spherical cavern of radius R, a closed-form solution can be found:

$$\theta_R^{\sim} - \theta_l(t) = \left[\theta_R^{\sim} - \theta_l(0)\right] \cdot \varphi(\xi, \upsilon) \tag{31}$$

where:

$$\begin{cases} \varphi(\xi,\upsilon) = W(\xi,\upsilon) + W(-\xi,\upsilon) \\ W(\xi,\upsilon) = \dfrac{1+\xi}{2\zeta} e^{(1+\xi)^2\upsilon} \operatorname{erfc}\left[(1+\xi)\sqrt{\upsilon}\right] \\ \xi^2 = \dfrac{3\chi - 4}{3\chi} \\ \upsilon = \dfrac{9\chi^2 k_{salt}^{th} t}{4R^2} = \dfrac{9}{4\pi}\chi^2 \dfrac{t}{t_c^{th}} \end{cases} \tag{32}$$

and the characteristic time can be more precisely defined: $2\,t_c^{th}$ is the time after which approximately 75 percent of the initial temperature difference has been removed.

6.3.4 A Case History

The EZ53 cavern was leached out during the spring of 1982 and is small (about 8,000 m^3, see Figure 15). The initial temperature difference was $\theta_R^{\infty} - \theta_1(0) = 45 - 26.5 = 18.5°C$. Figure 16 displays the measured evolution of cavern brine temperature, and Figure 17 displays the amount of brine expelled at the cavern well during two periods of time when the well was opened at ground level. The continuous line in Figure 16 is the computed thermal history of cavern brine temperature when the cavern is assumed to be approximately spherical with a characteristic time t_c^{th} = 0.5 year. An excellent comparison is observed. (Such a good comparison is no surprise; in most cases, temperature histories can be predicted correctly provided that the initial thermal conditions are well known.) The amount of brine expelled at ground level is strongly correlated to temperature history, as will be proven later.

RSI-1476-05-020

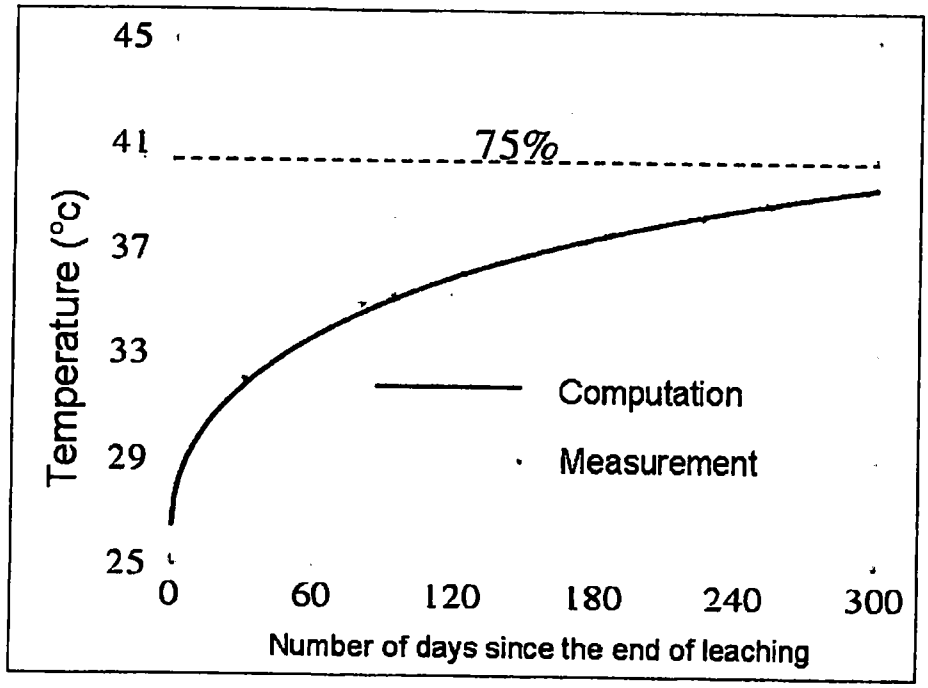

Figure 16. Temperature Evolution in the EZ53 Cavern.

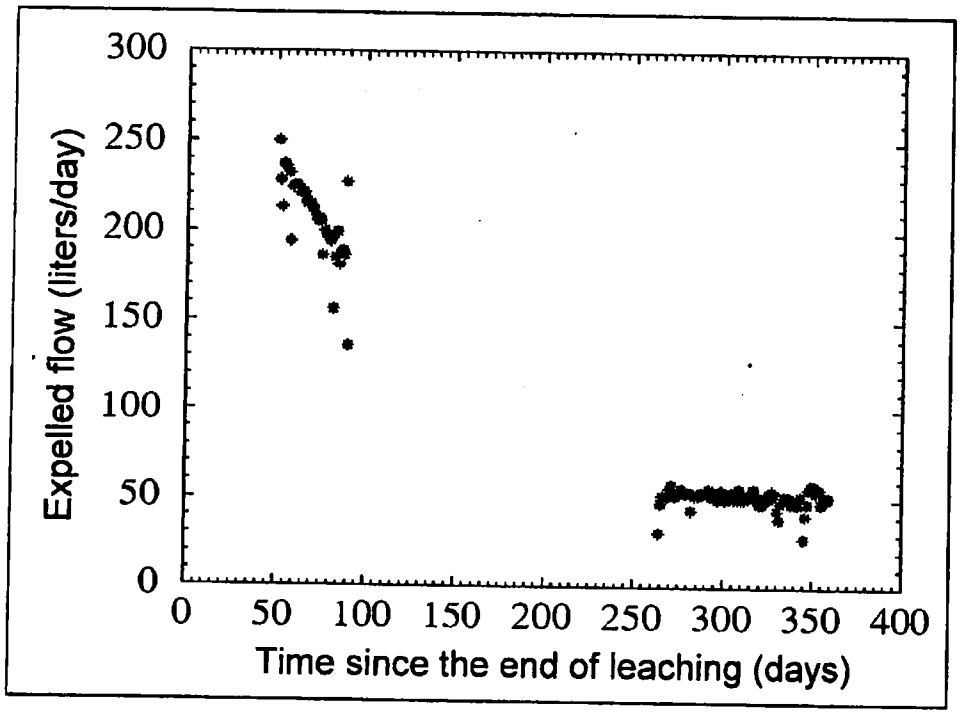

Figure 17. Measurement of Brine Flow Expelled From the EZ53 Cavern.

6.3.5 Temperature Increase Rate

The cavern temperature increase rate is

$$d\theta_l/dt = -\left[\theta_R^{\infty} - \theta_l(0)\right] \cdot \Omega_\tau'\left(\tau = t/t_c^{th}, t_c^{th}/\chi\right)/t_c^{th} \tag{33}$$

The rate of temperature increase is lower in a larger cavern, when t_c^{th} is larger.

6.3.6 Brine Thermal Expansion

Brine warming leads to brine thermal expansion. When the cavern is opened, the brine outflow rate because of brine thermal expansion is

$$Q_{th} = \alpha_b \cdot V \cdot \dot{\theta}_l = -\alpha_b \cdot V \cdot \left[\theta_R^{\infty} - \theta_l(0)\right] \cdot \Omega_\tau'\left(\tau = t/t_c^{th}, t_c^{th}/\chi\right)/t_c^{th} \tag{34}$$

where α_b is the brine thermal expansion coefficient, or $\alpha_b = 4.4 \cdot 10^{-4}$/°C. (Slightly larger values of α_b can be observed in a deep cavern, when temperature and pressure are high.)

For the EZ53 cavern, the measured brine outflow rates (Figure 17) are slightly larger (by a few percent) than the rates predicted by the above formula. This small difference between

observed and computed values is probably accounted for by the effect of cavern shrinkage caused by salt-mass creep.

When the cavern is shut in, brine warming leads to pressure increases or:

$$\dot{P}_I = \frac{\alpha_b}{\beta}\dot{\theta}_I \tag{35}$$

as β = 4 to $5 \cdot 10^{-4}$/MPa, because $\alpha_b/\beta \approx 1$ MPa/°C. For example, the average temperature increase rate, 0.057°C/day, observed during Days 31–81 in the EZ53 cavern, should have led to a pressure increase rate of 0.057 MPa/day (8 psi/day) had the cavern been shut-in during this period.[3]

In other words, in a small cavern, when an LLI is performed a few weeks after leaching is completed, brine thermal expansion (a phenomenon that precedes the test) can lead to a significant cavern pressure increase rate, $\dot{P}_I$, and the apparent leak underestimates the actual leak.

In a large cavern, the pressure increase rate is slower (as it is proportional to the inverse of the square of the characteristic length). However, in the case of an NIT, the picture changes, because gas compressibility must be taken into account. The most important factor, in this case, is the brine thermal expansion rate, or $Q_{th} = \alpha_b V \dot{\theta}_I$, and the apparent leak (Q_{app}) is linked to both Q_{th} and the actual leak (Q_{act}), see Chapter 13.0, Equation (155).

By way of comparison, in the 8,000-m^3 EZ53 cavern, the temperature increase rate for the period of 1 to 3 months after leaching was 0.057°C/day. The pressure increase rate should be 0.057 MPa/day if the cavern were closed, and the brine thermal expansion rate would be Q_{th} = 0.2 m^3/day. In a 500,000-m^3 cavern (3.1 MMbbls), the corresponding period is 16–48 months after leaching is completed (t_c^{th} is 16 times greater); at which time, the temperature increase rate should be 0.0035°C/day, and the pressure build-up rate should be $\dot{P}_I$ = 0.0035 MPa/day in a closed cavern. Therefore, brine thermal expansion is Q_{th} = 0.8 m^3/day, or Q_{th} = 290 m^3/year, a significant figure in the context of an MIT.

6.3.7 Brine Thermal Expansion During an MIT

As discussed earlier, brine warming is an important influence in MITs. A good example of its importance is provided in Figure 18. The three caverns (A, B, and C) were leached out at the same time in the same salt formation and are at comparable depths. For technical reasons, leaching was stopped for a couple of weeks. During the stoppage in cavern leaching, shut-in

[3] Coincidentally, because $\alpha_b/\beta = 1$ MPa/°C, the temperature increase rate (0.057°C/day) is numerically the same as the pressure increase rate (0.057 MPa/day).

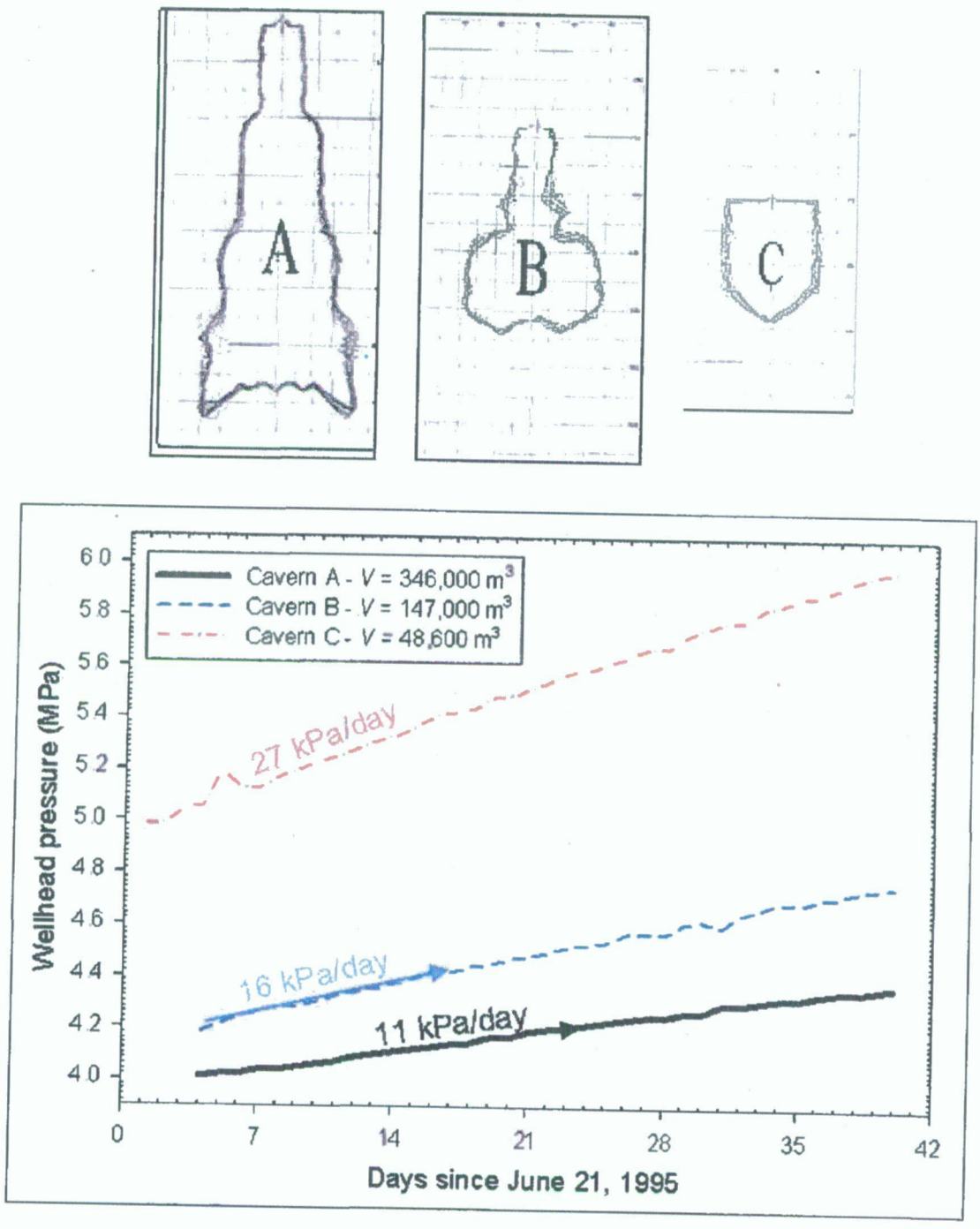

Figure 18. Pressure Build-Up Due to Brine Thermal Expansion in a Small, Big, and Medium Size Cavern. These caverns were being actively leached just prior to shut in for these tests. Thus the temperature gradient between the salt mass and the cavern brine was likely much greater than would be the case in a mature cavern that had not been recently leached.

pressure tests were performed. As observed, pressure increase rates were 4 MPa/year (11 kPa/day), 5.9 MPa/year (16 kPa/day), and 10 MPa/year (27 kPa/day) on the 346,000-m^3, 147,000-m^3, and 48,600-m^3 caverns, respectively. These differences in the rates of pressure increase are consistent with what is known from the laws of thermal conduction in a rock mass; viz, when the cavern is larger, the pressure increase rate is slower (see Section 6.3.6).

The cavern compressibility factor at this site is of the order of $\beta = 4 \cdot 10^{-4}$/MPa. (Cavern compressibility, or βV, is obtained by multiplying the compressibility factor, β, by the cavern volume, V; see Chapter 5.0). The pressure increases shown in Figure 18 would still be active during an LLI because the thermal expansion would not be modified by the test. Such pressure increases could partially mask the actual leak. If $P_2 - P_1$ is the pressure change because of thermal expansion during a given time interval, $t_2 - t_1$, the leak rate, which will be hidden by thermal expansion, is $\beta V(P_2 - P_1)/(t_2 - t_1)$ or, in the above-mentioned examples, 560 m^3/year (3,360 bbls/year), 360 m^3/year, and 300 m^3/year, respectively. When interpreting an LLI test, this "negative" leak should be added to the apparent leak to provide a corrected leak; in this case, the corrected leak is larger than the apparent leak.

6.3.8 What Can Be Done During an LLI

The effect of thermal expansion can be computed, provided that the cavern thermal history (volume and temperature of the fluids injected in or withdrawn from the cavern since leaching was completed) is known. However, it is more convenient to assess these effects before the test itself. This can be accomplished accurately and simply by performing a "shut-in pressure test" a few days before performing the MIT. After drawing down the products, the cavern is closed; no fluid injection is performed before the shut-in pressure test begins and the pressure-versus-time curve is recorded for 2 or 3 days. The pressure increase rate observed during the shut-in pressure test is added to the pressure drop rate observed during an LLI test. However, Thiel [personal communication] points out that a shut-in pressure in some cases may be difficult to interpret, for instance in the case of a LPG storage in a shallow cavern when the cavern was completely emptied of product before the shut-in test: "...in bedded salt (in mature caverns), it is common to have a washout above the bottom of the casing with trapped hydrocarbon. Thus, you may not be able to totally empty the cavern. It is also quite common in bedded salt to have minor "burping" of product from the cavern into the brine full annulus after "emptying." Thus shut-in data will commonly be impacted by the buildup of LPG (in a vapor state) in the annulus...".

A simpler, less time-consuming, and probably more accurate method can also be used that allows the thermal expansion effects during an LLI test to be eliminated. This method, the Pressure Difference Observation (PDO) is explained later in Chapter 10.0.

6.3.9 Simplified Equations for Pressure Change From Brine Temperature Change

The following approximation is valid when $t \ll t_c^{th}$, which can be helpful when an MIT is performed a few weeks or months after the cavern has been washed out and/or when the cavern is large:

$$\theta_l(t) - \theta_l(0) = \left[\theta_R^{-} - \theta_l(0)\right] \cdot \frac{3\chi}{\pi} \cdot \left(\frac{t}{t_c^{th}} + 2\sqrt{\frac{t}{t_c^{th}}} \right) \tag{36}$$

$$\dot{\theta}_l(t) = \left[\theta_R^{-} - \theta_l(0)\right] \cdot \frac{3\chi}{\pi} \cdot \left(\frac{1}{t_c^{th}} + \frac{1}{\sqrt{t \cdot t_c^{th}}} \right) \tag{37}$$

When $t \ll t_c^{th} = R^2/\pi k_{salt}^{th}$, $1/t_c^{th}$ is small when compared to $1/\sqrt{t \cdot t_c^{th}}$. Taking $\chi = 4/9$, $k_{salt}^{th} = 3 \cdot 10^{-6}$ m^2/s, $t_c^{th}(\text{days}) = 1.23\, R^2(\text{m}^2)$ and:

$$\theta_l(t) - \theta_l(0) = \frac{0.784}{R\,(\text{m})}\left[\theta_R^{-} - \theta_l(0)\right] \cdot \sqrt{t\,(\text{days})} \tag{38}$$

$$\dot{\theta}_l(t) = \frac{0.392}{R\,(\text{m})}\left[\theta_R^{-} - \theta_l(0)\right] \Big/ \sqrt{t\,(\text{days})} \tag{39}$$

After 16 days, in an R = 12.5-m spherical cavern (V = 8,000 m^3, t_c^{th} = 190 days) when the initial temperature gap is 25°C, the temperature increase rate is approximately 0.13°C/day.

Brine volumetric expansion (when $\alpha_b = 4.4 \cdot 10^{-4}$/°C) is

$$\frac{Q_{th}}{V} = \alpha \cdot \dot{\theta}_l(t) = \frac{1.72 \cdot 10^{-4}}{R\,(\text{m})}\left[\theta_R^{-} - \theta_l(0)\right] \Big/ \sqrt{t\,(\text{days})} \tag{40}$$

and pressure increase in a closed cavern (when $\alpha_b/\beta \approx 1$ MPa/°C) is

$$p_l - p_l^{i} = \frac{\alpha_b}{\beta}\left[\theta_l(t) - \theta_l(0)\right] = \frac{0.784}{R\,(\text{m})}\sqrt{t\,(\text{days})} \tag{41}$$

Keep in mind that this relation holds for a freshly washed out spherical cavern. For an idealized slender cylindrical cavern, a similar solution can be found:

$$\dot{\theta}_l(t) = \frac{2\chi}{\pi}\left[\theta_R^{-} - \theta_l(0)\right]\left(\frac{1}{2t_c^{th}} + \sqrt{\frac{t_c^{th}}{t}} \right) \approx \frac{0.26\left[\theta_R^{-} - \theta_l(0)\right]}{R\,(\text{m})} \Big/ \sqrt{t\,(\text{days})} \tag{42}$$

6.3.10 Brine Thermal Expansion Effects During an NIT

Brine thermal expansion leads to a brine volume increase and the nitrogen interface rises during an NIT. This effect must be subtracted from the apparent leak (during an NIT, the actual leak is overestimated). However this effect is small when the cavern is large, as the nitrogen pocket is "stiff" when compared to the large brine volume and hampers brine expansion particularly in a small cavern (see Chapter 13.0.)

Consider again the A, B, and C caverns shown in Figure 18. Assume that an NIT is performed in each of these three caverns. Nitrogen is injected in the cavern, its volume is $V_g^o = 40$ m^3, its compressibility factor at interface depth is $\beta_g = 1/P_g$ = 0.05/MPa, and nitrogen-column compressibility then is $\beta_g V_g^o = 2$ m^3/MPa.

$$Q_{leak}^{corr} = \left(1 + \frac{\beta_g V_g^o}{\beta V}\right) \cdot Q_{app} - \left(\frac{\beta_g V_g^o}{\beta V}\right) \cdot Q_{th} \qquad (43)$$

or:

$$Q_{leak}^{corr}\ (\text{m}^3/\text{year}) = 1.0015 \cdot Q_{app} - 8 \qquad \text{(Cavern A, } V = 346{,}000 \text{ m}^3\text{)}$$

$$Q_{leak}^{corr}\ (\text{m}^3/\text{year}) = 1.034 \cdot Q_{app} - 12 \qquad \text{(Cavern B, } V = 147{,}000 \text{ m}^3\text{)}$$

$$Q_{leak}^{corr}\ (\text{m}^3/\text{year}) = 1.10 \cdot Q_{app} - 30 \qquad \text{(Cavern C, } V = 48{,}600 \text{ m}^3\text{)}$$

For a large cavern, the apparent leak as measured in an NIT is close to the actual leak, but the difference becomes more significant for smaller caverns.

6.4 ADIABATIC PRESSURE INCREASE IN A CAVERN

6.4.1 Temperature Increase

When pressure is rapidly increased in a fluid-filled cavern ("adiabatic compression"), the cavern experiences an instantaneous temperature increase, which must be assessed because this temperature change causes subsequent heat transfer into the rock mass. This temperature increase is a fraction of a degree Celsius; i.e., much smaller than the temperature difference after cavern leaching that was discussed in Section 6.3. However, even though small, this temperature variation may be significant because, in sharp contrast with the temperature changes induced by leaching, this small temperature change is achieved during a short period of time (one or a few hours). This rapid temperature change is followed by brine cooling and a subsequent pressure drop in a closed cavern; moreover, the pressure drop rate is quite fast during a couple of days or so and may lead to misinterpretation of an LLI test. In this section, the initial temperature increase is discussed; a case history is described in Section 6.4.2. The subsequent brine cooling and pressure drop are discussed in Section 6.4.3.

The first law of thermodynamics states that any change in the internal energy of a given body is the sum of the amount of heat received by the body and the amount of work performed on the body. Density, temperature, and pressure are not independent variables, as these variables are linked together through a state equation. In the context of a salt cavern, it is convenient to select temperature and pressure as two independent variables (in fact, when brine is considered, there exists a third variable, which is brine concentration, or the amount of dissolved salt in the water; the role of this variable is discussed in Chapter 8.0). Hence the following equation can be written:

$$q_{heat} = \iint_S K_{salt}^{th} \frac{\partial \theta_R}{\partial n} dS = \rho_l \cdot V \cdot \left(C_l^p \dot{T}_l - \frac{\alpha_l T_l}{\rho_l} \dot{P}_l \right) \tag{44}$$

where:

q_{heat} = amount of heat crossing the cavern wall (W)
C_l^p = liquid heat capacity (when pressure is kept constant) (J/kg-°C)
α_l = liquid thermal expansion coefficient (/°C)
ρ_l = liquid density (kg/m^3)
T_l = liquid absolute temperature (K)
P_l = liquid pressure (Pa).

During a slow process, the last term of the right-hand side of this equation ($C_l^p \dot{T}_l \gg \alpha_l T_l \dot{P}_l / \rho_l$) can be neglected; such an approximation was made in Section 6.4.3. Conversely, when a rapid pressure change is considered, the first-term, right-hand side of the equation can be neglected, as heat exchange is a slow process. In other words, any rapid pressure increase (as occurs at the beginning of an MIT) will result in a (small) instantaneous temperature change.

In the case of a brine-filled cavern, C_b^p = 3,800 J/kg–°C, $\alpha_b = 4.4 \cdot 10^{-4}$/°C, T_l = 300 K, ρ_b = 1,200 kg/m^3, and the instantaneous temperature change is

$$\vartheta_l^1 \text{ (°C)} = \left(\frac{\alpha_b T_l}{\rho_b C_b^p} \right) p_l^1 = 2.9 \cdot 10^{-2} \, p_l^1 \text{ (MPa)} \tag{45}$$

For instance, a p_l^1 = 5 MPa rapid pressure increase generates a ϑ_l^1 = 0.15°C temperature increase. When the cavern contains liquid hydrocarbons and brine, the same phenomenon takes place in the two liquids, and the two liquids experience a distinct temperature change. In general, ρ_l and C_l^p are significantly smaller for oil, and the temperature increase is larger than for brine.

6.4.2 Adiabatic Temperature Increase in a Field Test

A field test was performed in a 900-m-deep, 400,000-m^3 cavern filled with oil with only a small amount of brine left at cavern bottom. Before December 12, 2002 ($t = 0$), the cavern was kept idle and its temperature gently increased; the change in temperature between December 18 and December 30 is shown in Figure 19. Temperature change with respect to time during this period can be fitted to a linear relation:

$$\theta_l(t)\ (°C) = 29.408 + 1.1714 \cdot 10^{-3} \cdot t\ (\text{days})$$

Brine and oil were withdrawn from the cavern from January 14 to January 31, 2003; during this period (Figure 19), the pressure dropped by $p_l^1 = -3.2$ MPa. Although no accurate temperature measurements were made during the withdrawal period, after January 31, the cavern was again kept idle, and temperature measurements were again available. The temperature measured on January 31 (44 days after December 12) was 28.98°C, instead of the 29.46°C predicted by the linear relation; i.e., 0.48°C less than what the temperature should have been had no withdrawal taken place.

The theoretical effect of the oil withdrawal on cavern temperature (adiabatic depressurization) can be computed easily:

$$\vartheta_l^1\ (°C) = \left(\frac{\alpha_{oil} T_l^o}{\rho_{oil} C_{oil}^p}\right) p_l^1 = 0.21 \cdot p_l^1\ (\text{MPa})$$

or $\vartheta_l^1 = -0.67$°C, a figure slightly higher than the as-measured temperature drop, or –0.48°C. This gap can be explained when remembering that fluid withdrawal took a couple of weeks to complete; by January 31, when temperature was measured again, there had been time for heat transfer from the rock to the oil.

6.4.3 Temperature Evolution

Before an MIT, thermal equilibrium does not typically exist. Usually, the brine temperature in the cavern is lower than the rock mass temperature, which results in a heat flux from the rock mass to the cavern. In some situations (for example in Kansas, USA, in the summer), a shallow cavern may have the heat flux reversed with the rock mass cooler than the cavern brine. An additional thermal equilibrium disturbance is created when the brine temperature increases at the beginning of the test because of the pressure increase. Because the equations that describe the temperature evolution are linear, the "old" brine warming process that preceded the MIT and the "new" cooling process triggered by the MIT are uncoupled. They will be discussed and computed independently. The overall temperature history of the cavern can be obtained through superposition of the solution for the "new" cooling process or $\vartheta_l = \vartheta_l(t)$ and the solution for the "old" warming process or $\theta_l = \theta_l(t)$.

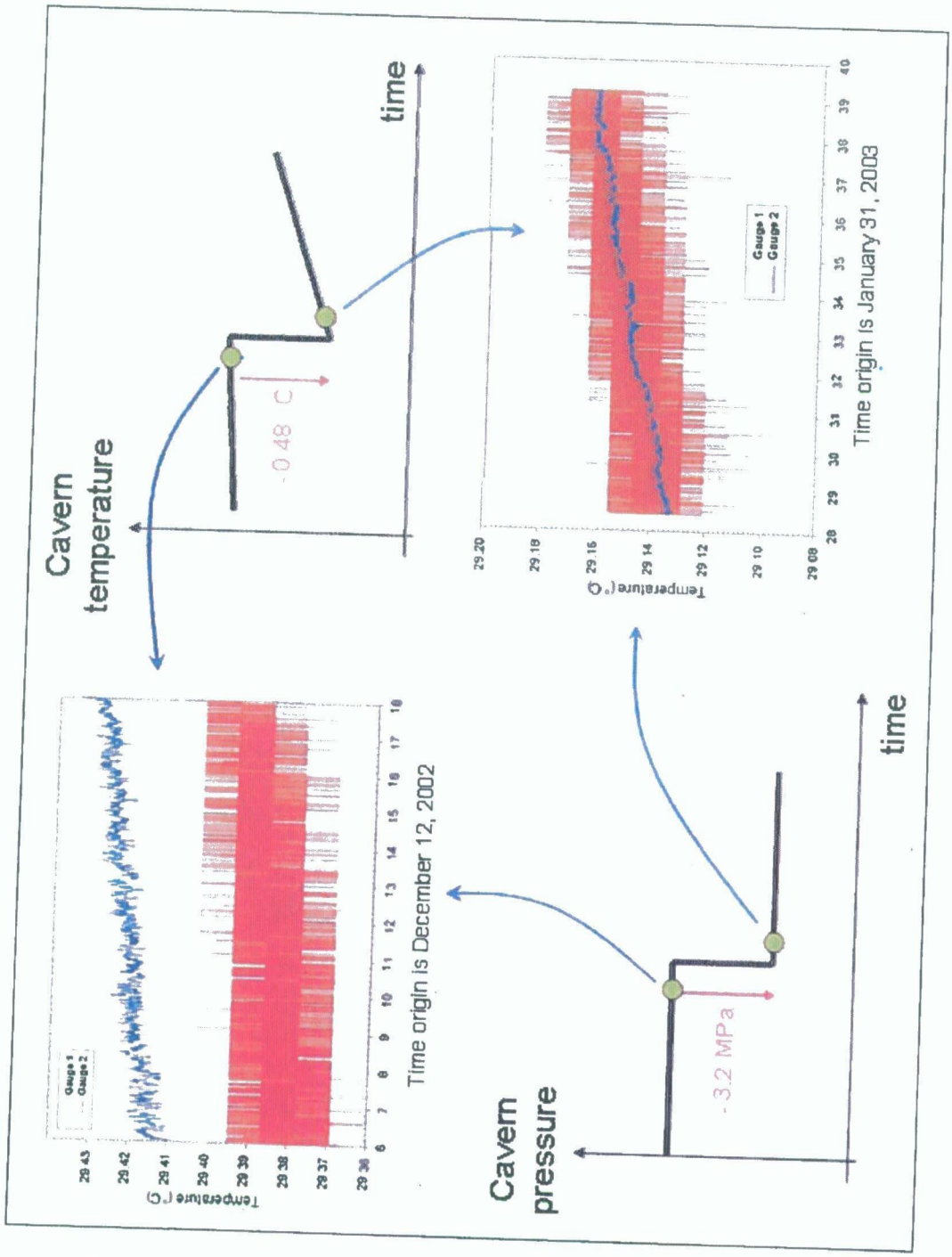

Figure 19. Cavern Temperature Evolution as Measured in a Large Oil-Filled Cavern. (Two temperature gauges were used. A small offset is clearly visible.) Temperature and rate of temperature increase are lower and higher, respectively, after depressurization.

The equations governing the cooling process triggered by the pressure increase are similar to the equations described in Section 6.3:

$$\begin{cases} \dfrac{\partial \vartheta_R}{\partial t} = k_{salt}^{th} \cdot \Delta \vartheta_R \\ q_{heat}^{ad} = \iint_S K_{salt}^{th} \dfrac{\partial \vartheta_R}{\partial n} dS = \rho_l C_l^p V \dot{\vartheta}_l \\ \vartheta_R(\infty, t) = 0 \\ \vartheta_R(\text{wall}, 0) = \vartheta_l(0) = \vartheta_l^1 \\ \vartheta_R(\text{rock mass}, 0) = 0 \end{cases} \tag{46}$$

where:

$\vartheta_R(\underline{x}, t)$ (°C) = the transient temperature distribution in the rock mass (because of pressure build-up alone)

q_{heat}^{ad} (W) = the heat flux crossing the cavern wall following liquid adiabatic warming

k_{salt}^{th} (m^2/s) = the salt thermal diffusivity

K_{salt}^{th} (W/m-°C) = the salt thermal conductivity

$\vartheta_l(t)$ (°C) = the cavern fluid temperature (because of pressure build-up alone)

$\vartheta_l(0) = \vartheta_l^1$ = the initial fluid temperature increase caused by the rapid pressure build-up p_l^1, or

$$\vartheta_l^1 = \left(\frac{\alpha_l T_l^o}{\rho_l C_l^p} \right) p_l^1 \tag{47}$$

We are mainly interested in the temperature change during testing duration, which is a few days long. It can be assumed that during this small interval of time, the temperature changes will not be large. In the case of a spherical cavern, radius R, a closed-form solution can be found:

$$q_{heat}^{ad} = q_{ad}^{ss} \cdot \left(1 + \sqrt{t_c^{th}/t} \right) \quad \text{where} \quad q_{ad}^{ss} = -4\pi R k_{salt}^{th} \rho_{salt} C_{salt} \vartheta_l^1 \quad \text{and} \quad t_c^{th} = \frac{R^2}{\pi k_{salt}^{th}} \tag{48}$$

where:

- q_{ad}^{ss} is the steady-state heat flow (reached after a very long period of time, when ϑ_l^1 is kept constant for a long period of time)
- t_c^{th} is the characteristic time for the thermal evolution.

and:

$$\vartheta_l - \vartheta_l(0) = -\frac{3\chi\alpha_l T_l^o}{\pi\rho_l C_l^p} p_l^1 \left(\frac{t}{t_c^{th}} + 2\sqrt{\frac{t}{t_c^{th}}} \right) \tag{49}$$

When $t << t_c^{th} = R^2 / k_{salt}^{th}$, $1/t_c^{th}$ is small when compared to $1/\sqrt{t_c^{th} t}$.

Taking $\chi = 4/9$, $k_{salt}^{th} = 3 \cdot 10^{-6} \text{m}^2/\text{s}$, $t_c^{th}(\text{days}) = 1.23\ R^2\ (\text{m}^2)$, and $\alpha_b T_l / \rho_b C_b^p = 2.9 \cdot 10^{-2}\ p_l^1\ (\text{MPa})$

$$\vartheta_l(t) - \vartheta_l(0) = -\frac{2.2 \cdot 10^{-2}}{R\ (\text{m})} p_l^1\ (\text{MPa}) \cdot \sqrt{t\ (\text{days})} \tag{50}$$

$$\dot{\theta}_l(t) = -\frac{1.1 \cdot 10^{-2}}{R\ (\text{m})} p_l^1\ (\text{MPa}) \Big/ \sqrt{t\ (\text{days})} \tag{51}$$

6.4.4 Pressure Decrease During an LLI in a Spherical Cavern

Brine volumetric contraction in a spherical cavern (where $\alpha_b = 4.4 \cdot 10^{-4}/°\text{C}$) is

$$\frac{Q_{th}^{ad}}{V} = -\alpha_b \dot{\vartheta}_l(t) = \frac{4.8 \cdot 10^{-6}}{R\ (\text{m})} p_l^1\ (\text{MPa}) \Big/ \sqrt{t\ (\text{days})} \tag{52}$$

and pressure build-up in a closed cavern (where $\alpha_b / \beta \approx 1\ \text{MPa}/°\text{C}$) is

$$p_l - p_l^1 = \frac{\alpha_b}{\beta}\left(\vartheta_l(t) - \vartheta_l^o\right) = \frac{-2.2 \cdot 10^{-2}}{R\ (\text{m})} p_l^1 \sqrt{t\ (\text{days})} \tag{53}$$

Note that $\dot{p}_l = \frac{1}{2}(p_l - p_l^1)/t$; when $R = 12.5$ m ($V = 8{,}000\ \text{m}^3$) and $p_l^1 = 5$ MPa, the pressure drop from cooling is 8.8 kPa after 1 day and 17.6 kPa (2.5 psi) after 4 days.

In real life, pressure build-up is not an "instantaneous" process; it is achieved after a period of 1 hour or more. The adiabatic temperature change is more gradual than assumed when deriving mathematical expressions. Figure 20 displays the results of a numerical computation considering several pressure increase rates. Brine cooling rate (and the resulting pressure drop rate) are somewhat slower when a slower pressure increase is applied. Here again, a significant part of the "apparent" leak can be avoided by waiting for a couple of days to allow stabilization

of the cavern, or, more precisely, to let enough time pass for the initial rapid cooling rate to dissipate.

RSI-1476-05-024

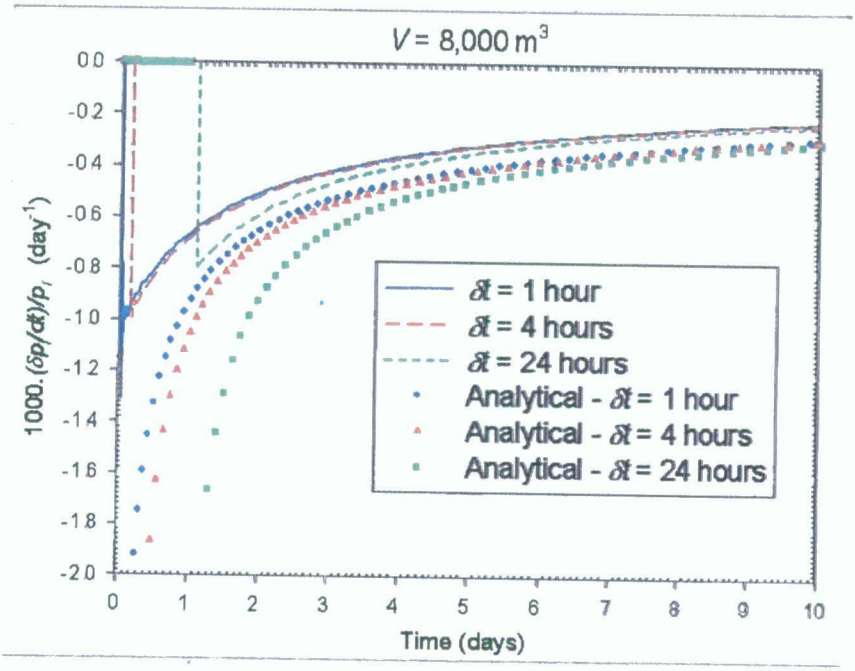

Figure 20. Numerical Computation of Relative Pressure History After a Rapid Pressure Increase. Only the effect of brine cooling following the adiabatic pressure increase is taken into account. δt is the time required for the initial pressure increase. The computed solution is compared to the closed-form ("analytical") solution when pressure is instantaneously increased instead of progressively increased over the δt-long period.

6.4.5 Brine Volume Decrease During an NIT

The effect of a rapid pressure increase in an NIT is described in Chapter 13.0 (where $Q = Q_{th}^{ad} = -\alpha V \dot{\vartheta}_1(t) > 0$).

6.5 ATMOSPHERIC PRESSURE, EARTH TIDES

Atmospheric pressure experiences small variations. Over a few days, the magnitude of these fluctuations is 0.1–1 kPa. These pressure fluctuations generate additional vertical and horizontal stresses in the rock formation which, in turn, generate small pressure variations in a closed cavern. Because the transfer through the rock is not 100 percent efficient, the magnitude of the cavern pressure change, or δP_1, is always smaller than the magnitude of the atmospheric pressure variations. Even so, cavern pressure changes are, however, commonly observed when the pressure measurement system has a high resolution.

Earth tides are generated by the moon and, to a smaller extent, by the sun. They induce small, but repeatable, deformations of the earth with a complex history with an apparent period is 12 hours and 25 minutes. The magnitude of these deformations is in the $\delta\varepsilon = 10^{-8}$ to 10^{-7} range. The resulting brine pressure fluctuations in a closed cavern are $\delta P_i = \delta\varepsilon/\beta$ or $10^{-7}/4 \cdot 10^{-10} = 250$ Pa (0.04 psi); i.e., smaller than the effect of atmospheric pressure fluctuations.

Both atmospheric pressure fluctuations and gravitational forces of the sun and moon are normally negligible in the context of an MIT, although they were observed during the test described in Section 12.8.

7.0 FLUID PERMEATION

7.1 EFFECTS OF STEADY-STATE AND TRANSIENT FLUID MICROPERMEATION INTO THE SALT

Pure rock salt exhibits a very low permeability because its matrix hydraulic conductivity is extremely small and because no fractures exist in a massive salt formation (except, perhaps, in some disturbed zones encountered at the fringes of salt domes). Permeability magnitudes as small as $K_{salt}^{hyd} = 10^{-22}$ to 10^{-20} m^2 are reported. Several authors believe that most of this (small) permeability is induced by cavern creation and operation (more precisely, either by tensile or high deviatoric stresses developed at the cavern wall, when the cavern fluid pressure is very high or very small, respectively). This generalization is likely different for bedded salt formations when the formation contains a fair amount of insoluble rocks (anhydrite or clay interbedded layers): the overall formation permeability may be strongly influenced by the presence of these insoluble layers.

In most cases, salt's permeability is so small that its measurement is beyond the standard techniques used for more permeable rocks (say, rocks with permeabilities greater than $K_{salt}^{hyd} = 10^{-17}$ m^2), and few reliable in situ test results are available. For example, experiments performed in an air-intake shaft at the Waste Isolation Pilot Plant (WIPP) site (bedded salt) provide permeabilities as small as $K_{salt}^{hyd} = 10^{-21}$ m^2 for undisturbed salt at a 1-meter depth behind the shaft wall [Dale and Hurtado, 1996]. Durup [1994] performed a 1-year test, supported by the Solution Mining Research Institute (SMRI), in a 1,000-meter-deep well in the Etrez *upper* salt formation, a bedded salt formation where anhydrite and clay interbeds are present. The insoluble content in this formation is approximately 10 percent. This test consisted of the incremental build-up of brine pressure in the well. Brine was injected daily to keep the well pressure constant during each step. Assuming Darcy's law, Durup computed an average permeability of $K_{salt}^{hyd} = 6 \cdot 10^{-20}$ m^2 in the 200-meter-long unlined deeper part of the well. Brouard et al. [2001] compiled a dozen similar, but shorter, tests performed in the Etrez *lower* salt formation and in the Tersanne (bedded) salt formation: respective back-calculated permeabilities were $K_{salt}^{hyd} = 4.6 \cdot 10^{-21}$ m^2 to $1.9 \cdot 10^{-20}$ m^2 (Etrez) and $K_{salt}^{hyd} = 8.6 \cdot 10^{-22}$ to $3.2 \cdot 10^{-21}$ m^2 (Tersanne). Incidentally, it is interesting to note that Tersanne salt has a higher creep rate than Etrez salt. More recently, at the Etrez site, an 18-month test (supported by the SMRI) in a full-size cavern (rather than in a well) provided $K_{salt}^{hyd} = 2 \cdot 10^{-19}$ m^2 [Bérest et al., 2001b]. This larger figure is consistent with the generally accepted effect of scale on rock permeability [Brace, 1980].

The consequences of salt permeability must be examined in the context of an MIT where it is believed that leaks also occur mainly through the cemented casing; however, leaks through the formation itself must be assessed. Steady-state leaks are extremely small. When the pressure in a 100,000-m^3 spherical cavern is larger than the natural pore pressure in the rock mass by

10 MPa and the permeability is $K_{salt}^{hyd} = 10^{-20}$ m^2, steady-state seepage flow of the brine is $Q_{perm} = 1$ m^3/year (6 bbls/year), and the brine pressure decay rate is $\dot{p}_i^1 = -25$ kPa/year (–3.5 psi/year), a figure that can be disregarded in the context of the MIT duration. However, the pressure decay rate is larger in a smaller cavern. An example is given in Section 11.8 where the leak rate because of steady-state brine permeation in an 8,000-m^3 cavern was –0.87 kPa/day, or –0.12 psi/day, when testing pressure was $p_i^1 = 2.7$ MPa.

Transient leaks following pressure increases may be more significant and are assessed below. We assume the following:

1. Darcy's law for fluid flow through porous media holds; i.e., fluid flow rate in the rock mass is proportional to the pressure (or hydraulic potential) gradient.
2. Only the additional (or incremental) flow because of pressure increases is considered. In other words, natural pore pressure is assumed to be *halmostatic* (pore pressure in the salt equals the cavern pressure as it was before the test began). The incremental pressure increase is defined as $p(r,t) = P_{pore} - P_o$ (Pa), which is the difference between the actual pore pressure P_{pore} and the initial (halmostatic) pore pressure P_o.
3. The hydraulic and mechanical processes are uncoupled.

As a consequence, pore pressure difference evolution can be described as

$$\frac{\partial p}{\partial t} = \frac{K_{salt}^{hyd}}{\mu_b \beta' \phi} \Delta p \qquad \left(\text{or } \frac{\partial p}{\partial t} = k_{salt}^{hyd} \Delta p\right) \tag{54}$$

where K_{salt}^{hyd} (m^2) is the salt-mass intrinsic permeability, μ_b (Pa·s) is the fluid (brine) dynamic viscosity, β' (/Pa) is the rock matrix compressibility factor, ϕ (-) is the rock mass porosity, and k_{salt}^{hyd} is the hydraulic conductivity of the salt mass.

7.1.1 Boundary Conditions

Boundary conditions are described below:

- At a large distance from the cavern, inside the rock mass, the pore pressure is undisturbed:

$$P_{pore} = P_{pore}(\infty, t) = P_o \quad \text{or} \quad p(\infty, t) = 0. \tag{55}$$

- At the cavern wall, pore pressure equals cavern pressure:

$$P_{pore}(\text{wall}, t) = P_i(t) \quad \text{or} \quad p(\text{wall}, t) = p_i(t) \tag{56}$$

In the following, we mostly are interested in the amount of brine that leaves the cavern or, more precisely, in the ratio between this amount of brine (Q_{perm}) and the cavern volume (V):

$$\frac{Q_{perm}}{V} = \frac{1}{V}\iint_S \frac{K_{salt}^{hyd}}{\mu_b}\frac{\partial p}{\partial n}dS \tag{57}$$

where $\partial p/\partial n$ is the pore pressure gradient at the cavern wall.

7.1.2 Steady-State Flow

When cavern pressure (P_i) is kept constant $\left(P_i = P_i^1,\ p_i = p_i^1\right)$ for a very long period of time, steady-state flow is reached, and the problem can be rewritten as

$$\begin{cases} \Delta p = 0 \\ p(\infty, t) = 0 \\ p(\text{wall}, t) = p_i^1 \\ \dfrac{Q_{perm}^{ss}}{V} = \dfrac{1}{V}\iint_S \dfrac{K_{salt}^{th}}{\mu_b}\dfrac{\partial p}{\partial n}dS \end{cases} \tag{58}$$

7.1.3 Boundary Condition During an MIT Test

An MIT test lasts a few days–typically not enough time to reach steady state. However, cavern pressure changes during an MIT are relatively small when compared with the large pretest pressure increase imposed on the cavern. Rather than an exact value, our goal here is to obtain orders of magnitude for the cavern fluid loss to the surrounding rock. For simplicity, assume that cavern pressure remains approximately constant during the MIT. Such an assumption is only valid when the characteristic time, t_c^{hyd}, is much longer than the MIT duration, or t_{test}.

$$\begin{cases} p_i(t) \approx p_i^1 \\ t < t_{test} << t_c^{hyd} \end{cases} \tag{59}$$

7.2 THE CASE OF A SPHERICAL CAVERN

Consider, first, the case of a spherical cavern with radius R and volume $V = 4\pi R^3/3$. Rock permeability is assumed to be constant throughout the entire rock mass. Then, the flow of brine from the cavern can be written as

$$Q_{perm} = Q_{perm}^{ss} \cdot \left(1 + \sqrt{t_c^{hyd}/t}\right) \tag{60}$$

Two important quantities to be defined are Q_{perm}^{ss} (steady-state brine flow) and t_c^{hyd} (characteristic time).

$$Q_{perm}^{ss} = \frac{4\pi K_{salt}^{hyd} R}{\mu_b} p_i' \qquad t_c^{hyd} = \frac{\mu_b \phi \beta' R^2}{\pi K_{salt}^{hyd}} \tag{61}$$

7.2.1 Steady-State Flow in a Spherical Cavern

In the following, we assume that the initial pressure increase, or testing pressure at the wellhead, is p_i' = 5 MPa--a typical value. (For a different pressure increase, the calculated steady-state flow must be adjusted proportionally.) Brine viscosity is $\mu_b = 1.2 \cdot 10^{-3}$ Pa·s. The steady-state flow, Q_{perm}^{ss}, or more precisely, the ratio Q_{perm}^{ss}/V, is especially significant when (a) the rock permeability is large and (b) the cavern volume is small.

Consider the somewhat extreme case of a cavern with V = 8,000 m^3 and $K_{salt}^{hyd} = 10^{-19}$ m^2. Even in this case, steady-state flow is small:

$$Q_{perm}^{ss} = 2 \text{ m}^3/\text{year} \qquad Q_{perm}^{ss}/V = 2.5 \cdot 10^{-4}/\text{year} \tag{62}$$

The steady-state relative flow rate, or Q_{perm}^{ss}/V, is even less significant when larger caverns and less permeable rocks are considered.

7.2.2 Characteristic Time in a Spherical Cavern

Consider now the characteristic time t_c^{hyd}; i.e., the time after which the brine flow equals twice the steady-state brine flow. Orders of magnitude are a little more difficult to assess, as the parameters are poorly defined. Rock porosity (ϕ) is correlated to rock permeability (K_{salt}^{hyd}). The following two cases can be considered:

1. A micropermeable cavern: $K_{salt}^{hyd} = 10^{-19}$ m^2, $\phi = 0.01$, $K_{salt}^{hyd}/\phi = 10^{-17}$ m^2
2. A poorly permeable cavern: $K_{salt}^{hyd} = 10^{-21}$ m^2, $\phi = 0.002$, $K_{salt}^{hyd}/\phi = 5 \cdot 10^{-19}$ m^2.

Matrix compressibility is difficult to assess. We assume that it is the same as the cavern compressibility factor (see below), or $\beta' = \beta = 4 \cdot 10^{-10}$/Pa. It follows, then:

1. A micropermeable cavern: t_c^{hyd} (year) $= \mu_b \phi \beta' R^2 / \pi K_{salt}^{hyd} = 5 \cdot 10^{-4} \; R^2$ (m^2)
2. A poorly permeable cavern: t_c^{hyd} (year) $= \mu_b \phi \beta' R^2 / \pi K_{salt}^{hyd} = 10^{-2} \; R^2$ (m^2).

As the square of the cavern radius ranges from R^2 = 150 m^2 (when V = 8,000 m^3) to R^2 = 2,500 m^2 (when V = 500,000 m^3), the characteristic time ranges from 1 month (in a small cavern excavated in a permeable salt formation) to several years (in a big cavern, when permeability is small). The characteristic time is much longer than the MIT duration.

7.3 CAVERN PRESSURE DROP CAUSED BY BRINE MICROPERMEATION

7.3.1 The Case of an LLI

The brine volume (v_{perm}) and the brine flow rate (Q_{perm}) permeating from a cavern can be expressed as

$$\frac{V_{perm}}{V} = \frac{3\phi\beta'}{\pi} \cdot p_i^1 \cdot \left(\frac{t}{t_c^{hyd}} + 2\sqrt{\frac{t}{t_c^{hyd}}} \right) \tag{63}$$

$$\frac{Q_{perm}}{V} = \frac{3\phi\beta'}{\pi} \cdot p_i^1 \cdot \left(\frac{1}{t_c^{hyd}} + \sqrt{\frac{1}{t \cdot t_c^{hyd}}} \right) \tag{64}$$

When $t < t_c^{hyd} = (R^2 \mu_b \phi \beta')/(\pi K_{salt}^{hyd})$, a condition always met in an MIT, these relations can be simplified. Consider the case of a permeable salt formation, $K_{salt}^{hyd} = 10^{-19}$ m^2, $\phi = 10^{-2}$, $\beta' = \beta = 4 \cdot 10^{-4}$ /MPa, $\mu_b = 1.2 \cdot 10^{-3}$ Pa·s, t_c^{hyd} (days) $= 0.177\ R^2$ (m^2), and:

$$\frac{V_{perm}}{V} \approx \frac{6 K_{salt}^{hyd}}{\mu_b R^2} p_i^1 \sqrt{t_c^{hyd} t} \approx \frac{1.36 \cdot 10^{-6}}{R\ (\text{m})} p_i^1\ (\text{MPa}) \cdot \sqrt{t\ (\text{days})} \tag{65}$$

and in an LLI:

$$\dot{p}_i = -\frac{Q_{perm}}{\beta V} \approx \frac{3 K_{salt}^{hyd}}{\beta \mu_b R^2} p_i^1 \left(1 + \sqrt{\frac{t_c^{hyd}}{t}} \right) \approx -\frac{1.7 \cdot 10^{-2}}{R\ (\text{m})} p_i^1\ (\text{MPa}) \Big/ \sqrt{t\ (\text{days})} \tag{66}$$

The largest pressure drop occurs when rock permeability is large–say, $K_{salt}^{hyd} = 10^{-19}$ m^2, $\phi = 0.01$, $\beta = \beta' = 4 \cdot 10^{-4}$/MPa, t_c^{hyd} (days) $= 0.177\ R^2$–and when the cavern size is small.

The pressure decay rate is smaller in a small cavern (for example, R = 12.5 m or V = 8,000 m^3), $\dot{p}_i / p_i^1 = -1.78 \cdot 10^{-3}$/day after 1 day, and the total pressure drop after 1 day is $\delta p_i / p_i^1 = -3.56 \cdot 10^{-3}$, or 17.8 kPa (2.5 psi) when the initial pressure build-up is p_i^1 = 5 MPa (725 psi).

The effect of brine permeation is comparable to the effect of an adiabatic pressure change (see Section 6.4). However, it must be kept in mind that in the case of brine permeation, such quantities as rock permeability or matrix compressibility are poorly known. When small permeabilities are considered ($K_{salt}^{hyd}\phi$ = 10^{-23} m^2), brine permeation can be neglected.

7.3.2 The Case of an NIT

During an NIT, brine permeation into the rock mass results in a (small) brine/nitrogen interface drop, see Chapter 13.0; the actual leak is slightly underestimated.

7.4 THE CASE OF A CYLINDRICAL CAVERN

Consider the case of a slender cavern whose radius, R, is much smaller than its height (note that a wellbore is a particular case of cylindrical cavern). The set of equations to be solved is the same as in Section 7.1, although cylindrical coordinates must be used.

For small values of t/t_c^{hyd}, a closed-form solution can be found. For such short periods of time, cavern pressure experiences small changes. The brine flux at the surface (per unit of length) is [Carlslaw and Jaeger, 1959, p.336]:

$$Q_{perm} = \frac{\pi K_{salt}^{hyd} R}{\mu_b}\left(1+2\sqrt{\frac{t_c^{hyd}}{t}}+\ldots\right)p_l^1 \tag{67}$$

which, following a procedure similar to the procedure used in Section 7.3, leads to

$$\frac{\dot{p}_l}{p_l^1} = -\frac{Q_{perm}^{hyd}}{\pi R^2} = -\frac{2\phi}{\pi}\frac{\beta'}{\beta}\Big/\sqrt{t\cdot t_c^{hyd}} \tag{68}$$

In most cases, the permeation effect for cylindrical caverns, which are typically larger volume than spherical caverns, is quite small and can be neglected in the context of an MIT.

7.5 THE CASE OF A WELLBORE

In this case, the volume of the unlined part of the well (through which permeation takes place) is only a fraction of the overall volume of the well. Let Φ be this fraction. Then, the above formula must be modified slightly:

$$\frac{\dot{p}_l}{p_l^1} = -\frac{2\phi\Phi}{\pi}\frac{\beta'}{\beta}\Big/\sqrt{t\cdot t_c^{hyd}} \tag{69}$$

In a wellbore, t_c^{hyd} is short (transient phenomena are rapid when the radius is small) and, following a rapid pressure increase, a subsequent rapid pressure drop is observed. In sharp contrast to the case of a large cavern, transient brine permeation is an important mechanism in a well. One consequence is that salt micropermeability is assessed conveniently through tests performed in a wellbore before the cavern is created (see Chapter 10.0, Example 2).

7.6 THE CASE OF A PERMEABLE LAYER

In a bedded salt formation, the "salt permeability" is expected to be associated with the permeability of insoluble layers whose permeability is larger than that of pure salt. Let R be the cavern radius at the depth of the insoluble layer, h be the insoluble layer thickness, and V be the volume of the cavern. The formula given in Section 7.5 can be used when one sets $\Phi = 2\pi Rh/V$. In most cases, brine permeation into insoluble layers can be neglected.

8.0 ADDITIONAL DISSOLUTION

8.1 EXAMPLE OF ADDITIONAL DISSOLUTION EFFECTS

During the leaching phase, the cavern brine is not fully saturated because soft water is continuously injected into the cavern. If the brine were saturated, no dissolution would take place. When injection stops, the brine/air interface in the well commonly drops for a few days, although both cavern shrinkage because of salt creep and brine thermal expansion caused by brine warming should lead to brine/air interface rising, as generally happens several days after injection has stopped.

This transient phenomenon (i.e., air/brine interface dropping for a few days) can be explained by additional salt dissolution. The brine volume is smaller than the sum of the volumes of its constituents (the dissolved rock salt and the water). Therefore, when dissolution continues in an idle cavern, the increase in brine volume is smaller than the increase in cavern volume, resulting in a brine interface drop (or resulting in a cavern pressure drop when the cavern is closed and pressurized). After a few days or weeks, dissolution is almost complete as the brine approaches saturation. Further volume changes caused by dissolution become negligible, and the cavern behavior is governed predominantly by thermal expansion and cavern creep, which causes the air/brine interface to rise and brine to be expelled from an open cavern (or the pressure to increase in a closed cavern).

Consider the case of a cavern with fully saturated brine where no additional dissolution takes place. If the pressure is rapidly built up in the cavern, the brine becomes slightly undersaturated at the new pressure because brine saturation, or the maximum amount of salt that can be dissolved in a given mass of soft water, is an increasing function of both fluid pressure and temperature, so additional dissolution takes place. This phenomenon lasts a few days. Here again, during the dissolution process, cavern volume increase is larger than brine volume increase, resulting in a transient cavern pressure decay, as more room is provided to the brine cavern. This phenomenon is quantified below.

8.2 ESTIMATION OF ADDITIONAL DISSOLUTION EFFECTS

Brine concentration (c) is the ratio between the salt mass and the (water + salt) mass in a given volume of brine. When brine is saturated, its concentration is c_{sat} (concentration at saturation). The concentration at saturation is a function of pressure and temperature. The following expression is given by ATG Manual [1985]:

$$c_{sat} = c_{ref} \cdot \left[1 + \Psi\left(P_l - P_{ref}\right) + \kappa\left(\theta_l - \theta_{ref}\right) + \xi\left(\theta_l - \theta_{ref}\right)^2\right] \tag{70}$$

where:

$$\left|\begin{array}{lll} c_{ref}=0.2655 & P_{ref}=0.1\ \text{MPa} & \theta_{ref}=25°\text{C} \\ \Psi=2.62\cdot10^{-4}/\text{MPa} & \kappa=4.07\cdot10^{-4}/°\text{C} & \xi=7.42\cdot10^{-6}/°\text{C}^2 \end{array}\right. \tag{71}$$

Brine density at saturation is also a function of temperature and pressure:

$$\rho_b^{sat}=\rho_b^{ref}\cdot\left[1+a_s\left(P_l-P_{ref}\right)-b_s\left(\theta_l-\theta_{ref}\right)\right] \tag{72}$$

where:

$$\rho_b^{ref}=1{,}198\ \text{kg/m}^3 \quad a_s=3.16\cdot10^{-4}/\text{MPa} \quad b_s=3.76\cdot10^{-4}/°\text{C} \tag{73}$$

In the following, we are mainly interested in the effect of pressure variations. Consider a cavern filled with saturated brine. Initial cavern volume, cavern pressure, saturated brine concentration, and density are V^o, P_l^o, c_{sat}^o, and ρ_{sat}^o, respectively. Then, a volume of liquid (brine or hydrocarbon), or v^{inj}, is injected in the cavern. In a Nitrogen Interface Test, in addition to this brine injection, gas is forced into the cavern, with v_g being the volume of the gas in the cavern.

The brine injection results in a cavern pressure increase of p_l^1; cavern pressure is $P_l^1=P_l^o+p_l^1$ immediately after injection. At this instant, the brine is no longer saturated because brine pressure and temperature conditions, to a smaller extent, have changed. Additional dissolution takes place over a few days. After some time, the brine becomes saturated again, and brine is said to have reached its "final state" (with regard to saturation): its concentration is then c_{sat}^f, its volume is V_b^f, its pressure is $P_l^f=P_l^o+p_l^f$, and its density is ρ_{sat}^f.

General Relations—It is assumed that fluid thermal expansion, cavern creep, adiabatic pressure increases and fluid seepage through the casing can be neglected.

The linearized state equations provided above allows:

$$\begin{cases} c_{sat}^f-c_{sat}^o=c_{sat}^o\Psi p_l^f \\ \rho_{sat}^f-\rho_{sat}^o=\rho_{sat}^o a_s p_l^f \end{cases} \tag{74}$$

and the following two mass-balance equations can be written:

$$\begin{cases} V_b^f\rho_{sat}^f c_{sat}^f=V_b^o\rho_{sat}^o c_{sat}^o+\rho_{salt}V_{salt} \\ V_b^f\rho_{sat}^f=V_b^o\rho_{sat}^o+\rho_{salt}V_{salt} \end{cases} \tag{75}$$

$\rho_{salt} v_{salt}$ is the mass of dissolved salt, and V_b^f and V_b^o are the cavern brine volume in the final and initial state, respectively. The first of Equation (75) is the salt-mass balance equation; the second of Equation (75) is the brine-mass balance equation.

From Equations (70)–(75):

$$v_{salt} = V_b^o \frac{\rho_{sat}^o}{\rho_{salt}} \frac{c_{sat}^o}{1 - c_{sat}^o} \Psi p_i^f = \lambda V_b^o p_i^f \tag{76}$$

When $c_{sat}^o = 0.2655$, $\rho_{sat}^o = 1{,}200\ \text{kg/m}^3$, $\rho_{salt} = 2{,}160\ \text{kg/m}^3$, and $\Psi = 2.6 \cdot 10^{-4}$ /MPa, one gets $\lambda = 0.52 \cdot 10^{-4}$ /MPa. In other words, when pressure is increased by $p_i^f = 5$ MPa in a $V_b^o = 10{,}000\ \text{m}^3$ brine-filled cavern, an additional 2.6 m^3 (5,600 kg) volume of salt is dissolved:

$$V_b^f - V_b^o = V_b^o \left(\frac{\rho_{salt}}{\rho_{sat}^o} \lambda - a_s \right) p_i^f \tag{77}$$

Equation (77) stipulates that brine volume change results from salt dissolution (volume increase) and from saturated brine pressurization (volume decrease). The net result is a volume decrease.

Now the change in cavern volume can be written as

$$V_c^f - V_c^o = v_{salt} + \beta_E V_c^o p_i^f = \left(\lambda V_b^o + \beta_E V_c^o \right) p_i^f \tag{78}$$

Equation (78) stipulates that cavern volume change results from the creation of new voids (v_{salt}), which are proportional to brine volume (V_b^o), and from the cavern volume increase, caused by a pressure increase, which is proportional to cavern volume (V_c^o). Equations (77) and (78) can be combined to obtain:

$$V_c^f - V_c^o = V_b^f - V_b^o + \left[\beta_E V_c^o + (a_s - \varpi) V_b^o \right] p_i^f \tag{79}$$

where $\varpi = \frac{\rho_{salt}}{\rho_{sat}^o} \lambda - \lambda = 0.8\lambda = 0.416\ 10^{-4}$/MPa.

Four different cases of changes caused by dissolution are considered next.

1. **The cavern is filled with brine.** (A small amount of hydrocarbon may be contained in the annular space.) Brine or liquid hydrocarbon is injected in the cavern. Then,

$$V_c^o = V_b^o \qquad V_c^f = V_b^f + v^{inj} \tag{80}$$

From Equation (79), we obtain

$$v^{inj} = \left[\beta_E + a_s - \varpi \right] V_c^o p_i^f \tag{81}$$

This can be compared to that obtained in Section 5.1:

$$v^{inj} = \left(\beta_E + \beta_b^{ad}\right) V_c^o p_i^1 \tag{82}$$

which leads to the apparent leak caused by additional dissolution:

$$v_{leak}^{app} = \left(\beta_E + \beta_b\right) V_c^o \left(p_i^1 - p_i^f\right) = \frac{a_s - \varpi - \beta_b^{ad}}{a_s - \varpi + \beta_E} v^{inj} \tag{83}$$

where $a_s = 3.16 \cdot 10^{-4}$ /MPa, $\beta_b^{ad} = 2.57 \cdot 10^{-4}$ /MPa, $\beta_E = 1.3 \cdot 10^{-4}$/MPa, and

$$v_{leak}^{app} = 0.043 \; v^{inj} \tag{84}$$

The following formula can also be useful:

$$\frac{v_{leak}^{app}}{v^{inj}} = \frac{p_i^1 - p_i^f}{p_i^1} \tag{85}$$

For example, when the initial pressure increase is $p_i^1 = 5$ MPa in a $V_c^o = 50{,}000$ m^3 cavern such that $\beta V_c^o = 20$ m^3/MPa, and when the injected volume is $v^{inj} = \beta V_c^o p_i^1 = 100$ m^3, the apparent leak caused by dissolution is 4.3 m^3, and the final pressure after dissolution is complete is $p_i^f = 4.79$ MPa, or about a 0.2 MPa pressure drop.

2. **The cavern is partially filled with hydrocarbon.** The initial volumes of brine and hydrocarbons are V_b^o and V_h^o, respectively, so:

$$V_c^f = v^{inj} + V_b^f + V_h^f \qquad V_c^o = V_b^o + V_h^o \tag{86}$$

Straight-forward algebra leads to

$$v_{leak}^{app} = \frac{\left(a_s - \varpi - \beta_b^{ad}\right)(1-x)}{\beta_E + \left(a_s - \varpi\right)(1-x) + \beta_h^{ad} x} v^{inj} \tag{87}$$

where $x = V_h^o / V_c^o$ is the ratio between the hydrocarbon volume and the cavern volume (see Section 5.2.2.4). When $x = 1$ (no brine), then $v_{leak}^{app} = 0$; when $x = 0$ (no gas), we get the same formula as Equation (83). Note, the apparent leak caused by additional dissolution is smaller when x is large, as expected. Equation (85) still applies and the injected volume is, upon rearrangement,

$$v^{inj} = \left[\beta_E + (1-x)\beta_b^{ad} + \beta_h^{ad}\right] V_c^o p_i^f \tag{88}$$

3. **The EZ53 Test.** In this section, the effect of pressure increase is reviewed when the partially filled central tubing is kept open after the pressure increase. This test is described

more completely in Section 12.2. During the first phase of this test, the annular space was filled with a light hydrocarbon; the wellhead was opened to atmospheric pressure, cavern depth was H = 950 m and the air/brine interface was $h^o_{\text{int}} = -290$ m below ground level, cavern pressure was P^o_l = 8 MPa, and hydrocarbon outflow was measured daily (Figure 21.a).

RSI-1476-05-025

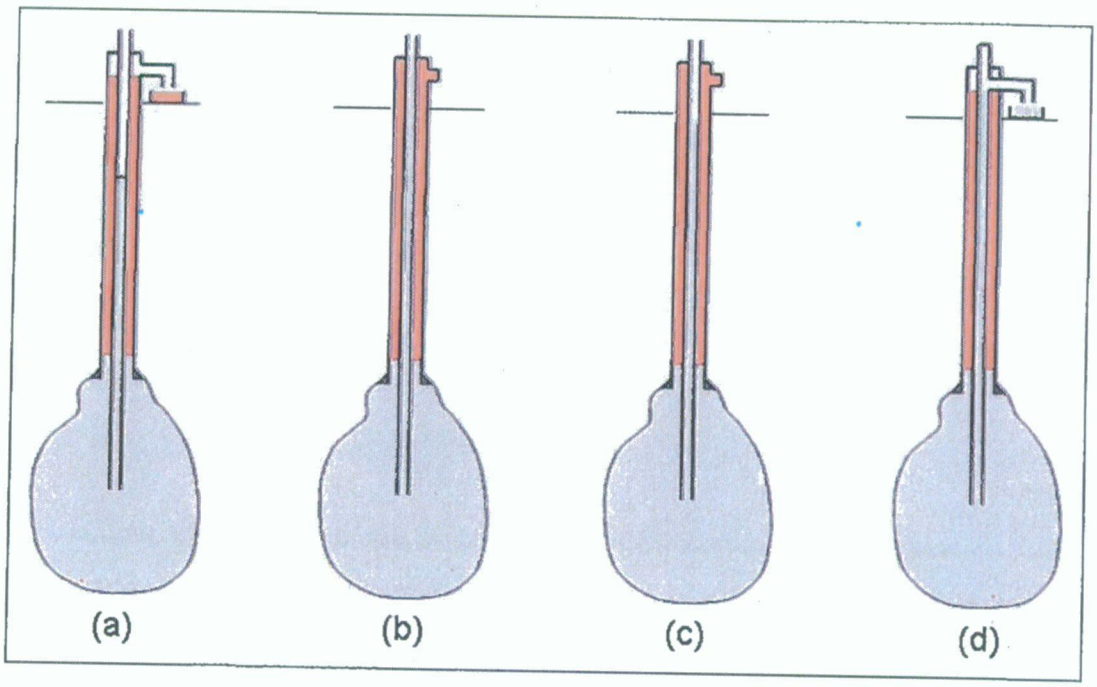

Figure 21. Evolution of Brine and Hydrocarbon in the Well at the End of EZ53 Transient Creep Test.

Brine was injected into the central tubing resulting in an increase in cavern pressure by p^1_l = 3.4 MPa (Figure 21.b; see also Figure 33). In the following days, the air/brine interface dropped (Figure 21.c; this drop results from additional dissolution and possibly transient creep, whose effects, during this period, are larger than the effects of steady-state creep and thermal expansion). After 12 days (Figure 21.d), the effects of transient creep and additional dissolution are negligible, and brine is expelled from the cavern; brine outflow is "constant" because of the effects of steady-state creep and brine thermal expansion.

In this problem, cavern pressure $P^f_l = P^o_l + p^f_l$ can be considered as being constant throughout the entire test (in fact, small transient pressure changes take place when the air/brine interface drops). Instead of Equation (86), the final and initial cavern volumes are given by:

$$V^f_c = v^{inj} - S_t h^o_{\text{int}} + V^f_b \qquad V^o_c = V^o_b \tag{89}$$

where S_t is the cross-sectional area of the central string. One obtains

$$v^{inj} - S_t h^o_{int} - \beta_E V^o_c p^f_i = (a_s - \varpi) V^o_c p^f_i \tag{90}$$

$S_t h^o_{int} + \beta V^o_c p^f_i$ is the volume of brine injected into the cavern during the first injection [from (a) to (b)], and $(a_s - \varpi - \beta^{ad}_b) V^o_c p^f_i = 0.174 \cdot 10^{-4}\ V^o_c p^f_i$ is the total volume of brine injected into the cavern during the following injections [from (b) to (d)].

4. **Nitrogen Interface Test.** During an NIT, a certain volume of brine, v^{inj}, is injected to prepressurize the cavern; then, nitrogen is injected in the annular space. Immediately after the gas injection takes place, v^1_g, P^1_g, and h^1 are the gas volume, gas pressure, and interface depth, respectively. At the end of the additional dissolution process, these quantities are v^f_g, P^f_g, and h^f, respectively:

$$\begin{cases} P^f_g v^f_g = P^1_g v^1_g \\ v^f_g - v^1_g = \Sigma(h^f - h^1) \\ p^f_i - p^1_i = P^f_g - P^1_g - (\rho^o_b - \rho^o_g) g (h^f - h^1) \end{cases} \tag{91}$$

where Σ is the cross-sectional area of the cavern neck at the interface depth, and $p^f_i - p^1_i$ is the cavern brine pressure variation.

The following equations can be written:

$$V^f_c = v^{inj} + v^f_g + V^f_b \qquad V^o_c = V^o_b \tag{92}$$

Note that the total amount of brine injected into the cavern is $v^{inj} + S_a H_{cs}$, where S_a is the annular average cross-sectional area down to the casing seat, and H_{cs} is casing seat depth; however, the final amount of gas in the cavern is $v^f_g - S_a H_{cs}$ and the following relation holds:

$$\Sigma(h^f - h^1)\left[1 + (\beta_E + a_s - \varpi) V^o_c \left(\frac{P^1_g}{v^1_g} + \frac{g(\rho^o_b - \rho^o_g)}{\Sigma}\right)\right] = -v^1_g - \frac{\beta^{ad}_b - a_s + \varpi}{\beta_E + \beta^{ad}_b} v^{inj} \tag{93}$$

The dissolution component of the apparent leak, or $v^{app}_{leak} = \Sigma(h^f - h^1)$ is **negative**; i.e., a portion of the actual leak could be hidden by the effect of the additional dissolution.

8.3 DISSOLUTION CHARACTERISTIC TIME

Brine saturation is a slow process. Brine saturation occurs through multiple processes, including diffusion inside the boundary layer at the cavern wall and convection and diffusion through the cavern brine body. The whole process is difficult, perhaps impossible, to compute

exactly. In the following development, assume that the dissolution process can be simply characterized by a time constant, t_c^{diss}; i.e.,

- During a POT, we have $p_l = p_l^f + \left(p_l^1 - p_l^f\right)\cdot\exp\left(-t/t_c^{diss}\right)$ or:

$$\frac{Q_{diss}}{V} = -\beta\dot{p}_l = \frac{\beta}{t_c^{diss}}\left(p_l^1 - p_l^f\right)\cdot\exp\left(-t/t_c^{diss}\right) = 0.043\ \frac{\beta}{t_c^{diss}}\ p_l^1\cdot\exp\left(-t/t_c^{diss}\right) \tag{94}$$

- During an NIT, we have $h = h^f + \left(h^1 - h^f\right)\cdot\exp\left(-t/t_c^{diss}\right)$ or:

$$\frac{Q_{diss}^{NLT}}{V} = -\Sigma\dot{h} = \left(v_g^1 + \frac{\beta_b^{ad} - a_s + \varpi}{\beta_c + \beta_b^{ad}}v^{inj}\right)\cdot\frac{\exp\left(-t/t_c^{diss}\right)}{t_c^{diss}}\Bigg/\left[1 + \left(\beta_c + a_s - \varpi\right)V_c^a\left(\frac{P_g^1}{v_g^1} + \frac{g\left(\rho_b^o - \rho_g^o\right)}{\Sigma}\right)\right] \tag{95}$$

where t_c^{diss} is a constant from empirical origin. From the results of the Etrez test described later (see Section 12.2), it can be inferred that t_c^{diss} is a few days long, say, t_c^{diss} = 2.5 days. However, Remizov et al. [2000] states this time is even shorter. The dissolution characteristic time may be less than this estimate.

Note that when crystallization (instead of dissolution) takes place after a pressure drop, the associated characteristic time is likely to be different.

9.0 CREEP

In this chapter, the effects of salt creep are discussed. Lessons drawn from in situ data are discussed in Section 9.1. The main features of rock salt mechanical behavior are described in Section 9.2. Steady-state creep and transient creep are defined in Sections 9.3 and 9.4. Section 9.5 provides discussion of other geological factors that affect creep and presents the stead-state creep closure rates for simple geometric forms. The transient effect of a rapid pressure build-up is computed in Section 9.6. It is proved that, in contrast with what is observed during in situ tests, numerical computations predict no cavern volume increase after a rapid pressure build-up, except when the pressure build-up is quite large. Additional testing and modeling should be needed to address this issue.

9.1 CASE STUDIES

All solution-mined cavities converge as they gradually, and quite slowly, close by salt creep. Prediction of the volume loss rate has led to numerous works. A few facts are presented here.

Subsidence is experienced at several storage sites; see, for example, Menzel and Schreiner [1983], Ratigan [1991], Durup [1991], Van Sambeek [1993], and Quintanihla de Menezes and Nguyen Minh [1996]. However, no ground level damage resulting solely from cavern convergence has been experienced as the subsidence bowl slope is small.

Some natural-gas storage facilities have experienced large losses of volume (several percent per year) (see Baar [1977], Röhr [1974], Boucly and Legreneur [1980], Boucly [1981], Staupendahl and Schmidt [1984], Quast and Schmidt [1983], Denzau and Rudolph [1997], and Cole [2002]).

Convergence rates in shallow, fluid-filled caverns are slow. Brouard [1998] measured brine outflow from the cavern well in a brine-filled, 950-meter-deep, 7,500 ± 500-m^3 cavern at the Etrez site. The test was performed 15 years after cavern leaching. In this small cavern, the effect of brine thermal expansion became negligible after such a length of time; the (as measured) 7.2 liters/day brine outflow can be attributed to cavern convergence. The relative volume loss rate was $\dot{V}/V = -3 \cdot 10^{-4}$/year, a very small figure when compared to what can be expected in a natural gas storage facility. More recently, Brouard et al. [2004] measured 20 liters/day outflow from a 700-meter-deep cavern of the Carresse site. The cavern volume was not known exactly, but the relative volume loss rate was probably close to $\dot{V}/V = -7 \cdot 10^{-4}$/year. However, faster closure rates can be expected in much deeper caverns; data from a cavern more than 2,000 meters deep can be found in You et al. [1994].

Data available for fluid-filled caverns are more-or-less related to the "steady-state behavior" of a cavern. For instance, the brine out-flow tests were performed by Brouard in caverns that had remained idle for several years preceding the test. Because of the long idle time, the thermal effects were negligible, and the cavern experienced constant pressure for a long period of time before the test began.

Few data are available when "transient behavior" is considered; i.e., when pressure changes rapidly before the test. Description of a test performed in the Kiel 101 cavern can be found in Baar [1977] where severe volume losses were experienced after a cavern pressure drop. However, complete interpretation of this test is not available, and the cavern pressure history in this case is not the type of pressure history in which we are interested. (In the Kiel case, transient consequences of a large pressure *drop* are observed; during an MIT test, a large pressure *increase* is experienced.)

The single "transient test" described in the literature, to our knowledge, is Hugout's [1984] test. Similar tests were performed recently by Brouard et al. [2004]; these Carresse caverns will be described in more detail later (Section 12.3).

9.2 ROCK MECHANICAL TESTING

Motivated by the needs of salt mining; hydrocarbon storage; and above all, nuclear waste disposal, no other rock has given rise to such a comprehensive set of laboratory experiments. The interested reader is invited to refer to the five *Proceedings of the Conferences on the Mechanical Behaviour of Salt* edited by Hardy et al. A full description of these efforts is beyond the scope of this report; we will focus on the main results, which are widely accepted by rock mechanics experts.

Salt behavior is elastic-ductile when short-term compression tests are considered; it is elastic-brittle when tensile tests are considered. The same behavior (elastic-brittle) is expected when a brine pore pressure greater than the smallest applied compressive stress is applied, a configuration met when hydrofracturing is performed in a well. However, in the long term, salt "flows" even under small deviatoric stresses (i.e., when the state of stress is not purely isotropic). In fact, steady-state creep (reached after several weeks or months when a constant load is applied to a sample) must be distinguished from transient creep (effective during a period of several weeks after mechanical loading is applied or after mechanical loading is changed). Furthermore, laboratory tests prove that salt creep is temperature-sensitive: under two identical mechanical loadings and two distinct temperatures, the higher temperature specimen will experience a faster creep rate than the specimen at the lower temperature.

9.3 STEADY-STATE CREEP

The following simple model, or Norton-Hoff model, captures the main features of the steady-state rock salt creep:

$$\dot{\varepsilon}_{ss} = -A \cdot \exp\left(-\frac{Q}{\Re T}\right) \cdot \sigma^n \tag{96}$$

where $\dot{\varepsilon}_{ss}$ is steady-state strain rate; σ is the differential stress applied to test samples; T is the (absolute) rock temperature; and A, $Q/\Re$, and n are model parameters. Values of the three constants collected by Brouard and Bérest [1998] are given in Table 2 for 15 different salts. The constant n is in the range n = 3–6, illustrating the highly nonlinear effect of the applied stress.

Table 2. Typical Salt Creep Parameters (After Brouard and Bérest [1998]. Original data can be found in Van Sambeek [1993], DeVries [1988], Munson et al. [1989], Wawersik [1984], Pouya [1991], Senseny [1984], Heusermann [1993].) $\dot{V}/V$ is the steady-state convergence rate of a hypothetical brine-filled spherical cavern opened to the atmosphere and located at a 1,000-m depth where the temperature is assumed to be 42°C (108°F)

No.	Facility	n	Q/R (K)	A (/year-MPa^n)	$(\dot{V}/V)^{\text{sphere}}_{1,000\text{ m}}$ (%/year)
1	Avery Island (DeVries)	3.14	6,495	$1.30 \cdot 10^4$	–0.29
2	WIPP	5.0	5,035	1.04	–0.0043
3	Salado	5.19	8,333	$3.67 \cdot 10^4$	–0.0044
4	Asse (Wawersik)	6.25	9,969	$2.51 \cdot 10^4$	–0.000016
5	West Hackberry WH1	4.73	6,606	452.31	–0.012
6	West Hackberry WH2	4.99	10,766	0.94	$-5 \cdot 10^{-11}$
7	Bryan Mound BM3C	4.54	7,623	$1.32 \cdot 10^3$	–0.0014
8	Bryan Mound BM4C	5.18	8,977	$1.04 \cdot 10^5$	–0.0016
9	Bayou Choctaw	4.06	5,956	64.03	–0.012
10	Etrez	3.1	4,100	0.64	–0.028
11	Avery Island (Senseny)	4.0	6,565	2081	–0.055
12	Salina	4.1	8,715	$2.7752 \cdot 10^5$	–0.0082
13	Palo Duro – Unit 4	5.6	9,760	$1.806 \cdot 10^5$	–0.00024
14	Palo Duro – Unit 5	5.3	9,810	$2.52 \cdot 10^5$	–0.00028
15	Asse (Heusermann)	5.0	6,495	65.7	–0.0027

9.4 TRANSIENT CREEP

The transient creep behavior of salt has been studied by several authors. Transient creep is triggered by any change in the applied load and is especially significant when the loading change is large and rapid. Keeping in mind that we are interested mainly in the mechanical behavior of a cavern during an MIT test, we focus on the case in which a "stress drop" is applied to the sample. In some cases, when the stress drop is large enough, sample height increases for a while after the stress drop was applied. This phenomenon was observed during laboratory creep tests and is referred to as "reverse creep" [Van Sambeek, 1993; Hunsche, 1991; Munson, 1997; Charpentier et al., 1999]. This phenomenon is not taken into account in the following.

The Munson [1997] creep law reduces to the following rheological model for temperature and stress conditions around a cavern:

$$\dot{\varepsilon}^{vp} = F \cdot \dot{\varepsilon}_{ss} \quad \text{with} \quad \dot{\varepsilon}_{ss} = A \cdot \exp\left(-\frac{Q}{\Re T}\right) \cdot \sigma^n \tag{97}$$

$$F = \begin{cases} e^{\Delta(1-\zeta/\varepsilon_t^*)^2}; & \zeta \le \varepsilon_t^* \\ 1 & \\ e^{-\delta(1-\zeta/\varepsilon_t^*)^2}; & \zeta \ge \varepsilon_t^* \end{cases} \tag{98}$$

$$\varepsilon_t^* = K_o e^{cT} \sigma^m \tag{99}$$

$$\Delta = \alpha_w + \beta_w \mathrm{Log}_{10} \frac{\sigma}{\mu} \tag{100}$$

The parameter ζ is an internal variable whose evolution is described by the following equation:

$$\dot{\zeta} = (F-1) \cdot \dot{\varepsilon}_{ss} \tag{101}$$

The constants of this model have been fitted to transient creep tests performed on different salts [Munson, 1998], and three sets of parameters are given in Table 3. Note that Munson law predicts no reverse creep during an uniaxial test. Munson law predicts that after a stress drop, the strain rate remains slow for a while, and that the strain rate is slower the longer the stress was applied before the stress drop.

For the SPR3 cavern (see Section 5.2.2.4), the following parameters were fitted to in situ experiments:

$$A \cdot \exp\left(-\frac{Q}{\Re T_R^{\infty}}\right) = 0.9 \cdot 10^{-8} / \mathrm{day} - \mathrm{MPa}^n \text{ and } n = 3.1 \tag{102}$$

$$\delta = 0.58, \quad K_o = 1.9 \cdot 10^{-3} / \mathrm{MPa}^n, \quad \alpha_w = 6, \quad \beta_w = 0, \quad m = 1.3 \tag{103}$$

The Norton-Hoff steady-state creep law and the Munson-Dawson transient creep law will be considered below.

Table 3. Typical Munson-Dawson Creep Parameters (After Munson [1999])

Salt	Waste Isolation Pilot Plant	Avery Island	Argillaceous Salt
A (/MPa^n-year)	$8.1 \cdot 10^7$	$1.1 \cdot 10^7$	$1.3 \cdot 10^8$
$Q/\Re$ (K)	12,590	12,590	12,590
n	5.5	5.5	5.5
α_w	−17.37	−13.20	−14.96
m	3.0	3.0	3.0
β_w	−7.738	−7.738	−7.738
c (/K)	0.0092	0.0092	0.0092
δ	0.58	0.58	0.58
K_o (/MPa^n)	$3.3 \cdot 10^{-7}$	$7.0 \cdot 10^{-7}$	$9.3 \cdot 10^{-7}$
μ (GPa)	12.4	12.4	12.4

9.5 CAVERN BEHAVIOR PREDICTION

The constitutive behavior of salt, the description of the geological layers, and the history of cavern pressure allow, in principle, the mechanical behavior of a cavern to be computed. However, a few general comments are useful.

1. The actual behavior of a salt formation may differ to some extent from the specimen behavior observed in the laboratory. This is sometimes referred to as "scale effect," which results from various factors, among which is the existence of nonsalt layers that, even when thin, may strongly influence the cavern response to mechanical loading. (The creep rate is slower when the salt formation contains interbedded anhydrite layers and faster when it contains carnallite layers.)

2. In a cavern, the effects of various physical phenomena intermingle; among these, mechanical phenomena are only one of the effective processes. For instance, during a shut-in pressure test, both cavern creep *and* brine warming contribute to the observed pressure changes. Brine warming is often the dominant factor in this context. After a

rapid pressure change, both transient rock mass creep *and* additional dissolution contribute to cavern volume changes.

3. During a laboratory test on a rock sample, the state of stress in the sample is assumed to be homogeneous. The same cannot be said of the rock mass in the vicinity of a cavern; there, the stress distribution is not homogeneous. Relatively large deviatoric stresses exist close to the cavern wall while the state of stress becomes isotropic at larger distances from the cavern wall. When a rapid pressure change is imposed on a cavern, the resulting measured pressure history is affected by two distinct transients:

   (a) The *rheological* transient behavior (transient creep), which can be described with a transient creep law

   (b) A *geometrical* transient behavior, resulting from the slow redistribution of the incremental stresses resulting in a new final steady-state stress distribution, which is reached after the (modified) cavern pressure is kept constant for a sufficient amount of time. This geometrical transient behavior cannot be observed during most laboratory tests, as stress distribution is uniform through the sample. The geometrical transient behavior is clearly recognized in the numerical modeling of underground salt-mining situations using steady-state creep laws.

9.5.1 Overburden Pressure, Cavern Pressure, Rock Temperature

The driving force for rock mass (salt) creep is the difference between the overburden pressure (stress), P_{ob}, and the cavern pressure, P_i. In other words, recalling Figure 1, the deeper the cavern, the faster the creep and subsequent cavern volume (when other conditions, cavern shape, distance between neighboring caverns and salt composition are identical). However, rock temperature also plays a role, and because temperature is usually warmer at greater depths, the behavior of a deep cavern is significantly different from the behavior of a shallow cavern.

The overburden pressure (resulting from gravitational forces) may be related to cavern depth (H) and rock mass density. A typical overburden distribution is

$$P_{ob}\ (\text{MPa}) = 0.022\ H\ (\text{m}) \tag{104}$$

For example, the overburden pressure is nominally 22 MPa at a depth of 1,000 meters (3,200 psi at 3,300 feet or about 1 psi/foot).

The cavern pressure (P_i), when the cavern is opened to the atmosphere and the well is filled with saturated brine, is the "halmostatic pressure" and is equal to:

$$P_o\ (\text{MPa}) = 0.012\ H\ (\text{m})\ \ [\text{or}\ P_o(\text{psi}) = 0.52\ H(\text{ft})] \tag{105}$$

However, when the cavern pressure is increased at the beginning of an MIT test by $p_i^!$ (testing pressure), the cavern pressure becomes $P_i = P_o + p_i^!$.

In general, cavern creep leads to cavern shrinkage; loss of cavern volume; and, for a closed cavern, increased cavern pressure. However, after a rapid pressure increase, as at the beginning of an MIT test, caverns of certain shapes can be enlarged as a result of transient creep.

9.5.2 Steady-State and Transient Creep for Simple Shapes

The Norton-Hoff creep model allows closed-form solutions for the steady-state creep closure of spherical or cylindrical caverns, idealized shapes that give a valuable approximation in the case of many actual caverns:

- Spherical cavern $$\frac{\dot{V}}{3V} = \frac{\dot{R}}{R} = -\frac{1}{2}\left[\frac{3}{2n}\left(P_- - P_o - p_i^!\right)\right]^n A \cdot \exp\left(-\frac{Q}{\Re T_R^-}\right) \quad (106)$$

- Cylindrical cavern $$\frac{\dot{V}}{2V} = \frac{\dot{R}}{R} = -\frac{\sqrt{3}}{2}\left[\frac{\sqrt{3}}{n}\left(P_- - P_o - p_i^!\right)\right]^n A \cdot \exp\left(-\frac{Q}{\Re T_R^-}\right) \quad (107)$$

Where R is the cavern radius, $\dot{R}$ is the wall velocity, and T_R^- is the absolute temperature ($T_R^- = \theta_R^- + 273$ in Kelvin, θ_R^- in degree Celsius). These formulae for the normalized closure of caverns have been given and discussed by Hardy et al. [1983] and Van Sambeek [1990]. They provide useful orders of magnitude and clearly explain that the volume loss-rate in a fluid-filled cavern is larger by two orders of magnitude when cavern depth is doubled. However, in an MIT test, we are mainly interested in the effects of transient creep.

9.6 TRANSIENT BEHAVIOR

In this section, the only delayed phenomenon taken into account in finite element computations is salt creep. Computations were performed with the help of Mehdi-Karimi Jarimi, École Polytechnique. The Munson-Dawson law is considered with the parameters given by Munson [1998] for WIPP salt (see Table 3). For the sake of simplicity, we consider the case of a spherical cavern. When the cavern is created, the elastic state of stress that develops inside the rock mass is such that the tangential stress is more compressive than the radial stress. After the cavern is kept idle for a long period of time, the gap between the tangential stress and the radial stress slowly decreases and eventually reaches its steady-state value. Now, when cavern pressure is significantly increased, the (instantaneous) elastic response is such that, in some cases, the tangential stress becomes less compressive than the radial stress. During a transient period, cavern volume may increase.

We considered a 1,000-meter-deep spherical cavern. The cavern is leached out in 100 days and kept idle during 1,900 days after leaching is completed. At Day 2,000, cavern pressure is suddenly increased by $p_i^!$. Three different values of $p_i^!$ were considered. After the test pressure is applied, the cavern pressure continues to slowly build up at a constant rate.

Figures 22 and 23 provide the cavern pressure history before, during, and after the test, respectively, for a pressure build-up of $p_i^!$ = 2 MPa. Figures 24 and 25 provide the cavity pressure evolution when the pressure increase is $p_i^!$ = 4 MPa. Figure 26 and 27 provide the cavity pressure evolution when the pressure increase is $p_i^!$ = 9 MPa.

The following conclusions can be drawn (for the modeled conditions):

- Cavern pressure continues to increase (cavern shrinks) after fluid injection when the pressure increase is 2 or 4 MPa,
- The rate of pressure increase is very slow immediately after fluid injection: it is slower than what it will be when steady-state is reached, and still slower than what it was before fluid injection,
- The rate of pressure increase is slower when the cavern had been kept idle during a longer period before fluid injection,
- Inverse creep (cavern volume increase leading to pressure decrease) is not observed. This result is not unexpected, as the Munson-Dawson transient creep law used for these runs does not include inverse creep.[4]

[4] Moreover, based on the results of in situ tests (see Chapter 12.0), it is clear that inverse creep is not observed except when the initial pressure build-up is large ($p_i^!$ = 9 MPa) and when the cavern is squat (presumably a large roof area compared to the cavern wall area). Additional modeling efforts are needed to capture this feature of cavern mechanical behavior. However, at this stage, the existing database is too small to provide a sound basis for such an effort.

RSI-1476-05-026

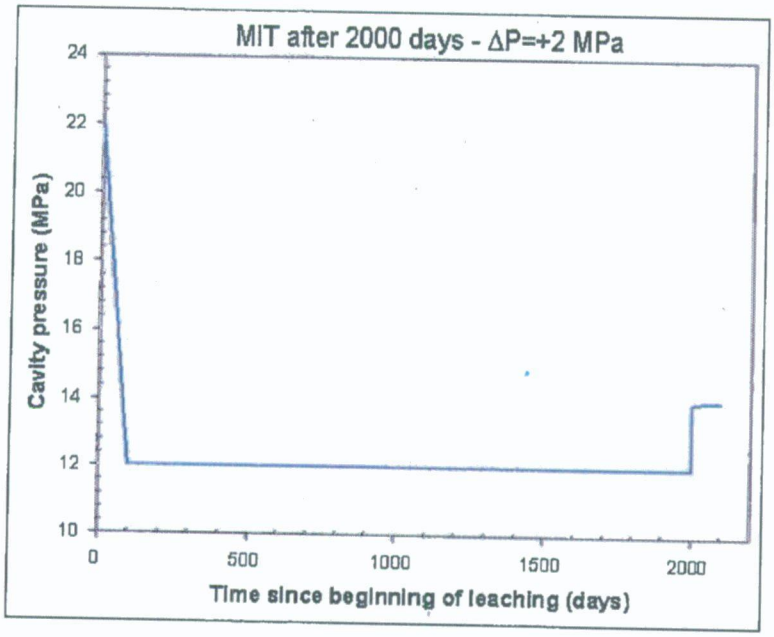

Figure 22. Cavity Pressure History (MIT Performed 2,000 Days After the End of Leaching, p_i^1 =+2 MPa).

RSI-1476-05-027

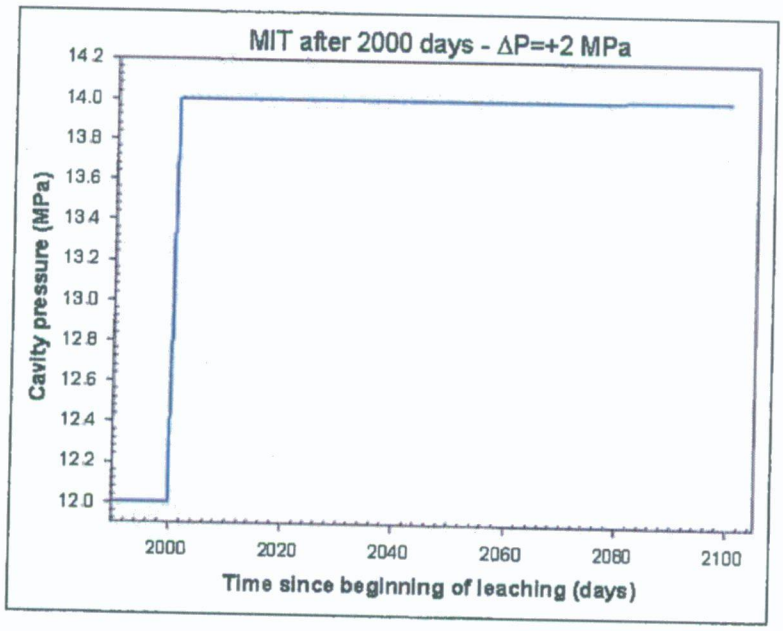

Figure 23. Cavity Pressure After Pressure Build-Up (MIT Performed 2,000 Days After the End of Leaching, p_i^1 = +2 MPa) [zoomed from Figure 22].

RSI-1476-05-028

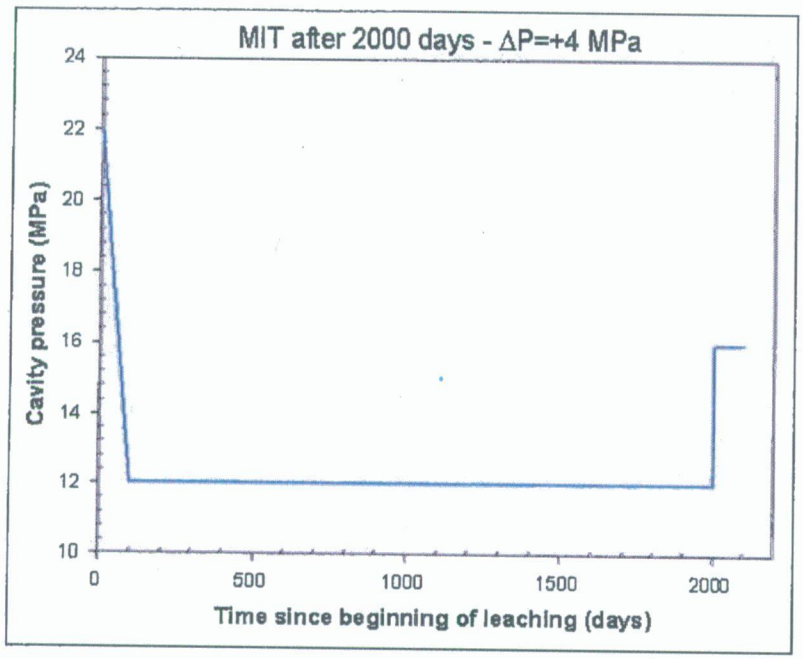

Figure 24. Cavity Pressure History (MIT Performed 2,000 Days After the End of Leaching, $p_i^1 = +4$ MPa).

RSI-1476-05-029

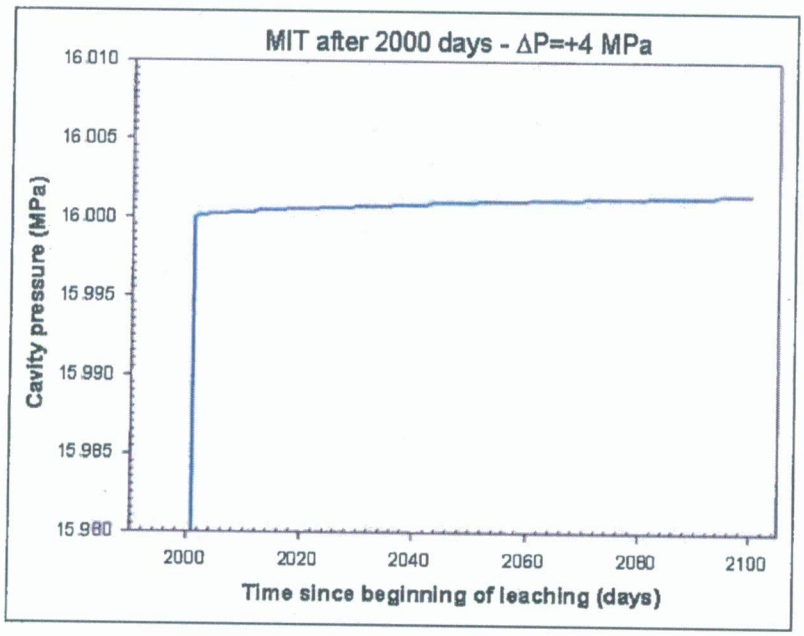

Figure 25. Cavity Pressure After Pressure Build-Up (MIT Performed 2,000 Days After the End of Leaching, $p_i^1 = +4$ MPa) [zoomed from Figure 24].

RSI-1476-05-030

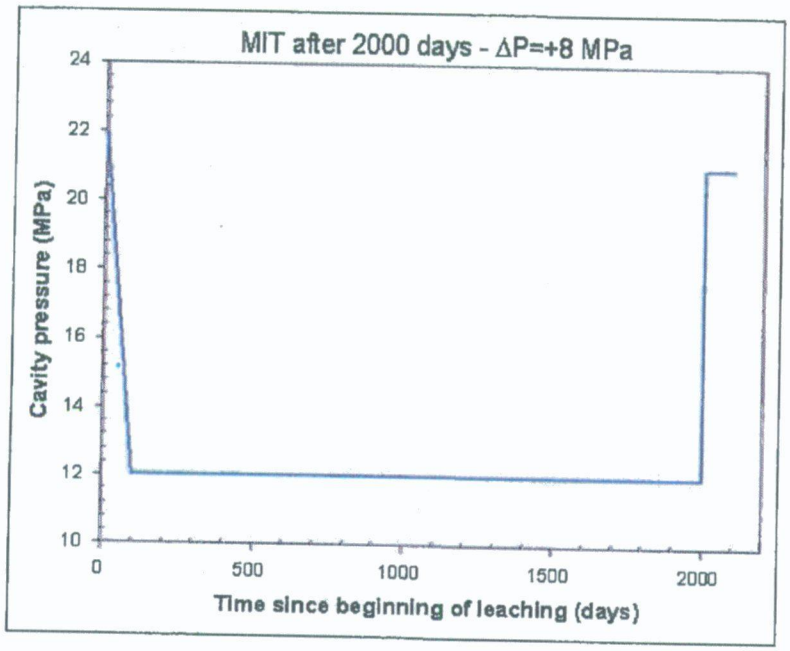

Figure 26. Cavity Pressure History (MIT Performed 2,000 Days After the End of Leaching, p_i^1 = +9 MPa).

RSI-1476-05-031

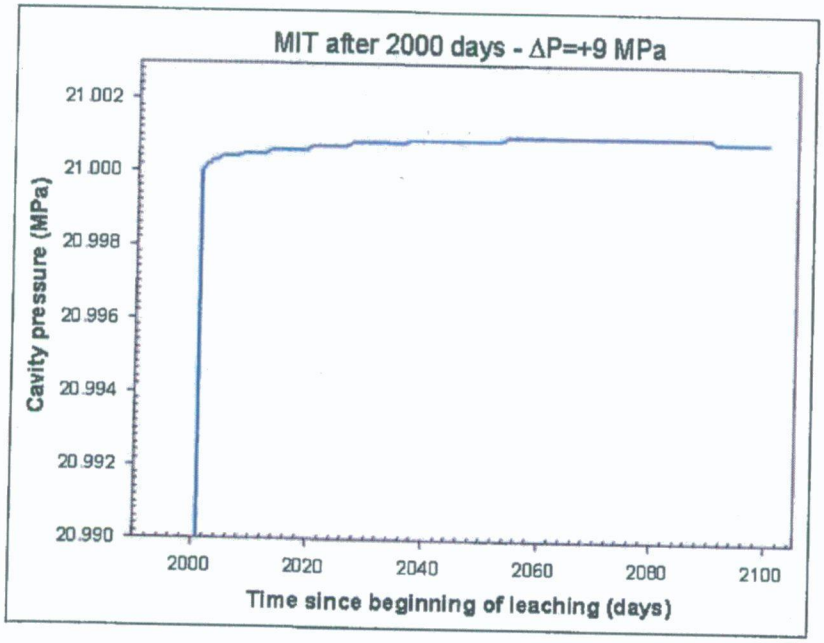

Figure 27. Cavity Pressure After Pressure Build-Up (MIT Performed 2,000 Days After the End of Leaching, p_i^1 = +9 MPa) [zoomed from Figure 26].

10.0 LIQUID-LIQUID INTERFACE TEST: ANALYSIS OF PRESSURE OBSERVATION AND PRESSURE DIFFERENCE OBSERVATION TESTS

The Pressure Observation Test (POT) [Thiel and Russel, 2004] consists of lowering a light liquid or liquefied hydrocarbon column in the annular space. In some cases, when the cavern is filled with hydrocarbons before the test is performed, one simply can withdraw enough hydrocarbon from the cavern to allow the brine-hydrocarbon interface to be located a few meters below the casing shoe [Thiel and Russel, 2004]. During the test, the change in brine and hydrocarbon pressures is measured at the wellhead. A severe pressure-drop rate (especially when linear) is a clear sign of poor tightness. More precisely, the brine pressure drop, $P_2 - P_1 < 0$, during a given interval of time, $t_2 - t_1$, is multiplied by the cavern compressibility, βV, to obtain an apparent-leak flow rate, $Q_{app} = -\beta V \cdot (P_2 - P_1)/(t_2 - t_1)$ [Thiel and Russel, 2004].

However, a more sophisticated interpretation is possible when considering the changes in the difference between the (hydrocarbon-filled) annular space pressure and the (brine-filled) central string pressure [Diamond, 1989; Diamond et al., 1993; Bérest et al., 2001a]. This method (the Pressure Difference Observation, or PDO) is explained below.

10.1 ADVANTAGES OF THE TWO PRESSURE TEST METHODS

The POT and PDO tests are simpler than the Nitrogen Interface Test and have the following advantages:

- For a given cavern test pressure, hydrocarbon, which is heavier than nitrogen, involves lower wellhead pressures.
- Pressure change is recorded at the wellhead; thus, no logging tool is necessary.
- Costs are lower (no logging tool, no nitrogen injection).
- There is no nitrogen contamination [Thiel and Russel, 2004].
- When the test is performed in a cavern used for storing light liquid hydrocarbon, complete product removal is not necessary.
- The stored liquid can be used as a testing liquid, making liquid-leak assessment more realistic.

The POT and PDO also have several disadvantages:

- There are different safety concerns than there are when using nitrogen.
- The POT is a little less demanding from the perspective of checking tightness (pressures are smaller near the surface; in comparable conditions, nitrogen leaks are larger and more easily detected than hydrocarbon leaks).
- In a POT, the entire cavern is tested; the actual leak (through the casing and casing shoe) can not be separated from the phenomena which affect the cavern.
- The main weakness of the POT and the PDO tests is that the high viscosity of liquid/liquefied hydrocarbons (when compared to the viscosity of nitrogen) reduces test sensitivity (see Section 4.6).

10.2 A TYPICAL POT

During a POT, the well is equipped with a length of central tubing a little longer than the length of the last cemented casing. The annular space is filled with a liquid hydrocarbon. The hydrocarbon/brine interface in the annular space is located below the last casing shoe. Pressure is increased in the annular space to the test pressure. In fact, pressure is increased in two steps. During the prepressurization phase, the pressure is increased rapidly to a pressure somewhat smaller than the test pressure. After a stabilization period lasting a few days, the pressure is increased slowly (in one or a few hours) to the test pressure. It is important that the injected brine density is constant during the prepressurization and final pressurization phases. The second phase data are used to measure the cavern compressibility, or βV, in m^3/MPa or bbls/psi (see Figure 28). Cavern compressibility is best measured during this second phase because:

1. The cavern pressure is close to the test conditions.
2. Small head losses are expected during this slow pressure increase phase, which provides more accurate data.

After the test pressure is reached, injection stops and the pressure change at the wellhead is recorded versus time. Both the annular space pressure and the central tubing pressure are recorded. Figure 29 gives typical pressure versus time curves (after Thiel and Russel [2004]). The observed rate of pressure decrease (it is convenient to use MPa/year, or psi/year) is multiplied by cavern compressibility (as measured during pressurization) to get the (apparent) leak rate in m^3/year or bbls/year, which, in this case, is about 490 m^3/year. According to Thiel and Russel [2004], 1,000 bbls/year (160 m^3/year) is a typical maximum admissible leak rate. When the rate is larger than this figure, a second test ("second cycle") is performed in which pressure is built up again to the test pressure and the change in pressure is recorded (see Figure 29).

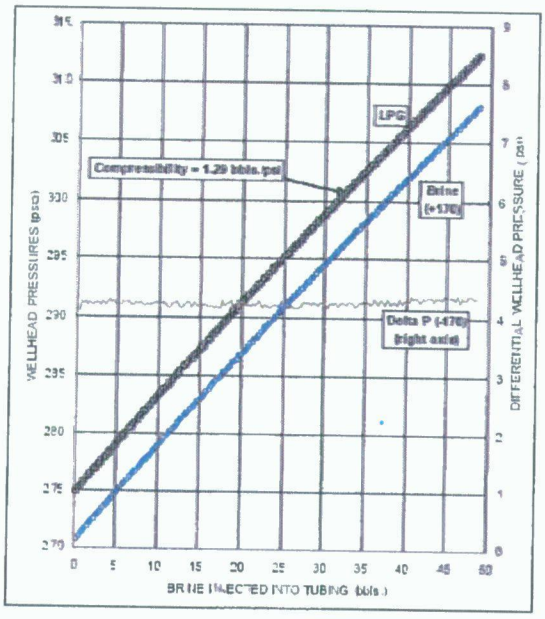

Figure 28. Pressurization Data During a Pressure Observation Test in Kansas (Thiel and Russel [2004]). The plotted brine pressures were increased by 170 psi so it could be plotted on the same scale as the LPG pressure. Similarly, the ΔP (brine pressure minus LPG pressure) was reduced by 170 psi for plotting.

10.3 A TYPICAL PDO TEST

During a POT, the annular pressure-versus-time curve and the central tubing-versus-time curve are not perfectly parallel, even though from a hydraulics perspective, the annular space and the central tubing are linked through the cavern at the bottom of the well.

The difference between the slopes of the two curves can be explained as follows: saturated brine (density = ρ_b = 1,200 kg/m^3) is heavier than hydrocarbon (density = ρ_h = 900 kg/m^3, approximately). If a hydrocarbon leak occurs (through the cemented casing or through the casing shoe), both the central tubing pressure and the cavern pressure decrease by the same amount. In addition, the hydrocarbon/brine interface rises because of the hydrocarbon leak. (Let $Q_{leak} > 0$ be the leak rate; Σ is the cross-sectional area of the cavern neck at the interface depth (in m^2 or ft^2), and Q_{leak}/Σ is the interface rise rate.) The column composition after a leak is different than when a test begins because the hydrocarbon column is shorter. Therefore, the subsequent $\Delta P = P^{wh}_{ann} - P^{wh}_{tub}$ changes whenever an additional pressure drop takes place in the annular space.

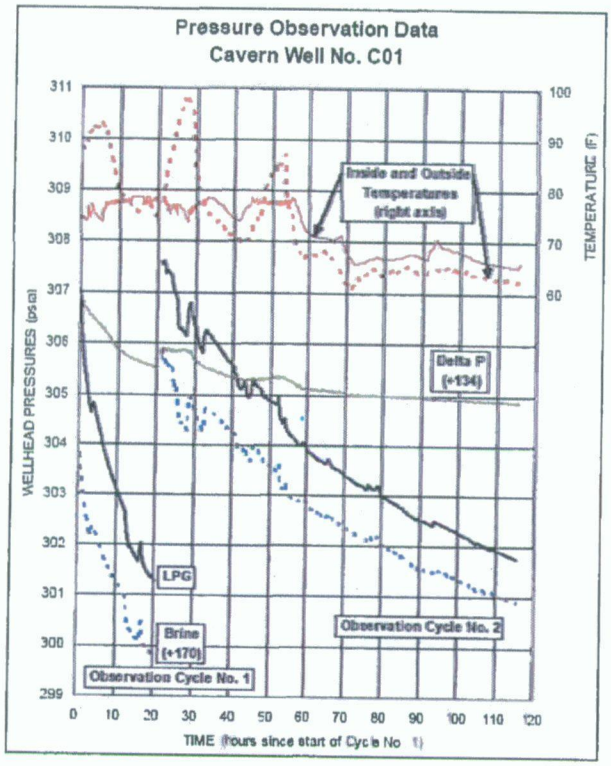

Figure 29. Two Different Curves Are Plotted Associated With Two Observation Cycles. (Initial pressurization and pressure increase again after 20 Hours. $\Delta P = P_{ann}^{wh} - P_{tub}^{wh}$ is the pressure difference; the cavern neck cross section at interface depth is unknown). The brine pressure and ΔP are modified by the amounts indicated for plotting (After Thiel and Russel [2004]).

This pressure difference effect can be computed as follows. Let Q (in m^3/s or bbl/s) be the brine or cavern volume change rate because of phenomena such as transient creep, additional dissolution, thermal expansion, etc.

$$Q = Q_{th} - Q_{perm}^{tr} - Q_{th}^{ad} - Q_{cr}^{tr} - Q_{diss} + Q_{cr}^{ss} - Q_{perm}^{ss} \tag{108}$$

Note that $Q > 0$ when thermal expansion prevails and $Q < 0$ when additional dissolution and transient creep prevail. When a hydrocarbon leak takes place ($Q_{leak} > 0$ in m^3/s, or bbls/s), the following occurs:

- Cavern pressure and wellhead tubing pressure decrease at a rate given by:

$$\frac{dP_i}{dt} = \frac{dP_{tub}^{wh}}{dt} = \frac{Q - Q_{leak}}{\beta V} < 0 \tag{109}$$

- Wellhead annular space pressure decreases by a larger amount as the interface rises (g = 9.8 m²/s):

$$\frac{dP_{ann}^{wh}}{dt} = \frac{Q - Q_{leak}}{\beta V} - (\rho_b - \rho_h) g \frac{Q_{leak}}{\Sigma} < 0 \qquad (110)$$

The exact value of Q is sometimes difficult to assess, as discussed above. However, when one considers the change in the difference of the two pressure rates as measured at the wellhead (instead of separately considering the changes in the two pressure rates), one gets:

$$\frac{dP_{ann}^{wh}}{dt} - \frac{dP_{tub}^{wh}}{dt} = -(\rho_b - \rho_h) g \frac{Q_{leak}}{\Sigma} < 0 \qquad (111)$$

This phenomenon is observed clearly during the test presented in Figure 29 (ΔP is the pressure difference at wellhead). A second example is described in Section 12.8. .Note that the PDO method can be used **in addition to** the POT method with only small or no additional costs. A similar method described in Section 12.7 provides for detection of a leak through the central tubing (from the wellhead, for example), but the procedure is more complicated.

The PDO method does not work when

- Brine leaks at the wellhead.
- The central tubing is not tight, and hydrocarbon accumulates at the top of the central tubing. Nevertheless, the leak from the annular space to the tubing can be calculated if the annular cross section is relatively large.

However, in both of these instances, leaks are easy to detect or observe. Furthermore, P_{tub}^{wh} and P_{ann}^{wh} experience fluctuations related to ground temperature variations (Section 6.2). These fluctuations can be partially removed by considering 24-hour-long periods.

10.4 CROSS-SECTIONAL AREA AT THE INTERFACE DEPTH

In the PDO method discussed above, the value of the interface cross-sectional area, Σ, at interface depth must be accurately known to convert the pressure difference rate into a leak rate. In some cases, this information can be obtained readily when the exact shape of the cavern is known (through sonar surveys) or when the cavern neck exhibits a perfectly cylindrical shape. In many cases, either this information is not available or the exact location of the brine/hydrocarbon interface is not known. In these cases, the following procedure may be used.

The maximum admissible leak rate is, say, 1,000 bbls/year. In fact, in most cases, the actual hydrocarbon leak rate is much smaller–say, 200 bbls/year. With a test duration of 10 days, the amount of leaked hydrocarbon during this period will be approximately 5 bbls or less. Before the test, the brine/hydrocarbon interface is located at a depth slightly less than the test interface depth. Then, 5 bbls of hydrocarbon are injected into the cavern, and the difference

between the changes in brine pressure and hydrocarbon pressure are measured accurately at the wellhead. The change in the difference between the two pressures, as a function of the hydrocarbon-injected volume, can be plotted. This measurement is quite similar to the measurement of cavern compressibility; however, hydrocarbon, instead of brine, is injected.

When the test proper is performed, the pressure difference versus injected volume curve can be used to interpret the test: the pressure difference change is converted into a leaked volume (see Figure 30).

RSI-1476-05-034

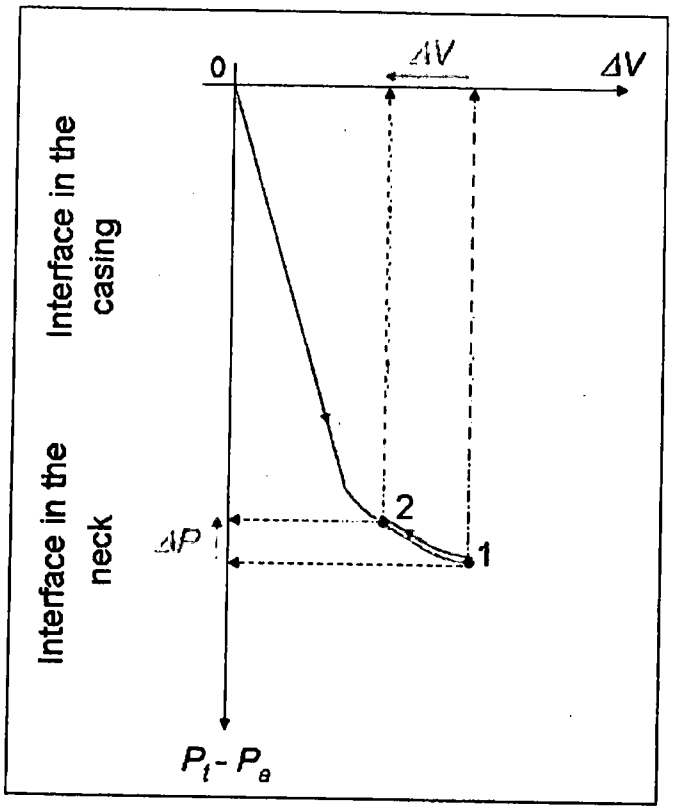

Figure 30. The 0-1 Curve Is the Wellhead Pressure Difference Versus Injected Volume as Observed at the End of the Pressurization Period. ΔP (during 1-2) is the pressure difference drop as observed during the test, which can easily be converted in a leaked volume ΔV using the 0-1 curve.

10.5 TEST SEQUENCE

A proposed test sequence (or list of test steps) is as follows:

1. Remove product from the cavern (wellhead) pressure.
2. Set the brine/hydrocarbon interface in the annular space a few meters above the casing shoe by injecting hydrocarbon and allowing brine to flow from the tubing.

3. Close the wellhead and perform a shut-in pressure test (3 days) to measure the tubing pressure increase rate in the closed cavern. (No pressurization is performed at this step.)

4. Prepressurize the cavern (brine injection) to a pressure slightly smaller than the test pressure.

5. Let the cavern stabilize (5 days).

6. Inject (1 hour) a small amount of hydrocarbon in the annular space to reach the desired test interface location. Plot the pressure-versus-injected volume curve for both the annular space and the central tubing.

7. Let the cavern stabilize (a few hours).

8. Record the pressure-versus-time changes, both in the annular space and in the central tubing. Use precision instrumentation as described, for example, by Thiel and Russel [2004].

9. Withdraw the hydrocarbon, measure its volume, back-calculate the brine/hydrocarbon interface location and check that the interface was located below the casing shoe during the test.

10. Check that no hydrocarbon is contained at the top of the central brine string.

11. Interpretation

    a. **Apparent Leak**: Add to the central-tubing pressure drop rate (computed on a 24-hour, 48-hour, or 72-hour basis) the pressure increase rate that was observed during the shut-in pressure test (from Step 3). Divide by cavern compressibility to get the apparent leak rate.

    b. **Hydrocarbon Leak**: Plot the pressure difference change (annular pressure minus tubing pressure). Compare with the pressure difference change-versus-injected volume curve recorded during Step 6 to get the hydrocarbon leaked volume.

10.6 ACCURACY OF THE PDO TEST

Actual hydrocarbon leaks through the casing and the casing shoe are expected to be smaller than the apparent leaks observed through a standard POT. Assume, for instance, that we try to detect a 30-m^3/year (180 bbls/year) hydrocarbon (ρ_h = 900 kg/m^3) leak; i.e., a 0.1-m^3/day (0.63-bbls/day) leak. Here, the decrease in daily pressure is

$$P_{ann}^{wh} - P_{tub}^{wh}\ (\text{kPa}) = 0.3/\Sigma\ (\text{m}^2) \quad \text{or} \quad P_{ann}^{wh} - P_{tub}^{wh}\ (\text{psi}) = 4\cdot 10^{-3}/\Sigma\ (\text{ft}^2) \tag{112}$$

For example, when the cross section of the cavern neck at the interface depth is $\Sigma = 1$ m^2 (10 ft^2), the daily pressure-drop rate is $\dot{P}_{ann}^{wh} - \dot{P}_{tub}^{wh} = 3$ kPa/day or 0.4 psi/day when the neck cross

section is 0.1 m^2. This last figure is easy to detect; as seen later in Figure 45, the measurement system proposed by Thiel and Russel [2004] provides sufficient accuracy to detect this level of pressure decrease.

In fact, the accuracy is extremely good when cavern neck shape is well known and/or easy to measure. However, problems may occur with "no-neck" caverns, as emphasized in Section 12.9.

11.0 THEORETICAL ANALYSIS OF THE NITROGEN INTERFACE TEST (NIT)

11.1 MATHEMATICAL BASIS

The simplest interpretation of the NIT consists of multiplying the interface rise rate, or $\dot{h}$ (m/day or ft/day), by the cavern cross-sectional area at interface depth or Σ (in liters/m or bbls/m) to get the nitrogen volume change rate, or apparent leak Q_{app}:

$$Q_{app} = -\Sigma \dot{h} > 0 \quad \text{(in liters/day or bbls/day)} \tag{113}$$

This interpretation suffers from a fundamental flaw: the nitrogen leak is assumed to be the only factor that leads to interface displacement.

A better interpretation consists of taking temperature and pressure variations into account to compute the change in gas mass ($\dot{m}_g$) rather than in gas volume ($\dot{V}_g$):

$$\dot{m}_g = \frac{d}{dt}\int_0^h \rho_g(z,t) S_a(z)\, dz = \int_0^h \dot{\rho}_g(z,t) S_a(z)\, dz + \dot{h} \rho_g(h,t) S_a(h) \tag{114}$$

From the nitrogen equation of state, $P_g = r_g \rho_g T_g$, we have:

$$\dot{\rho}_g / \rho_g = \dot{P}_g / P_g + \dot{T}_g / T_g \tag{115}$$

where P_g is the gas pressure, ρ_g is the gas density, T_g is the gas (absolute) temperature, S_a is the annular space cross-sectional area at depth z, and r_g is a gas-specific constant. It is assumed that gas temperature T_g equals rock mass temperature at depth z. Gas temperature (T_g) and gas pressure (P_g) can be measured and/or computed through pressure and temperature logs; however, the accuracy of these measurements is often no better than that for measuring the interface displacement.

In the following, we propose a theoretical analysis of the NIT method.

11.1.1 Gas Equation of State

Nitrogen pressure distribution in the annular space column can be obtained easily through the equilibrium equation, provided that the gas pressure at the wellhead or $P_g^{wh}(t) = P_g(z=0,t)$, the nitrogen state equation, $\rho_g = \rho_g(P_g, T_g)$, and the geothermal temperature distribution, $T_R = T_R(z)$, are known:

$$\frac{\partial P_g}{\partial z} = \rho_g g \tag{116}$$

where z is the depth below ground, P_g is the nitrogen pressure, g is the gravitational acceleration constant, and P_g and ρ_g are functions of z and t.

As a first approximation, the nitrogen state equation can be written as $P_g = r_g \rho_g T_g$, where T_g is the (absolute) geothermal temperature (in Kelvin), $T_g = T_R^{\circ}(z) = T_g^{\circ} + G^{th} z$. Then:

$$\frac{1}{\rho_g}\frac{\partial \rho_g}{\partial z} = \frac{1}{P_g}\frac{\partial P_g}{\partial z} - \frac{1}{T_g}\frac{\partial T_g}{\partial z} = \left[\frac{g}{r_g} - G^{th}\right] \cdot \frac{1}{T_g} \tag{117}$$

So when $g/r_g = 3.3 \cdot 10^{-2}$ °C/m and the geothermal gradient is $G^{th} = 3 \cdot 10^{-2}$ °C/m, only a small error is introduced when assuming the gas density to be uniform along the well:

$$\rho_g(z,t) = \lambda P_g^{wh}(t) \tag{118}$$

where P_g^{wh} is the gas pressure measured at the wellhead. This assumption considerably simplifies further calculations. A more precise description of gas-pressure distribution in the well can easily be obtained using a computer, as shown by Nelson and Van Sambeek [2003]. In the case of nitrogen, $\lambda = 11.5$ m^3/kg-MPa.

11.1.2 Pressure Equilibrium

Let h be the brine/nitrogen interface depth (in m or ft). At the interface depth, the brine and nitrogen pressures are equal to P_g^{int}; let P_b^{wh} and P_g^{wh} be the brine pressure and nitrogen pressure as measured at the wellhead in the central tubing and the annular space, respectively:

$$P_b^{wh}(t) + \rho_b g h = P_g^{wh}(t) + \rho_g g h = P_g^{int} = 1/\beta_g^{int} \tag{119}$$

where ρ_b and ρ_g are the average brine density and nitrogen density in the well, respectively, and $\beta_g^{int} = 1/P_g^{int}$ is the (isothermal) gas compressibility (see Section 5.2.2.3).

11.1.3 Gas Mass

Let h^o be the interface depth at the beginning of the test (after the initial pressure increase). Σ is the annular space cross-sectional area at interface depth, and V_g^o is the initial gas volume (when $h = h^o$). The gas mass contained in the well can be written as

$$m_g = \rho_g \left[V_g^o + \Sigma(h - h^o)\right] \tag{120}$$

11.1.4 Other Factors

Let Q be the brine volume increase ($Q > 0$) because of brine thermal expansion (or the cavern volume loss ($Q > 0$) caused by cavern shrinkage). The cavern volume change caused by cavern brine pressure build-up ($\dot{P}_b = \dot{P}_b^{wh}$) is $\beta V \cdot \dot{P}_b$, where β is the cavern compressibility factor and V is the cavern volume (see Section 5.1). Then the apparent leak rate, deduced from interface location measurements, or $Q_{app} = -\Sigma\dot{h} > 0$ ($\dot{h} < 0$ when the interface rises), is

$$Q_{app} = -\Sigma\dot{h} = Q - \beta V \dot{P}_b \tag{121}$$

11.1.5 Interface Rise Rate

Combining Equations (113) to (121) leads to a relation between the corrected nitrogen leak rate ($Q_{leak}^{corr} > 0$), the apparent gas leak (Q_{app}), and (for instance) the brine thermal expansion ($Q > 0$):

$$Q_{leak}^{corr} = C \cdot Q_{app} - \beta_g^{int}\left[V_g^o + \Sigma(h - h^o)\right] \cdot Q/\beta V \tag{122}$$

where C is defined as follows:

$$C = 1 + \beta_g^{int}\left[V_g^o + \Sigma(h - h^o)\right]\left[1/(\beta V) + (\rho_b - \rho_g)g/\Sigma\right] \tag{123}$$

11.2 PRACTICAL APPLICATION

The apparent leak rate (Q_{app}) may consist of the gas leak ($Q_{leak}^{corr} > 0$), brine thermal expansion, or other phenomena ($Q > 0$). For illustration purposes, it is useful to present some orders of magnitude for these phenomena. We assume that Σ (the cavern neck cross-sectional area) is not very small; for instance, $\Sigma = 1\ m^2$, $P_g^{int} = 20$ MPa, $V_g^o = 40\ m^3$, $\rho_g = 230\ kg/m^3$ and $\beta_g^{int} V_g^o (\rho_b - \rho_g) g/\Sigma = 0.019$ is small when compared to 1. At the beginning of the test, when $h \approx h_0$, $C \approx 1 + \beta_g^{int} V_g^o / \beta V$ and:

$$Q_{app} = \left[\frac{Q_{leak}}{\beta_g^{int} V_g^o} + \frac{Q}{\beta V}\right] \Big/ \left[\frac{1}{\beta_g^{int} V_g^o} + \frac{1}{\beta V}\right] \tag{124}$$

As a general rule, Q/V is a decreasing function of cavern size; however, this does not apply to cavern creep. When the cavern is very large ($\beta V \gg \beta_g V_g^o$) and Q and Q_{leak} have the same order of magnitude, the simplest interpretation of the NIT results (i.e., $Q_{app} \approx Q_{leak}$) is correct.

During an actual test, Q_{app} can be measured ($Q_{app} = -\Sigma\dot{h}$) and Q can be estimated. Let Q' be an estimate of the effect of the various factors (other than the actual leak) which contribute to the apparent leak. Then:

$$Q_{leak}^{corr} = \left(1 + \frac{\beta_g^{int} V_g^o}{\beta V}\right) \cdot Q_{app} - \left(\frac{\beta_g^{int} V_g^o}{\beta V}\right) \cdot Q^{\bullet} \qquad (125)$$

Numerical examples are discussed in Section 6.3.9.